Searches for additional Higgs bosons and for vector leptoquarks in $\tau\tau$ final states in proton-proton collisions at $\sqrt{s} = 13$ TeV

The CMS collaboration

E-mail: cms-publication-committee-chair@cern.ch

Abstract: Three searches are presented for signatures of physics beyond the standard model (SM) in $\tau\tau$ final states in proton-proton collisions at the LHC, using a data sample collected with the CMS detector at $\sqrt{s} = 13$ TeV, corresponding to an integrated luminosity of $138\,\mathrm{fb}^{-1}$. Upper limits at 95% confidence level (CL) are set on the products of the branching fraction for the decay into τ leptons and the cross sections for the production of a new boson ϕ, in addition to the H(125) boson, via gluon fusion (ggϕ) or in association with b quarks, ranging from $\mathcal{O}(10\,\mathrm{pb})$ for a mass of $60\,\mathrm{GeV}$ to $0.3\,\mathrm{fb}$ for a mass of $3.5\,\mathrm{TeV}$ each. The data reveal two excesses for ggϕ production with local p-values equivalent to about three standard deviations at $m_\phi = 0.1$ and $1.2\,\mathrm{TeV}$. In a search for t-channel exchange of a vector leptoquark U_1, 95% CL upper limits are set on the dimensionless U_1 leptoquark coupling to quarks and τ leptons ranging from 1 for a mass of $1\,\mathrm{TeV}$ to 6 for a mass of $5\,\mathrm{TeV}$, depending on the scenario. In the interpretations of the M_h^{125} and $M_\mathrm{h,EFT}^{125}$ minimal supersymmetric SM benchmark scenarios, additional Higgs bosons with masses below $350\,\mathrm{GeV}$ are excluded at 95% CL.

Keywords: Beyond Standard Model, Hadron-Hadron Scattering, Higgs Physics

Contents

1 Introduction

The discovery of a Higgs boson with a mass of around 125 GeV, H(125), at the LHC in 2012 [1–3] has turned the standard model (SM) of particle physics into a theory that could be valid up to the Planck scale. In the SM, H(125) emerges from the spontaneous breaking of the electroweak $SU(2)_L$ symmetry. While the nature of the underlying mechanism leading to this symmetry breaking and the exact form of the required symmetry-breaking potential are still to be explored, the measured couplings of H(125) to fermions and gauge bosons, with 5–20% experimental precision [4–7], are in good agreement with the expectation for an SM Higgs boson with a mass of 125.38 ± 0.14 GeV [8]. The SM still leaves several fundamental questions related to particle physics unaddressed, including the presence of dark matter and the observed baryon asymmetry in nature. Many extensions of the SM that address these questions require a more complex structure of the part of the theory that is related to $SU(2)_L$ breaking, often referred to as the Higgs sector. Such models usually predict additional spin-0 states and modified properties of H(125) with respect to the SM expectation. Models incorporating supersymmetry (SUSY) [9, 10] are prominent examples. In the minimal extension of the SM, the minimal supersymmetric SM (MSSM) [11, 12], the model predicts three neutral and two charged Higgs bosons.

Searches for additional heavy neutral Higgs bosons in the context of the MSSM were carried out in electron-positron collisions at the LEP collider at CERN [13] and in proton-antiproton collisions at the Fermilab Tevatron [14–17]. At the LHC such searches have been carried out by the ATLAS and CMS Collaborations in the b quark [18–21], dimuon [22–25], and $\tau\tau$ [22, 26–33] final states. The $\tau\tau$ final state has a leading role in these searches, since τ leptons can be identified with higher purity than b quarks and backgrounds from genuine $\tau\tau$ events can be estimated with higher accuracy, while the branching fractions for the decay into τ leptons are typically larger than those for the decay into muons because of the larger τ lepton mass. There are several other examples of extended Higgs sectors, which are summarized in ref. [34], that could give appreciable resonant $\tau\tau$ production rates in addition to the known SM processes at the LHC. Furthermore, models that include additional coloured states carrying both baryon and lepton quantum numbers, known as leptoquarks [35, 36], can lead to an enhancement in the nonresonant production rates of $\tau\tau$ pairs with large invariant masses via the leptoquark t-channel exchange. Searches for resonant and nonresonant $\tau\tau$ signatures are thus complementary in the exploration of physics beyond the SM (BSM) at the LHC. Recent searches for single- and pair-production of third-generation leptoquarks at the LHC are reported in refs. [37–45].

In this paper the results of three searches for both resonant and nonresonant $\tau\tau$ signatures are presented:

i) The first search, which is meant to be as model independent as possible, targets the production of a single narrow spin-0 resonance ϕ, in addition to H(125), via gluon fusion (ggϕ) or in association with b quarks (bbϕ). Assumptions that have been made for this search are that the width of ϕ is small compared with the experimental resolution, and that the ϕ transverse momentum (p_T) spectrum for ggϕ production
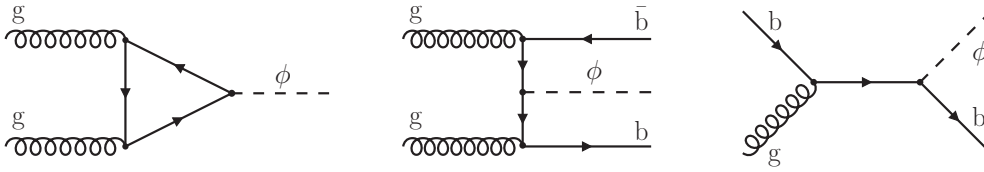
Figure 1. Diagrams for the production of neutral Higgs bosons ϕ (left) via gluon fusion, labelled as $\mathrm{gg}\phi$, and (middle and right) in association with b quarks, labelled as $\mathrm{bb}\phi$ in the text. In the middle diagram, a pair of b quarks is produced from the fusion of two gluons, one from each proton. In the right diagram, a b quark from one proton scatters from a gluon from the other proton. In both cases ϕ is radiated off one of the b quarks.

as well as the relative contributions of t- and b-quarks to $\mathrm{gg}\phi$ production are as expected for an SM Higgs boson at the tested mass value.

  ii) The second search targets the t-channel exchange of a vector leptoquark $\mathrm{U_1}$.

  iii) The third search exploits selected benchmark scenarios of the MSSM that rely on the signal from three neutral Higgs bosons, one of which is associated with H(125).

The results are based on the proton-proton (pp) collision data collected at the LHC during the years 2016–2018, at $\sqrt{s} = 13\,\mathrm{TeV}$, by the CMS experiment. The data correspond to an integrated luminosity of $138\,\mathrm{fb}^{-1}$. The analysis is performed in four $\tau\tau$ final states: $\mathrm{e}\mu$, $\mathrm{e}\tau_\mathrm{h}$, $\mu\tau_\mathrm{h}$, and $\tau_\mathrm{h}\tau_\mathrm{h}$, where e, μ, and τ_h indicate τ decays into electrons, muons, and hadrons, respectively. For this analysis the most significant backgrounds are estimated from data, which includes all SM processes with two genuine τ leptons in the final state, and processes where quark- or gluon-induced jets are misidentified as τ_h, denoted as jet $\to \tau_\mathrm{h}$.

The paper is organized as follows. Section 2 gives an overview of the phenomenology of the BSM physics scenarios under consideration. Section 3 describes the CMS detector, and section 4 describes the event reconstruction. Section 5 summarizes the event selection and categorization used for the extraction of the signal. The data model and systematic uncertainties are described in sections 6 and 7. Section 8 contains the results of the analysis. Section 9 briefly summarizes the paper. A complete set of tabulated results of this search for all tested mass hypotheses is available in the HEPData database [46].

2   Signal models

Neutral (pseudo)scalar bosons ϕ appear in many extensions of the SM. They may have different couplings to the upper and lower components of the $\mathrm{SU(2)_L}$ fermion fields (associated with up- and down-type fermions) and gauge bosons. In several models, like the MSSM models discussed in section 2.2, the ϕ couplings to down-type fermions are enhanced with respect to the expectation for an SM Higgs boson of the same mass, while the couplings to up-type fermions and vector bosons are suppressed. This makes down-type fermion final states, such as $\tau\tau$, particularly interesting for searches for neutral Higgs bosons in addition

to H(125). An enhancement in the couplings to down-type fermions also increases the bbϕ production cross section relative to ggϕ, which is another characteristic signature of these models and motivates the search for enhanced production cross sections in this production mode with respect to the SM expectation. In a first interpretation of the data, which is meant to be as model independent as possible, we search for ϕ production via the ggϕ and bbϕ processes in a range of $60 \leq m_\phi \leq 3500\,\text{GeV}$, where m_ϕ denotes the hypothesized ϕ mass. Diagrams for these processes are shown in figure 1. In a second, more specific interpretation of the data, we search for nonresonant $\tau\tau$ production in a model with vector leptoquarks. Finally, in a third interpretation of the data, we survey the parameter space of two indicative benchmark scenarios of the MSSM, which predict multiresonance signatures, one of which is associated with H(125). The most important characteristics of the vector leptoquark model and the MSSM are described in the following.

2.1 Vector leptoquarks

Leptoquarks are hypothetical particles that carry both baryon and lepton numbers [47], and are predicted by various BSM theories, such as grand unified theories [48–51], technicolour models [52–55], compositeness scenarios [56, 57], and *R*-parity violating SUSY [9–11, 58–64]. In recent years there has been a renewed interest in leptoquark models as a means of explaining various anomalies observed by a number of b physics measurements performed in different experiments [65–72], most notably the apparent violation of lepton flavour universality in neutral-current [73] and charged-current [74–80] B meson decays. Models that contain a TeV-scale vector leptoquark (U$_1$), characterized by its quantum numbers $(\text{SU(3)}_\text{C}, \text{SU(2)}_\text{L}, \text{U(1)}_\text{Y}) = (\mathbf{3}, \mathbf{1}, 2/3)$, are particularly appealing because they can explain both neutral- and charged-current anomalies at the same time [66–72].

The Lagrangian for the U$_1$ coupling to SM fermions is given by [72]

$$\mathcal{L}_\text{U} = \frac{g_\text{U}}{\sqrt{2}} \text{U}^\mu \left[\beta_\text{L}^{i\alpha}(\bar{q}_\text{L}^i \gamma_\mu l_\text{L}^\alpha) + \beta_\text{R}^{i\alpha}(\bar{d}_\text{R}^i \gamma_\mu e_\text{R}^\alpha) \right] + \text{h.c.}, \tag{2.1}$$

with the coupling constant g_U, where q_L and d_R (l_L and e_R) denote the left- and right-handed quark (lepton) doublets, and β_L and β_R are left- and right-handed coupling matrices, which are assumed to have the structures:

$$\beta_\text{L} = \begin{pmatrix} 0 & 0 & \beta_\text{L}^{\text{d}\tau} \\ 0 & \beta_\text{L}^{\text{s}\mu} & \beta_\text{L}^{\text{s}\tau} \\ 0 & \beta_\text{L}^{\text{b}\mu} & \beta_\text{L}^{\text{b}\tau} \end{pmatrix}, \quad \beta_\text{R} = \begin{pmatrix} 0 & 0 & 0 \\ 0 & 0 & 0 \\ 0 & 0 & \beta_\text{R}^{\text{b}\tau} \end{pmatrix}. \tag{2.2}$$

The motivations for the assumed structures of these matrices are given in ref. [72]. The normalization of g_U is chosen to give $\beta_\text{L}^{\text{b}\tau} = 1$. Two benchmark scenarios are considered, with different assumptions made about the value of $\beta_\text{R}^{\text{b}\tau}$. In the first benchmark scenario ("VLQ BM 1"), $\beta_\text{R}^{\text{b}\tau}$ is assumed to be zero. In the second benchmark scenario ("VLQ BM 2"), $\beta_\text{R}^{\text{b}\tau}$ is assumed to be -1, which corresponds to a Pati–Salam-like [49, 68] U$_1$ leptoquark. The $\beta_\text{L}^{\text{s}\tau}$ couplings are set to their preferred values from global fits to the low-energy observables presented in ref. [72], as summarized in table 1. The $\beta_\text{L}^{\text{d}\tau}$, $\beta_\text{L}^{\text{s}\mu}$, and $\beta_\text{L}^{\text{b}\mu}$

Benchmark	$\beta_{\mathrm{L}}^{\mathrm{s}\tau}$
VLQ BM 1	$0.19^{+0.06}_{-0.09}$
VLQ BM 2	$0.21^{+0.05}_{-0.09}$

Table 1. Summary of the preferred values and uncertainties of $\beta_{\mathrm{L}}^{\mathrm{s}\tau}$ in the two considered U_1 benchmark scenarios from ref. [72].
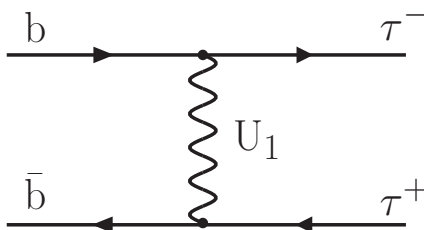
Figure 2. Diagram for the production of a pair of τ leptons via the t-channel exchange of a vector leptoquark U_1.

couplings are small and have negligible influence on the $\tau\tau$ signature, and therefore have been set to zero.

If the U_1 leptoquark mass (m_{U}) is sufficiently small, the U_1 particle will contribute to the $\tau\tau$ spectrum via pair production with each U_1 subsequently decaying to a $\mathrm{q}\tau$ pair. For larger m_{U}, the pair production cross section is suppressed because of the decreasing probability that the initial-state partons possess sufficiently large momentum fractions of the corresponding protons to produce on-shell U_1 pairs. In this case the dominant contribution to the $\tau\tau$ spectrum is via U_1 t-channel exchange in the $\mathrm{b\bar{b}}$ initial-state as illustrated in figure 2, with subdominant contributions from the equivalent $\mathrm{b\bar{s}}$, $\mathrm{s\bar{b}}$, and $\mathrm{s\bar{s}}$ initiated processes. In our analysis we target the kinematic region of $m_{\mathrm{U}} \gtrsim 1\,\mathrm{TeV}$, motivated by the experimental exclusion limits on m_{U} by direct searches, e.g. in ref. [42]. The contribution to the $\tau\tau$ spectrum from U_1 pair production is negligible in this case, and we therefore consider only production through the t-channel exchange.

2.2 The MSSM

In the MSSM, which is a concrete example of the more general class of two Higgs doublet models (2HDMs) [81, 82], the Higgs sector requires two SU(2) doublets, Φ_{u} and Φ_{d}, to provide masses for up- and down-type fermions. In CP-conserving 2HDMs, this leads to the prediction of two charged ($\mathrm{H}^{\pm}$) and three neutral ϕ bosons (h, H, and A), where h and H (with masses $m_{\mathrm{h}} < m_{\mathrm{H}}$) are scalars, and A (with mass m_{A}) is a pseudoscalar. The physical states h and H arise as mixtures of the pure gauge fields with a mixing angle α.

At tree level in the MSSM, the masses of these five Higgs bosons and α can be expressed in terms of the known gauge boson masses and two additional parameters, which can be chosen as m_{A} and the ratio of the vacuum expectation values of the neutral components

of Φ_u and Φ_d,

$$\tan\beta = \frac{\langle\Phi_u^0\rangle}{\langle\Phi_d^0\rangle}. \tag{2.3}$$

Dependencies on additional parameters of the soft SUSY breaking mechanism enter via higher-order corrections in perturbation theory. In the exploration of the MSSM Higgs sector these additional parameters are usually set to fixed values in the form of indicative benchmark scenarios to illustrate certain properties of the theory. The most recent set of MSSM benchmark scenarios provided by the LHC Higgs Working Group has been introduced in refs. [83–85] and summarized in ref. [86]. The corresponding predictions of masses, cross sections, and branching fractions can be obtained from ref. [87]. With one exception (the M_H^{125} scenario), in these scenarios h takes the role of H(125), and H and A are nearly degenerate in mass ($m_H \approx m_A$) in a large fraction of the provided parameter space.

For values of m_A much larger than the mass of the Z boson, the coupling of H and A to down-type fermions is enhanced by $\tan\beta$ with respect to the expectation for an SM Higgs boson of the same mass, while the coupling to vector bosons and up-type fermions is suppressed. For increasing values of $\tan\beta$, bbϕ (with ϕ = H, A) is enhanced relative to ggϕ production. The larger contribution of b quarks to the loop in figure 1 (left) in addition leads to softer spectra of the H and A transverse momentum. Extra SUSY particles influence the production and decay via higher-order contributions to the interaction vertices that belong to b quark lines. They also contribute directly to the loop in figure 1 (left).

3 The CMS detector

The central feature of the CMS apparatus is a superconducting solenoid of 6 m internal diameter, providing a magnetic field of 3.8 T. Within the solenoid volume are a silicon pixel and strip tracker, a lead tungstate crystal electromagnetic calorimeter (ECAL), and a brass and scintillator hadron calorimeter, each composed of a barrel and two endcap sections. Forward calorimeters extend the pseudorapidity (η) coverage provided by the barrel and endcap detectors. Muons are measured in gas-ionization detectors embedded in the steel flux-return yoke outside the solenoid. Events of interest are selected using a two-tiered trigger system. The first level (L1), composed of custom hardware processors, uses information from the calorimeters and muon detectors to select events at a rate of around 100 kHz within a fixed latency of about 4 μs [88]. The second level, known as the high-level trigger (HLT), consists of a farm of processors running a version of the full event reconstruction software optimized for fast processing, and reduces the event rate to around 1 kHz before data storage [89]. A more detailed description of the CMS detector, together with a definition of the coordinate system used and the relevant kinematic variables, can be found in ref. [90].

4 Event reconstruction

The reconstruction of the pp collision products is based on the particle-flow (PF) algorithm [91], which combines the information from all CMS subdetectors to reconstruct a set

of particle candidates (PF candidates), identified as charged and neutral hadrons, electrons, photons, and muons. In the 2016 (2017–2018) data sets the average number of interactions per bunch crossing was 23 (32). The primary vertex (PV) is taken to be the vertex corresponding to the hardest scattering in the event, evaluated using tracking information alone, as described in ref. [92]. Secondary vertices, which are displaced from the PV, might be associated with decays of long-lived particles emerging from the PV. Any other collision vertices in the event are associated with additional, mostly soft, inelastic pp collisions, referred to as pileup (PU).

Electrons are reconstructed using tracks from hits in the tracking system and energy deposits in the ECAL [93, 94]. To increase their purity, reconstructed electrons are required to pass a multivariate electron identification discriminant, which combines information on track quality, shower shape, and kinematic quantities. For this analysis, a working point with an identification efficiency of 90% is used, for a rate of jets misidentified as electrons of ≈1%. Muons in the event are reconstructed by combining the information from the tracker and the muon detectors [95]. The presence of hits in the muon detectors already leads to a strong suppression of particles misidentified as muons. Additional identification requirements on the track fit quality and the compatibility of individual track segments with the fitted track can reduce the misidentification rate further. For this analysis, muon identification requirements with an efficiency of ≈99% are chosen, with a misidentification rate below 0.2% for pions.

The contributions from backgrounds to the electron and muon selections are further reduced by requiring the corresponding lepton to be isolated from any hadronic activity in the detector. This property is quantified by an isolation variable

$$I_{\mathrm{rel}}^{\mathrm{e}(\mu)} = \frac{1}{p_{\mathrm{T}}^{\mathrm{e}(\mu)}} \left(\sum p_{\mathrm{T}}^{\mathrm{charged}} + \max \left(0, \sum E_{\mathrm{T}}^{\mathrm{neutral}} + \sum E_{\mathrm{T}}^{\gamma} - p_{\mathrm{T}}^{\mathrm{PU}} \right) \right), \qquad (4.1)$$

where $p_{\mathrm{T}}^{\mathrm{e}(\mu)}$ corresponds to the electron (muon) p_{T} and $\sum p_{\mathrm{T}}^{\mathrm{charged}}$, $\sum E_{\mathrm{T}}^{\mathrm{neutral}}$, and $\sum E_{\mathrm{T}}^{\gamma}$ to the p_{T} (or transverse energy E_{T}) sum of all charged particles, neutral hadrons, and photons, in a predefined cone of radius $\Delta R = \sqrt{(\Delta\eta)^2 + (\Delta\varphi)^2}$ around the lepton direction at the PV, where $\Delta\eta$ and $\Delta\varphi$ (measured in radians) correspond to the angular distances of the particle to the lepton in the η and azimuthal φ directions. The chosen cone size is $\Delta R = 0.3\,(0.4)$ for electrons (muons). The lepton itself is excluded from the calculation. To mitigate any distortions from PU, only those charged particles whose tracks are associated with the PV are included. Since an unambiguous association with the PV is not possible for neutral hadrons and photons, an estimate of the contribution from PU ($p_{\mathrm{T}}^{\mathrm{PU}}$) is subtracted from the sum of $\sum E_{\mathrm{T}}^{\mathrm{neutral}}$ and $\sum E_{\mathrm{T}}^{\gamma}$. This estimate is obtained from tracks not associated with the PV in the case of I_{rel}^{μ} and the mean energy flow per area unit in the case of $I_{\mathrm{rel}}^{\mathrm{e}}$. For negative values, the $I_{\mathrm{rel}}^{\mathrm{e}(\mu)}$ is set to zero.

For further characterization of the event, all reconstructed PF candidates are clustered into jets using the anti-k_{T} algorithm with a distance parameter of 0.4, as implemented in the FASTJET software package [96, 97]. To identify jets resulting from the hadronization of b quarks (b jets) the DEEPJET algorithm is used, as described in refs. [98, 99]. In this analysis a working point of this algorithm is chosen that corresponds to a b jet identification

	D_e (%)	D_μ (%)	D_{jet} (%)
$e\tau_h$	54 (0.05)	71.1 (0.13)	
$\mu\tau_h$	70 (2.60)	70.3 (0.03)	49 (0.43)
$\tau_h\tau_h$		71.1 (0.13)	

Table 2. Efficiencies for the identification of τ_h decays and corresponding misidentification rates (given in parentheses) for the working points of D_e, D_μ, and D_{jet}, chosen for the $\tau\tau$ selection, depending on the $\tau\tau$ final state. The numbers are given as percentages.

efficiency of $\approx 80\%$ for a misidentification rate for jets originating from light-flavour quarks or gluons of $\mathcal{O}(1\%)$ [100]. Jets with $p_T > 30\,\text{GeV}$ and $|\eta| < 4.7$ and b jets with $p_T > 20\,\text{GeV}$ and $|\eta| < 2.4$ are used in 2016. From 2017 onwards, after the upgrade of the silicon pixel detector, the b jet η range is extended to $|\eta| < 2.5$.

Jets are also used as seeds for the reconstruction of τ_h candidates. This is done by exploiting the substructure of the jets using the "hadrons-plus-strips" algorithm, as described in refs. [101, 102]. Decays into one or three charged hadrons with up to two neutral pions with $p_T > 2.5\,\text{GeV}$ are used. Neutral pions are reconstructed as strips with dynamic size in η-φ from reconstructed photons and electrons contained in the seeding jet, where the latter originate from photon conversions. The strip size varies as a function of the p_T of the electron or photon candidates. The τ_h decay mode is then obtained by combining the charged hadrons with the strips. To distinguish τ_h candidates from jets originating from the hadronization of quarks or gluons, and from electrons or muons, the DEEPTAU (DT) algorithm is used, as described in ref. [102]. This algorithm exploits the information of the reconstructed event record (comprising tracking, impact parameter, and calorimeter cluster information), the kinematic and object identification properties of the PF candidates in the vicinity of the τ_h candidate and those of the τ_h candidate itself, and quantities that estimate the PU density of the event. It results in a multiclassification output y_α^{DT} ($\alpha = \tau$, e, μ, jet) equivalent to a Bayesian probability of the τ_h candidate to originate from a genuine τ lepton, the hadronization of a quark or gluon, an electron, or a muon. From this output three discriminants are built according to

$$D_\alpha = \frac{y_\tau^{DT}}{y_\tau^{DT} + y_\alpha^{DT}}, \quad \alpha = \text{e, } \mu, \text{ jet.} \tag{4.2}$$

For the analysis presented here, predefined working points of D_e, D_μ, and D_{jet} [102] are chosen depending on the $\tau\tau$ final state, for which the τ_h selection efficiencies and misidentification rates are given in table 2. Since the jet $\to \tau_h$ misidentification rate strongly depends on the p_T and initiating parton type of the misidentified jet, it should be viewed as approximate.

The missing transverse momentum vector $\vec{p}_T^{\text{miss}}$ is also used for further categorization of the events. It is calculated as the negative vector p_T sum of all PF candidates, weighted by their probability to originate from the PV [103], and exploits the pileup-per-particle identification algorithm [104] to reduce the PU dependence. With p_T^{miss} we refer to the magnitude of this quantity.

5 Event selection and categorization

5.1 Selection of ττ candidates

Depending on the final state, the online selection in the HLT step is based either on the presence of a single electron, muon, or τ_h candidate, or an $e\mu$, $e\tau_h$, $\mu\tau_h$, or $\tau_h\tau_h$ pair in an event. In the offline selection further requirements on p_T, η, and $I_{rel}^{e(\mu)}$ are applied in addition to the object identification requirements described in section 4, as summarized in table 3.

In the $e\mu$ final state an electron and a muon with $p_T > 15\,\text{GeV}$ and $|\eta| < 2.4$ are required. Depending on the trigger path that has led to the online selection of an event, a stricter requirement of $p_T > 24\,\text{GeV}$ is imposed on one of the two leptons to ensure a sufficiently high trigger efficiency of the HLT selection. Both leptons are required to be isolated from any hadronic activity in the detector according to $I_{rel}^{e(\mu)} < 0.15\,(0.2)$.

In the $e\tau_h$ ($\mu\tau_h$) final state, an electron (muon) with $p_T > 25\,(20)\,\text{GeV}$ is required if the event was selected by a trigger based on the presence of the $e\tau_h$ ($\mu\tau_h$) pair in the event. From 2017 onwards, the threshold on the muon is raised to 21 GeV. If the event was selected by a single-electron trigger, the p_T requirement on the electron is increased to 26, 28, or 33 GeV for the years 2016, 2017, or 2018, respectively. For muons, the p_T requirement is increased to 23 (25) GeV for 2016 (2017–2018), if selected by a single-muon trigger. The electron (muon) is required to be contained in the central part of the detector with $|\eta| < 2.1$, and to be isolated according to $I_{rel}^{e(\mu)} < 0.15$. The τ_h candidate is required to have $|\eta| < 2.3$ and $p_T > 35\,(32)\,\text{GeV}$ if selected by an $e\tau_h$ ($\mu\tau_h$) pair trigger, or $p_T > 30\,\text{GeV}$ if selected by a single-electron (single-muon) trigger. In the $\tau_h\tau_h$ final state, both τ_h candidates are required to have $|\eta| < 2.1$ and $p_T > 40\,\text{GeV}$. For events only selected by a single τ_h trigger, the τ_h candidate that has been identified with the triggering object is required to have $p_T > 120\,(180)\,\text{GeV}$ for events recorded in 2016 (2017–2018).

The selected τ lepton decay candidates are required to be of opposite charge and to be separated by more than $\Delta R = 0.3$ in the η-φ plane in the $e\mu$ final state and by more than 0.5 otherwise. The closest distance of their tracks to the PV is required to be $d_z < 0.2\,\text{cm}$ along the beam axis. For electrons and muons, an additional requirement of $d_{xy} < 0.045\,\text{cm}$ in the transverse plane is applied. In rare cases, where more than the required number of τ_h candidates fulfilling all selection requirements is found, the candidate with the highest D_{jet} score is chosen. For electrons and muons, the most isolated candidate is chosen.

To avoid the assignment of single events to more than one final state, events with additional electrons or muons, fulfilling looser selection requirements than those given for each corresponding $\tau\tau$ final state above, are rejected from the selection. These requirements also help with the suppression of background processes, such as $Z/\gamma^* \to ee$ or $Z/\gamma^* \to \mu\mu$.

5.2 Event categorization

5.2.1 Standard categories and signal extraction

To increase the sensitivity of the searches, all selected events are further split into categories. Events with at least one b jet, according to the selection requirements given in section 4,

Final state	Obs.	First lepton			Second lepton		
		2016	2017	2018	2016	2017	2018
eμ	p_T		$> 15\,(24)$			$> 24\,(15)$	
	$\lvert\eta\rvert$		< 2.4			< 2.4	
	I^e_{rel}		< 0.15			< 0.20	
eτ_h	p_T	$> 25\,(26)$	$> 25\,(28)$	$> 25\,(33)$		$> 35\,(30)$	
	$\lvert\eta\rvert$		< 2.1			< 2.3	
	I^e_{rel}		< 0.15			$-$	
$\mu\tau_h$	p_T	$> 20\,(23)$	$> 21\,(25)$	$> 21\,(25)$		$> 32\,(30)$	
	$\lvert\eta\rvert$		< 2.1			< 2.3	
	I^μ_{rel}		< 0.15			$-$	
$\tau_h\tau_h$	p_T	$> 40\,(120)$	$> 40\,(180)$			> 40	
	$\lvert\eta\rvert$		< 2.1			< 2.1	

Table 3. Offline selection requirements applied to the electron, muon, and τ_h candidates used for the selection of the τ pair. The expressions first and second lepton refer to the label of the final state in the first column. The p_T requirements are given in GeV. For the eμ final state two lepton pair trigger paths, with a stronger requirement on the p_T of the electron (muon), are used for the online selection of the event. For the eτ_h, $\mu\tau_h$, and $\tau_h\tau_h$ final states, the values (in parentheses) correspond to the lepton pair (single lepton) trigger paths that have been used in the online selection. A detailed discussion is given in the text.

are combined into a global "b tag" category, used to target bbϕ production and to control the background from top quark pair ($t\bar{t}$) production. All other events are subsumed into a global "no b tag" category. The events in the $\tau_h\tau_h$ final state are not further categorized beyond that point. In the eτ_h and $\mu\tau_h$ final states, more categories are introduced in the global "b tag" and "no b tag" categories, based on the transverse mass of the e (μ)-$\vec{p}_T^{\,miss}$ system defined as

$$m_T^{e(\mu)} = m_T(\vec{p}_T^{\,e(\mu)}, \vec{p}_T^{\,miss}), \quad \text{with} \quad m_T(\vec{p}_T^{\,i}, \vec{p}_T^{\,j}) = \sqrt{2\,p_T^i\,p_T^j\,(1 - \cos\Delta\varphi)}, \tag{5.1}$$

where $\Delta\varphi$ refers to the azimuthal angular difference between $\vec{p}_T^{\,i}$ and $\vec{p}_T^{\,j}$. Events are divided into a tight-m_T ($m_T^{e(\mu)} < 40\,\text{GeV}$) and a loose-$m_T$ ($40 < m_T^{e(\mu)} < 70\,\text{GeV}$) category. The ϕ signal is expected to be concentrated in the tight-m_T category. However, the loose-m_T category increases the acceptance for $m_\phi \gtrsim 700\,\text{GeV}$.

In the eμ final state, events are categorized based on the observable D_ζ [105] defined as

$$D_\zeta = p_\zeta^{miss} - 0.85\,p_\zeta^{vis}; \qquad p_\zeta^{miss} = \vec{p}_T^{\,miss} \cdot \hat{\zeta}; \qquad p_\zeta^{vis} = \left(\vec{p}_T^{\,e} + \vec{p}_T^{\,\mu}\right) \cdot \hat{\zeta}, \tag{5.2}$$

where $\hat{\zeta}$ corresponds to the bisectional direction between $\vec{p}_T^{\,e}$ and $\vec{p}_T^{\,\mu}$. The scalar products p_ζ^{miss} and p_ζ^{vis} can take positive or negative values. Their linear combination has been optimized to maximize the sensitivity of the search. For events originating from W boson production in association with jets (W+jets) or $t\bar{t}$ production, the $\vec{p}_T^{\,e}$, $\vec{p}_T^{\,\mu}$, and $\vec{p}_T^{\,miss}$ directions are more isotropically distributed leading to nonpeaking distributions in D_ζ.
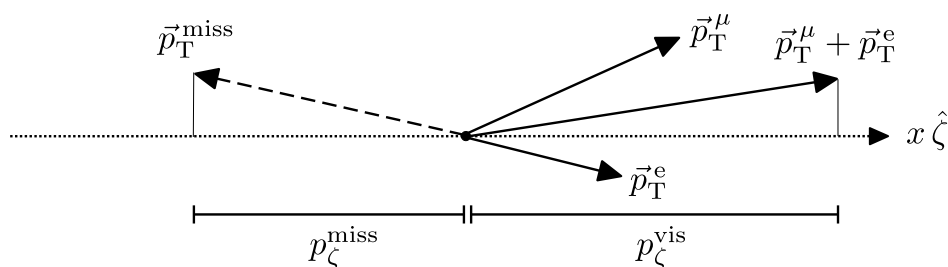
Figure 3. Inputs to the reconstruction of the event observable D_ζ in the eμ final state, as described in the text.

For $\tau\tau$ events from resonant decays, $\vec{p}_T^{\,\mathrm{miss}}$ is expected to roughly coincide with $\hat{\zeta}$, and a stronger correlation between p_ζ^{miss} and p_ζ^{vis} is expected to lead to a peaking distribution about $D_\zeta \approx 0\,\mathrm{GeV}$. The inputs to the reconstruction of D_ζ are illustrated in figure 3. Three further categories are introduced as high-D_ζ ($D_\zeta > 30\,\mathrm{GeV}$), medium-$D_\zeta$ ($-10 < D_\zeta < 30\,\mathrm{GeV}$), and low-$D_\zeta$ ($-35 < D_\zeta < -10\,\mathrm{GeV}$). A ϕ signal is expected to be concentrated in the medium-D_ζ category. However, the low- and high-D_ζ categories still contribute to an increase of the sensitivity of the model-independent ϕ search in the eμ final state by $\approx 10\%$. A control category in the eμ final state with at least one b jet and $D_\zeta < -35\,\mathrm{GeV}$ is used to constrain the normalization of $t\bar{t}$ events in the fit used for signal extraction.

In summary, this leads to 17 event categories per data-taking year. Figure 4 shows the D_ζ and m_T^μ distributions in the eμ and $\mu\tau_\mathrm{h}$ final states, before splitting the events into the categories described above. The category definitions are indicated by the vertical dashed lines in the figures. An overview of the categories described above is given in figure 5.

In all cases the signal is extracted from distributions of the total transverse mass [26] defined as

$$m_T^{\mathrm{tot}} = \sqrt{m_T^2(\vec{p}_T^{\,\tau_1}, \vec{p}_T^{\,\tau_2}) + m_T^2(\vec{p}_T^{\,\tau_1}, \vec{p}_T^{\,\mathrm{miss}}) + m_T^2(\vec{p}_T^{\,\tau_2}, \vec{p}_T^{\,\mathrm{miss}})}, \tag{5.3}$$

where $\tau_{1(2)}$ refers to the first (second) τ final state indicated in the eμ, eτ_h, $\mu\tau_\mathrm{h}$, and $\tau_\mathrm{h}\tau_\mathrm{h}$ final state labels, and m_T between two objects with transverse momenta $\vec{p}_T^{\,\tau_1}$ and $\vec{p}_T^{\,\tau_2}$ is defined in eq. (5.1). This quantity is expected to provide superior discriminating power between resonant signals with $m_\phi \gtrsim 250\,\mathrm{GeV}$ and nonpeaking backgrounds, such as W+jets or $t\bar{t}$ production in the high-mass tails of the distribution.

This strategy is used for the model-independent ϕ search, to extract the expected signal for hypothesized values of $m_\phi \geq 250\,\mathrm{GeV}$. It is also used for the extraction of the A and H signal (for m_A, $m_H \gtrsim 250\,\mathrm{GeV}$), when interpreting the data in MSSM benchmark scenarios, and for the vector leptoquark search, which is most sensitive to an excess over the background expectation for $m_T^{\mathrm{tot}} \gtrsim 250\,\mathrm{GeV}$ as will be discussed in section 6.4.2.

To increase the sensitivity of the analyses for the model-independent ϕ search for hypothesized values of $m_\phi < 250\,\mathrm{GeV}$ and the low-mass resonance h for the interpretation of the data in MSSM benchmark scenarios, this signal extraction strategy is modified as discussed in the following sections.
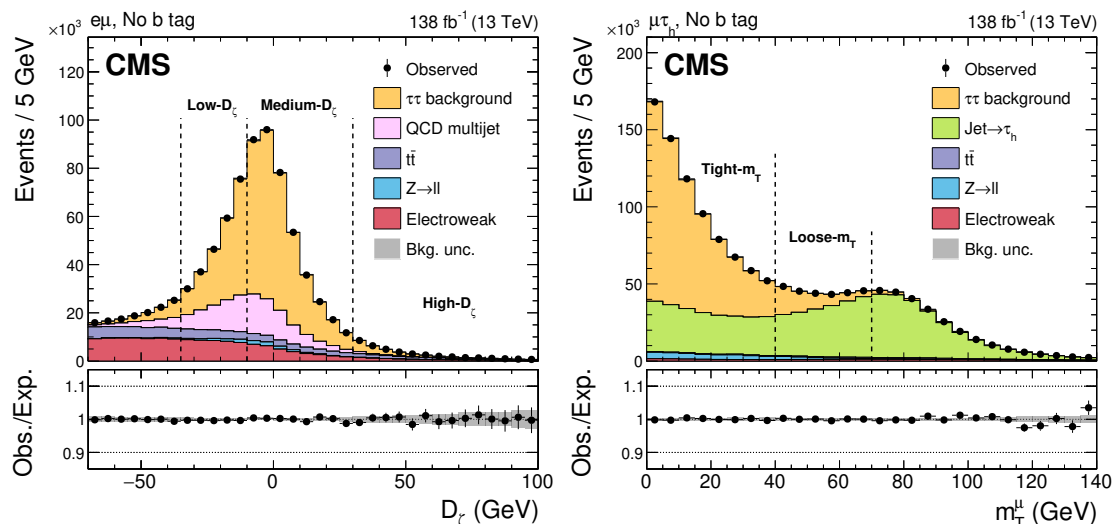
Figure 4. Observed and expected distributions of (left) D_ζ in the eμ final state and (right) m_{T}^μ in the $\mu\tau_{\mathrm{h}}$ final state. The distributions are shown in the global "no b tag" category before any further event categorization and after an individual background-only fit to the data in each corresponding variable. The grey shaded band represents the complete set of uncertainties used for signal extraction, after the fit. A detailed discussion of the data modelling is given in section 6. The vertical dashed lines indicate the category definitions in each of the final states, as described in the text. In the lower panels of each figure the ratio of the observed numbers of events per bin to the background expectation is shown.

Figure 5. Overview of the categories used for the extraction of the signal for the model-independent ϕ search for hypothesized values of $m_\phi \geq 250\,\mathrm{GeV}$, the vector leptoquark search, and the interpretation of the data in MSSM benchmark scenarios.

	No b tag		b tag	

eμ

Medium-D_ζ — $p_T^{\tau\tau} < 50\,\text{GeV}$ / $50 < p_T^{\tau\tau} < 100\,\text{GeV}$ / $100 < p_T^{\tau\tau} < 200\,\text{GeV}$ / $p_T^{\tau\tau} > 200\,\text{GeV}$

High-D_ζ — $p_T^{\tau\tau} < 50\,\text{GeV}$ / $50 < p_T^{\tau\tau} < 100\,\text{GeV}$ / $100 < p_T^{\tau\tau} < 200\,\text{GeV}$ / $p_T^{\tau\tau} > 200\,\text{GeV}$

Medium-D_ζ

High-D_ζ

eτ_h

Tight-m_T — $p_T^{\tau\tau} < 50\,\text{GeV}$ / $50 < p_T^{\tau\tau} < 100\,\text{GeV}$ / $100 < p_T^{\tau\tau} < 200\,\text{GeV}$ / $p_T^{\tau\tau} > 200\,\text{GeV}$

Tight-m_T

$\mu\tau_h$

Tight-m_T — $p_T^{\tau\tau} < 50\,\text{GeV}$ / $50 < p_T^{\tau\tau} < 100\,\text{GeV}$ / $100 < p_T^{\tau\tau} < 200\,\text{GeV}$ / $p_T^{\tau\tau} > 200\,\text{GeV}$

Tight-m_T

$\tau_h\tau_h$

$p_T^{\tau\tau} < 50\,\text{GeV}$ / $50 < p_T^{\tau\tau} < 100\,\text{GeV}$ / $100 < p_T^{\tau\tau} < 200\,\text{GeV}$ / $p_T^{\tau\tau} > 200\,\text{GeV}$

$t\bar{t}(e\mu)$

$D_\zeta < -35\,\text{GeV}$

Signal region (SR)

Control region

Figure 6. Overview of the categories used for the extraction of the signal for the model-independent ϕ search for $60 \leq m_\phi < 250\,\text{GeV}$.

5.2.2 Modifications for the low-mass model-independent ϕ search

For hypothesized values of $m_\phi < 250\,\text{GeV}$, the background from $Z/\gamma^* \to \tau\tau$ production, which features a peaking mass distribution in a region close to the signal mass, starts to exceed the nonpeaking backgrounds. The m_T^{tot} distribution loses discrimination power and some of the categories that were introduced to increase the acceptance for high-mass signals are not useful anymore. Therefore, the signal extraction strategy is modified in the following way. The low-D_ζ and loose-m_T categories are removed. The remaining "no b tag" categories are further split by $p_T^{\tau\tau}$, obtained from the vectorial sum p_T of the visible τ decay products and $\vec{p}_T^{\text{miss}}$, according to $p_T^{\tau\tau} < 50\,\text{GeV}$, $50 < p_T^{\tau\tau} < 100\,\text{GeV}$, $100 < p_T^{\tau\tau} < 200\,\text{GeV}$, and $p_T^{\tau\tau} < 200\,\text{GeV}$, where $p_T^{\tau\tau}$ is used as an estimate for the ϕ p_T (p_T^ϕ) in data. No further splitting based on $p_T^{\tau\tau}$ is applied to the "b tag" categories because of the lower event populations in these categories. In summary, this leads to 26 event categories per data-taking year. An overview of this modified set of categories is given in figure 6.

Search		Categories	Additional selections	Discr. variable
Model-independent (ϕ)	$m_\phi < 250\,\mathrm{GeV}$	Figure 6	—	$m_{\tau\tau}$
	$m_\phi \geq 250\,\mathrm{GeV}$	Figure 5	—	$m_{\mathrm{T}}^{\mathrm{tot}}$
Vector leptoquark (U_1)		Figure 5	—	$m_{\mathrm{T}}^{\mathrm{tot}}$
MSSM benchmark scenarios (A, H, h)		NN-analysis	$m_{\tau\tau} < 250\,\mathrm{GeV}$, $D_\zeta > -35\,\mathrm{GeV}$ (in eμ)	y_l
		Figure 5	$m_{\tau\tau} > 250\,\mathrm{GeV}$	$m_{\mathrm{T}}^{\mathrm{tot}}$

Table 4. Event categories and discriminants used for the extraction of the signals, for the searches described in this paper. We note that m_ϕ refers to the hypothesized mass of the model-independent ϕ search, while $m_{\tau\tau}$ refers to the reconstructed mass of the $\tau\tau$ system before the decays of the τ leptons, and thus to an estimate of m_ϕ in data. The variable y_l refers to the output functions of the NNs used for signal extraction in ref. [109].

In these categories, the signal is extracted from a likelihood-based fit of the invariant mass of the $\tau\tau$ system, $m_{\tau\tau}$, before the decay of the τ leptons [106]. This estimate combines the measurement of $\vec{p}_{\mathrm{T}}^{\mathrm{miss}}$ and its covariance matrix with the measurements of the visible $\tau\tau$ decay products, utilizing the matrix elements for unpolarized τ decays [107] for the decay into leptons and the two-body phase space [108] for the decay into hadrons. On average the resolution of $m_{\tau\tau}$ amounts to about 10–25%, depending on the kinematic properties of the $\tau\tau$ system and the $\tau\tau$ final states, where the latter is related to the number of neutrinos that escape detection. This approach exploits the better m_ϕ resolution of $m_{\tau\tau}$ compared to $m_{\mathrm{T}}^{\mathrm{tot}}$, together with the usually harder p_{T}^ϕ, compared to the $\mathrm{Z}/\gamma^* \to \tau\tau$ p_{T} spectrum.

5.2.3 Modifications for the MSSM interpretation

The MSSM predicts three neutral Higgs bosons ϕ, one of which is identified with H(125). Each benchmark scenario has to match the observed H(125) properties. To exploit the best possible experimental knowledge about H(125) all events in the global "no b tag" category are split by $m_{\tau\tau}$. For events with $m_{\tau\tau} > 250\,\mathrm{GeV}$, the categories described in section 5.2.1 are used. For events with $m_{\tau\tau} < 250\,\mathrm{GeV}$, the neural-network-based (NN) analysis, which was used for the stage-0 simplified template cross section measurements of ref. [109], is used to obtain the most precise estimates from data for H(125) production via gluon fusion (ggh), vector boson fusion (VBF), and vector boson associated production (Vh). Although the NN is trained specifically to target events with an SM-like ϕ with $m_\phi = 125\,\mathrm{GeV}$, signal events for the additional Higgs bosons can also enter the NN categories for $m_\phi \lesssim 250\,\mathrm{GeV}$, and the y_l discriminators contribute to the separation of such events from the background.

This modification adds 18 background and 8 signal categories from the NN-analysis per data-taking year. We will refer to these as the "NN categories" throughout this paper. In these categories, the H(125) signal is extracted from distributions of the NN output functions y_l in each signal and background category l. For the NN-analysis in ref. [109], $m_{\mathrm{T}}^{\mathrm{e}\mu}$ calculated from $\vec{p}_{\mathrm{T}}^{\mathrm{e}} + \vec{p}_{\mathrm{T}}^{\mu}$ and $\vec{p}_{\mathrm{T}}^{\mathrm{miss}}$ is required to be less than $60\,\mathrm{GeV}$ in the eμ final state, to prevent event overlap with analyses of other H(125) decay modes in the SM interpretation. For the analysis presented here, this requirement is replaced by $D_\zeta > -35\,\mathrm{GeV}$.

Background process	Final-state signature	Estimation method			
		τ-emb.	F_{F}	SS	Sim.
Z/γ^*	$\tau\tau$	✓	—	—	—
	Jet$\to\tau_{\mathrm{h}}$	—	✓	—	—
	$\ell\ell$	—	—	—	✓
$t\bar{t}$	$\tau\tau$	✓	—	—	—
	Jet$\to\tau_{\mathrm{h}}$	—	✓	—	—
	$\ell + \mathrm{X}$	—	—	—	✓
Diboson+single t	$\tau\tau$	✓	—	—	—
	Jet$\to\tau_{\mathrm{h}}$	—	✓	—	—
	$\ell + \mathrm{X}$	—	—	—	✓
W+jets	Jet$\to\tau_{\mathrm{h}}$	—	✓	—	—
	Jet$\to\ell$	—	—	—	✓
QCD multijet	Jet$\to\tau_{\mathrm{h}}$	—	✓	—	—
	QCD(eμ)	—	—	✓	—
H(125)	$\tau\tau$	—	—	—	✓

Table 5. Background processes contributing to the event selection, as discussed in section 5. The symbol ℓ corresponds to an electron or muon. The second column refers to the experimental signature in the analysis, the last four columns indicate the estimation methods used to model each corresponding signature, as described in sections 6.1–6.4. Diboson and single t production are part of the process group iv) discussed in section 6. QCD(eμ) refers to QCD multijet production with an eμ pair in the final state.

A summary of the categories and discriminating variables used for signal extraction for each of the analyses presented in this paper is given in table 4.

6 Background and signal modelling

All SM background sources that are relevant after the event selection described in section 5 are listed in table 5. The expected background composition depends on the $\tau\tau$ final state, event category, and the tested signal mass hypothesis. The most abundant source of background in the "b tag" categories is $t\bar{t}$ production. In the "no b tag" categories Z/$\gamma^* \to \tau\tau$ forms the largest fraction of background processes, followed by W+jets production and events containing purely quantum chromodynamics (QCD) induced gluon and light-flavour quark jets, referred to as QCD multijet production. These backgrounds are grouped according to their experimental signatures into:

i) events containing genuine τ lepton pairs ($\tau\tau$);

ii) events with quark- or gluon-induced jets misidentified as τ_{h} candidates (jet $\to \tau_{\mathrm{h}}$) or light leptons (jet $\to \ell$) in the eμ final state;

iii) $t\bar{t}$ events where an intermediate W boson decays into an electron, muon, or τ lepton, which do not fall into the previous groups (labelled as "$t\bar{t}$" in later figures);

iv) remaining background processes that are of minor importance for the analysis and not yet included in any of the previous event groups (labelled as "others" in later figures).

Event group (i) mostly contains $Z/\gamma^* \to \tau\tau$ events, with smaller contributions from $t\bar{t}$, diboson, and single t quark production. These events are modelled using the τ-embedding method [110], labelled "τ-emb." in table 5, and discussed in section 6.1. Event group (ii) contains events from QCD multijet, W+jets, Z+jets, $t\bar{t}$, diboson and single t quark production with jet $\to \tau_h$ misidentification, and QCD multijet production with jet $\to \ell$ misidentification in the eμ final state. The events with jet $\to \tau_h$ misidentification are estimated from the "fake factor" (F_F) method, labelled "F_F" in table 5, and discussed in section 6.2. The events with jet $\to \ell$ misidentification in the eμ final state are estimated from the "same-sign" (SS) method, labelled "SS" in table 5, and discussed in section 6.3. Event group (iv) comprises diboson and single t quark production (labelled as "electroweak" in figure 4 left), H(125) production, $Z/\gamma^* \to \mu\mu$ and $Z/\gamma^* \to$ ee events, and W+jets events with jet $\to \ell$ misidentification. Events from event groups iii) and iv), and all signal processes are estimated from full event simulation, labelled "Sim." in table 5, and discussed in section 6.4.

6.1 Backgrounds with genuine τ lepton pairs ($\tau\tau$)

For all events where the decay of a Z boson results in two genuine τ leptons, the τ-embedding method, as described in ref. [110], is used. For this purpose, $\mu\mu$ events are selected in data. All energy deposits of the muons are removed from the event record and replaced by simulated τ lepton decays with the same kinematic properties as the selected muons. In this way the method relies only on the simulation of the well-understood τ lepton decay and its energy deposits in the detector, while all other parts of the event, such as the identification and reconstruction of jets, including b jets, or the non-τ related parts of $\vec{p}_T^{\,\mathrm{miss}}$ are obtained from data. This results in an improved modelling of the data compared with the simulation of the full process. In turn, several simulation-to-data corrections, as detailed in section 6.5, are not needed. The selected muons predominantly originate from $Z/\gamma^* \to \mu\mu$ events. However, contributions from other processes resulting in two genuine τ leptons, like $t\bar{t}$ or diboson production, are also covered by this model. For a selection with no (at least one) b jet in the event, as described in section 5, 97% (84%) of the $\mu\mu$ events selected for the τ-embedding method are expected to originate from $Z/\gamma^* \to \mu\mu$ and <1% (14%) from $t\bar{t}$ production. A detailed discussion of the selection of the original $\mu\mu$ events, the exact procedure itself, its range of validity, and related uncertainties is reported in ref. [110].

6.2 Backgrounds with jets misidentified as hadronically decaying τ leptons (jet → τ_h)

The main processes contributing to jet → τ_h events in the $\mathrm{e}\tau_\mathrm{h}$, $\mu\tau_\mathrm{h}$, and $\tau_\mathrm{h}\tau_\mathrm{h}$ final states are QCD multijet, W+jets, and $\mathrm{t\bar{t}}$ production. These events are estimated using the F_F method described in refs. [32, 111], and adapted to the analyses described in this paper.

For this purpose, the signal region (SR), defined by the event selection given in section 5, is complemented by three additional regions: the application region (AR) and two determination regions DR^i, where i stands for QCD or W+jets. For the AR a looser working point for the identification of the τ_h candidate is chosen and the events from the SR are excluded, which is the only selection difference with respect to the SR. In this way the AR forms an orthogonal, though still adjacent, sideband to the SR that is enriched in jet → τ_h events. The events in the AR are then multiplied with a transfer function, which is obtained from each corresponding DR^i or simulation, to estimate the contribution of jet → τ_h events in the SR. The background processes in the AR and each corresponding DR^i that are not targeted by this method are estimated either from simulation or the τ-embedding method and subtracted from the data.

In the $\tau_\mathrm{h}\tau_\mathrm{h}$ final state, where QCD multijet production contributes $\gtrsim 95\%$ of the events in the AR, the transfer function is determined from DR^QCD only, for which the charges of the two selected τ_h candidates are required to be of same sign. This function is assumed to be applicable also for the small fraction of W+jets and $\mathrm{t\bar{t}}$ events in the AR. In this final state, both τ_h candidates usually originate from jet → τ_h misidentification. We require only the τ_h candidate with the larger p_T to fulfil the AR requirements, which provides an estimate for events where only this τ_h candidate is misidentified. Events in which the τ_h candidate with the larger p_T is a genuine τ lepton and the one with the lower p_T is misidentified, which constitute $\approx 2\%$ of the total jet → τ_h background, are modelled from simulation.

In the $\mathrm{e}\tau_\mathrm{h}$ ($\mu\tau_\mathrm{h}$) final state, where the sharing of processes contributing to the AR is more equal, separate contributions to the transfer function F_F^i are used, where the index i runs over the processes of QCD multijet, W+jets, and $\mathrm{t\bar{t}}$ production. For QCD multijet and W+jets production each F_F^i is derived in its corresponding DR^i. For DR^QCD we require $0.05 < I_\mathrm{rel}^{\mathrm{e}(\mu)} < 0.15$ and the charges of the selected $\mathrm{e}(\mu)$ and the τ_h candidate to be of same sign. For $\mathrm{DR}^\mathrm{W+jets}$ we require $m_\mathrm{T}^{\mathrm{e}(\mu)} > 70\,\mathrm{GeV}$ and the absence of b jets. The estimate of $F_\mathrm{F}^\mathrm{t\bar{t}}$ is obtained from simulation. Each F_F^i is then used to estimate the yield N_SR and kinematic properties of the combination of the main contributing backgrounds i in the SR from the number of events N_AR in the AR according to

$$N_\mathrm{SR} = \left(\sum_i w_i F_\mathrm{F}^i \right) N_\mathrm{AR}, \qquad i = \mathrm{QCD,\ W+jets,\ t\bar{t}}. \qquad (6.1)$$

Each F_F^i is combined into a weighted sum, using the simulation-based estimate of the fractions w_i of each process in the AR. A template fit to the data in the AR yields a similar result for the w_i.

Each F_F^i is computed on an event-by-event basis. It mainly depends on the p_T of the τ_h candidate with the larger p_T, $p_T^{\tau_h}$, the ratio $p_T^{jet}/p_T^{\tau_h}$ where p_T^{jet} corresponds to the p_T of the jet seeding the τ_h reconstruction, and the jet multiplicity N_{Jets}. Each F_F^i is further subject to a number of residual corrections derived from both control regions in data and simulation to take subleading dependencies of the F_F^i into account. Depending on the transfer function F_F^i and the $\tau\tau$ final state these are dependencies on p_T^ℓ, the invariant mass of the visible decay products of the $\tau\tau$ system, I_{rel}^ℓ, or $p_T^{\tau_h}$ of the second-leading τ_h candidate.

6.3 Backgrounds with jets misidentified as electron-muon pairs (QCD(eμ))

The background from QCD multijet production where two quark- or gluon-induced jets are misidentified as an eμ pair is estimated using the SS method. In this case, an AR is distinguished from the SR by requiring the charges of the electron and muon to have the same sign. A sideband region DR is defined requiring the muon to be nonisolated $(0.2 < I_{rel}^\mu < 0.5)$. From this DR an SS to opposite-sign (OS) transfer function F_T is obtained to extrapolate the number N_{AR} of events in the AR to the number N_{SR} of events in the SR according to

$$N_{SR} = F_T \, N_{AR}. \tag{6.2}$$

The function F_T primarily depends on the distance $\Delta R(e, \mu)$ between the e and μ trajectories in η-φ and N_{Jets}. Additional dependencies on the electron and muon p_T enter via a bias correction, ranging from 0.85–0.9. To validate the method, a second transfer function F_T' is calculated from a modified DR$'$ with an isolated muon $(I_{rel}^\mu < 0.2)$ and nonisolated electron $(0.15 < I_{rel}^e < 0.5)$, which is applied to the SS selection of the DR. The resulting event yield and shapes of the m_T^{tot} and $m_{\tau\tau}$ distributions are compared to the OS selection of the DR. This test reveals a consistent result within the statistical uncertainties of the estimate, for events with $N_{b\text{-}jets} = 0$. For events with $N_{b\text{-}jets} \geq 1$, a global correction factor r_b is required, with a value of 0.71–0.75 depending on the year of data-taking.

A potential bias from requiring the muon to be nonisolated in the definition of DR is checked from a third definition of the transfer function F_T'', in a DR$''$ with a nonisolated muon $(0.2 < I_{rel}^\mu < 0.5)$ and electron $(0.15 < I_{rel}^e < 0.5)$. This test reveals another correction of 0.94–0.95, depending on the year of data-taking, to correct for the fact that r_b, with an isolated muon, is systematically smaller by $\approx 5\%$ than in the case of a nonisolated muon.

6.4 Simulated backgrounds and signal

In the $\tau_h\tau_h$ final state, the τ-embedding and F_F methods cover 97% of all expected background events. The fractions of expected background events described by these two methods are 83% in the $e\tau_h$ and 90% in the $\mu\tau_h$ final states. In the eμ final state, 53% of all events are obtained by either the τ-embedding or SS method. All remaining events originate from processes such as Z boson, $t\bar{t}$, or diboson production, where at least one decay of a vector boson into an electron or muon is not covered by any of the previously discussed methods. These backgrounds and the signal processes are modelled using the simulation of the full processes.

6.4.1 Background processes

The W+jets and $Z/\gamma^* \to \ell\ell$ processes are simulated at leading order (LO) accuracy in the strong coupling α_S, using the MADGRAPH5_aMC@NLO 2.2.2 (2.4.2) event generator [112, 113] for the simulation of the data taken in 2016 (2017–2018). To increase the number of simulated events in regions of high signal purity, supplementary samples are generated with up to four outgoing partons in the hard interaction. For diboson production, MADGRAPH5_aMC@NLO is used at next-to-LO (NLO) precision in α_S. In each case, the FxFx [114] (MLM [115]) prescription is used to match the NLO (LO) matrix element calculation with the parton shower model. For $t\bar{t}$ [116] and (t-channel) single t quark production [117], samples are generated at NLO precision in α_S using POWHEG 2.0 [118–121]. The POWHEG version 1.0 at NLO precision is used for single t quark production in association with a W boson (tW channel) [122].

When compared with data, W+jets, $Z/\gamma^* \to \ell\ell$, $t\bar{t}$, and single t quark events in the tW channel are normalized to their cross sections at next-to-NLO (NNLO) precision in α_S [123–125]. Single t quark (t-channel) and diboson events are normalized to their cross sections at NLO precision in α_S or higher [125–127].

6.4.2 Signal processes

The kinematic properties of single h production are simulated at NLO precision in α_S using POWHEG 2.0 separately for the production via ggh [128], VBF [129], or in association with a Z (Zh) or W (Wh) boson [130, 131]. For ggh production, the distributions of the h boson p_T and the jet multiplicity in the simulation are tuned to match the NNLO accuracy obtained from full phase space calculations with the NNLOPS event generator [132, 133]. For this purpose, h is assumed to behave as expected from the SM. This applies to the modelling of H(125) as part of the background for the model-independent ϕ search, as well as for the SM and the MSSM hypotheses for the interpretation of the data in MSSM benchmark scenarios, where h is associated with H(125) with properties as expected from the SM.

The production of ϕ, H, and A bosons via gluon fusion is simulated at NLO precision in α_S using the 2HDM implementation of POWHEG 2.0 [128]. To account for the multiscale nature of the process in the NLO plus parton shower prediction, the p_T spectra corresponding to the contributions from the t quark only, b quark only, and tb-interference are each calculated separately. The POWHEG damping factor h_{damp}, which controls the matching between the matrix element calculation and the parton shower, is set specifically for each contribution as proposed in refs. [134–136].

For the model-independent ϕ search, the individual distributions are combined according to their contribution to the total cross section as expected for an SM-like Higgs boson with given mass. For the tests of MSSM benchmark scenarios, where the contributions of the individual distributions also depend on the model parameters, these distributions are scaled using the effective Yukawa couplings as predicted by the corresponding benchmark model [87], before combining them into one single prediction. In this context, the $\tan\beta$-enhanced SUSY corrections to the ϕbb couplings are also included via the corre-
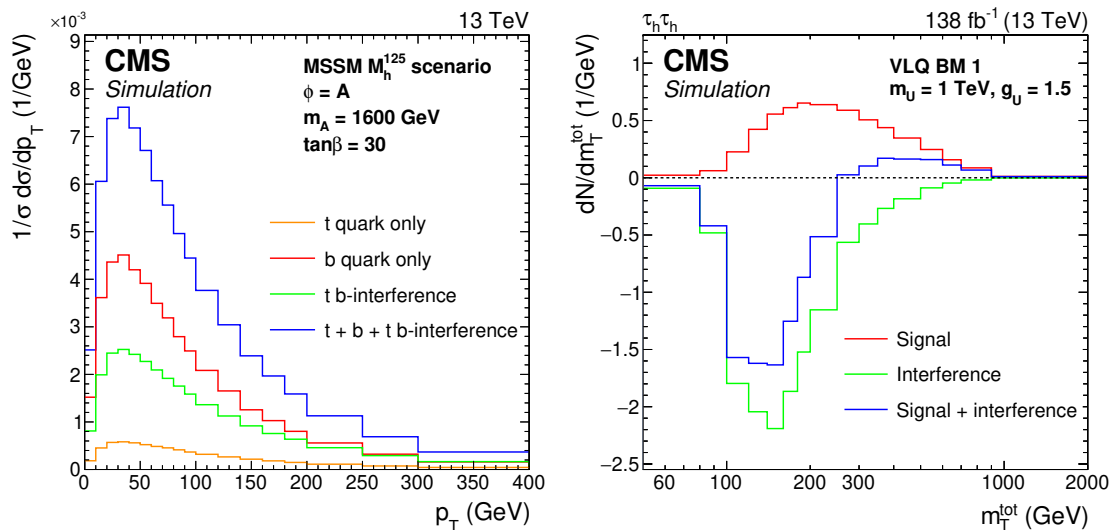
Figure 7. Composition of the signal for the MSSM interpretation of the data and the vector leptoquark search. The left figure shows the generator level A boson p_T density for the MSSM M_h^{125} scenario for $m_A = 1.6\,\text{TeV}$ and $\tan\beta = 30$, split by the contributions from the t quark only, the b quark only, and the tb-interference term. The right figure shows the distribution of m_T^{tot} at reconstruction level in the $\tau_h\tau_h$ final state for U_1 t-channel exchange with $m_U = 1\,\text{TeV}$ and $g_U = 1.5$, for the signal with and without the interference term for the VLQ BM 1 scenario. The $\tau_h\tau_h$ final state is shown, since it is the most sensitive one for this search. The bins of the distributions are divided by their width and the distribution is normalized to the expected signal yield for $138\,\text{fb}^{-1}$.

sponding effective Yukawa couplings, where appropriate. Other SUSY contributions have been checked to amount to less than a few percent and are neglected. An example of the A boson p_T spectrum for $m_A = 1.6\,\text{TeV}$ and $\tan\beta = 30$ is shown in figure 7 (left). The $bb\phi$ production is simulated at NLO precision in α_S using the corresponding POWHEG 2.0 implementation [137] in the four-flavour scheme (4FS).

The signal process of the U_1 t-channel exchange is simulated in the five-flavour scheme (5FS) at LO precision in α_S using the MADGRAPH5_aMC@NLO event generator, v2.6.5 [138]. Events are generated with up to one additional outgoing parton from the matrix element calculation and matched following the MLM prescription, with the matching scale Q_{match} set to $40\,\text{GeV}$. The contribution from on-shell $U_1 \to q\tau$ production and decay is excluded during the event generation. Samples are produced with $g_U = 1$, for several values of m_U between 1 and $5\,\text{TeV}$. We observe no large dependence, neither of the templates used for signal extraction nor of the overall cross section, on the assumed U_1 decay width Γ, even after variations of factors of 0.5 and 2 and therefore, for each considered value of m_U, we choose Γ to approximately match the value predicted for U_1 production with couplings as obtained from the global fit presented in ref. [72].

We expect a sizeable effect of destructive interference between the U_1 signal and $Z/\gamma^* \to \tau\tau$ production, where the relative sizes of the interference and noninterference contributions depend on g_U. To include this dependence we generate separate samples for

each contribution to form signal templates, which are negative in case of the interference contribution. These are scaled by g_U^4 (for the noninterference contribution) and g_U^2 (for the interference contribution), respectively, and combined to form the overall signal distributions for any value of g_U. Finally, the resulting signal event yields are normalized to the cross sections for the inclusive U_1 mediated $pp \to \tau\tau$ process, computed at LO precision in α_S. The contribution of the U_1 t-channel exchange to the m_T^{tot} distribution in the $\tau_h\tau_h$ final state for $m_U = 1\,\text{TeV}$ and $g_U = 1.5$ for the VLQ BM 1 scenario is shown in figure 7 (right). As visible from the figure, a complex contribution of the signal to the overall $\tau\tau$ event yield in m_T^{tot} is expected, with a reduction for $m_T^{tot} \lesssim 250\,\text{GeV}$ and an enhancement otherwise. Both features may contribute to the signal inference, while the sensitivity of the analysis relies on the yield enhancement for $m_T^{tot} \gtrsim 250\,\text{GeV}$, as will be discussed in more detail in section 8.2. We note that for the ϕ searches presented in this paper interference effects with $\tau\tau$ backgrounds, e.g., from $Z/\gamma^* \to \tau\tau$ production are not an issue due to the different spin configurations of the $\tau\tau$ final states.

6.4.3 Common processing

The PDF4LHC15 [139] (NNPDF3.1 [140]) parton distribution functions (PDFs) are used for the simulation of the $gg\phi$ and $bb\phi$ (U_1) signal processes. For all other processes, the NNPDF3.0 [141] (NNPDF3.1) PDFs are used for the simulation of the data taken in 2016 (2017–2018). The description of the underlying event is parameterized according to the CUETP8M1 [142] and CP5 [143] tunes for the simulation of the data taken in 2016 and 2017–2018, respectively.

Parton showering and hadronization, as well as the τ lepton decays, are modelled using the PYTHIA event generator [144], where versions 8.212 and 8.226 are used for the simulation of the data taken in 2016, and version 8.230 is used for the data taken in 2017–2018. For all simulated events, additional inclusive inelastic pp collisions generated with PYTHIA are added according to the expected PU profile in data. All events generated are passed through a GEANT4-based [145] simulation of the CMS detector and reconstructed using the same version of the CMS event reconstruction software used for the data.

6.5 Corrections to the model

The capability of the model to describe the data is monitored in various control regions orthogonal to the signal and background classes, and corrections and corresponding uncertainties are derived where necessary. All corrections that have been applied to the model are described in the following. Their uncertainties are discussed in section 7.

The following corrections apply equally to simulated and τ-embedded events, where the τ decay is also simulated. Since the simulation part of τ-embedded events happens under detector conditions that are different from the case of fully simulated events, corrections and related uncertainties may differ, as detailed in ref. [110]. Corrections are derived for residual differences in the efficiencies of the selected triggers, differences in the electron and muon tracking efficiencies, and in the efficiencies of the identification and isolation requirements for electrons and muons. These corrections are obtained in bins of p_T and η of the corresponding lepton, using the "tag-and-probe" method, as described in ref. [146],

with $Z/\gamma^* \to ee$ and $Z/\gamma^* \to \mu\mu$ events. They usually do not amount to more than a few percent. The electron energy scale is adjusted to the scale measured in data using the Z boson mass peak in $Z/\gamma^* \to ee$ events.

In a similar way, corrections are obtained for the efficiency of triggering on the τ_h decay signature and for the τ_h identification efficiency. The trigger efficiency corrections are obtained from parametric fits to the trigger efficiency, as a function of p_T, derived for simulated events and data. The identification efficiency corrections are also derived as a function of the p_T of the τ_h candidate. For $p_T^{\tau_h} > 40\,\text{GeV}$, a correction is moreover derived for each τ_h decay mode individually, which is used only in the $\tau_h\tau_h$ final state. For each data-taking year and each τ_h decay mode, corrections to the energy scale of the τ_h candidates and of electrons misidentified as τ_h candidates are derived from likelihood scans of discriminating observables, such as the reconstructed τ_h candidate mass. For muons misidentified as τ_h candidates, the energy scale correction has been checked to be negligible.

Corrections are applied to the magnitude and resolution of $\vec{p}_T^{\,\text{miss}}$ in τ-embedded events to account for rare cases of an incomplete removal of the energy deposits from the muons that are replaced by simulated τ decays during the embedding procedure. These corrections are derived by comparing p_T^{miss} in τ-embedded events with fully simulated events.

The following corrections only apply to fully simulated events. During the 2016 and 2017 data taking, a gradual shift in the timing of the inputs of the ECAL L1 trigger in the region at $|\eta| > 2.0$ caused a specific trigger inefficiency [88]. For events containing an electron (a jet) with p_T larger than $\approx 50\,(\approx 100)\,\text{GeV}$, in the region of $2.5 < |\eta| < 3.0$ the efficiency loss is 10–20%, depending on p_T, η, and time. Corresponding corrections have been derived from data and applied to the simulation, where this effect is not present.

The energies of jets are corrected to the expected response of the jet at the stable hadron level, using corrections measured in bins of the jet p_T and η. These corrections are usually less than 10–15%. Residual data-to-simulation corrections are applied to the simulated event samples. They usually range from subpercent level at high jet p_T in the central part of the detector to a few percent in the forward region. The energy resolution of simulated jets is also adjusted to match the resolution in data. A correction is applied to the direction and magnitude of $\vec{p}_T^{\,\text{miss}}$ based on differences between estimates of the hadronic recoil in $Z/\gamma^* \to \mu\mu$ events in data and simulation. This correction is applied to the simulated $Z/\gamma^* \to \ell\ell$, W+jets, h, and ϕ signal events, where a hadronic recoil against a single particle is well defined. The efficiencies for genuine and misidentified b jets to pass the working points of the b jet identification discriminant, as given in section 5, are determined from data, using $t\bar{t}$ events for genuine b jets and jet-associated Z boson production for jets originating from light-flavour quarks. Data-to-simulation corrections are obtained for these efficiencies and used to correct the number of b jets in the simulation.

Data-to-simulation corrections are further applied to simulated events where an electron (muon) is reconstructed as a τ_h candidate, to account for residual differences in the $e(\mu) \to \tau_h$ misidentification rate between data and simulation. In a similar way, a correction is applied to account for residual differences in the $\mu \to e$ misidentification rate between data and simulation.

The dilepton mass and p_T spectra in simulated $Z/\gamma^* \to \ell\ell$ events are corrected to better match the data. To do this, the dilepton mass and p_T are measured in data and simulation in $\mu\mu$ events, and the simulated events are corrected to match the spectra in data. In addition, all simulated $t\bar{t}$ events are weighted to better match the top quark p_T distribution observed in data [147]. The overall normalization of $t\bar{t}$ events is constrained using the $t\bar{t}$ control region described in section 5.

7 Systematic uncertainties

The uncertainty model used for the analysis comprises theoretical and experimental uncertainties, and uncertainties due to the limited population of template distributions available for the background model. The last group of uncertainties is incorporated for each bin of each corresponding template individually following the approach proposed in refs. [148, 149]. All other uncertainties lead to correlated changes across bins either in the form of normalization changes or as general nontrivial shape-altering variations. Depending on the way they are derived, correlations may also arise across data-taking years, samples, or individual uncertainties.

7.1 Uncertainties related to the τ-embedding method or the simulation

The following uncertainties, related to the reconstruction of electrons, muons, and τ_h candidates after selection, apply to simulated and τ-embedded events. Unless stated otherwise, they are partially correlated across τ-embedded and simulated events.

7.1.1 Uncertainties common to signal and background events

Uncertainties in the identification efficiency of electrons and muons amount to 2%, correlated across all years. Since no significant dependence on the p_T or η of each corresponding lepton is observed, these uncertainties are introduced as normalization uncertainties. A similar reasoning applies to uncertainties in the electron and muon trigger efficiencies, which also amount to 2% each. Because of differences in the online selections they are treated as uncorrelated for single-lepton and dilepton triggers. This may result in shape-altering effects in the overall model, since the two trigger types act on different ranges of lepton p_T.

For fully simulated events, an uncertainty in the electron energy scale is derived from the calibration of ECAL crystals, and applied on an event-by-event basis. For τ-embedded events, uncertainties of 0.5–1.25%, determined separately for the ECAL barrel and endcap regions, are derived for the corrections described in section 6.5. Because of the varying detector conditions, and the different ways the uncertainties are determined, they are treated as uncorrelated across simulated and τ-embedded events. They lead to shape-altering variations and are treated as correlated across data-taking years. The muon momentum is precisely known, and a variation within the expected uncertainties was verified to have no effect on the analysis.

Uncertainties in the τ_h identification efficiency are between 3–9% in bins of τ_h lepton p_T. These are dominated by statistical uncertainties and are, therefore, treated as

uncorrelated across decay modes, p_T bins, and data-taking years. The same is true for the uncertainties in the τ_h energy scale, which amount to 0.2–1.1%, depending on the τ_h lepton p_T and decay mode. For the energy scale of electrons misidentified as τ_h candidates, the uncertainties are 1–6.5%. All τ_h energy scale uncertainties are also treated as uncorrelated across data-taking years as they are predominantly statistical in nature. The uncertainty in the energy scale of muons misidentified as τ_h is 1%. Uncertainties in the τ_h trigger efficiencies are typically $\mathcal{O}(10\%)$, depending on the τ_h lepton p_T. They are obtained from parametric fits to data and simulation, and are treated as uncorrelated across triggers and data-taking years. All uncertainties discussed in this paragraph lead to shape-altering variations.

Four further sources of uncertainty are considered for τ-embedded events. A 4% normalization uncertainty arises from the efficiency of the $\mu\mu$ selection in data, which is unfolded during the τ-embedding procedure. Most of this uncertainty originates from the triggers used for selection. Since the trigger configurations changed over time, this uncertainty is treated as uncorrelated across data-taking years. An additional shape uncertainty is introduced to quantify the consistency of the embedding method in a sample of $\mu\mu$ events. For this purpose, dedicated event samples are produced where the muons selected in data are replaced by simulated muons instead of τ lepton decays. These events are compared with the originally selected $\mu\mu$ events in data and residual differences in the $\mu\mu$ mass and p_T spectra are used as uncertainties. Another shape- and normalization-altering uncertainty in the yield of $t\bar{t} \rightarrow \mu\mu + X$ decays, which are part of the τ-embedded event samples, ranges from subpercent level to 8%, depending on the event composition of the model. For this uncertainty, the number and shape of $t\bar{t}$ events contained in the τ-embedded event samples are estimated from simulation, where the corresponding decay has been selected at the parton level. This estimate is then varied by $\pm 10\%$ to account for the $t\bar{t}$ cross section and acceptance uncertainties. Finally, an uncertainty in the p_T^{miss} correction for the τ-embedded events described in section 6.5 is applied. Since this correction is derived from a comparison with fully simulated events, this uncertainty is related to the imperfect $\vec{p}_T^{miss}$ reconstruction in the simulation.

For fully simulated events, the following additional uncertainties arise. Uncertainties in the $e(\mu) \rightarrow \tau_h$ misidentification rate are 18–40% for electrons and 7–65% for muons, depending on the η of the τ_h candidate. These uncertainties apply only to simulated $Z/\gamma^* \rightarrow ee$ and $Z/\gamma^* \rightarrow \mu\mu$ events, which are of marginal importance for the analysis. The same is true for the uncertainty in the reweighting in the $Z/\gamma^* \rightarrow \ell\ell$ dilepton mass and p_T, discussed in section 6.5, which is typically smaller than 1%. A normalization uncertainty due to the timing shift of the inputs of the ECAL L1 trigger described in section 6.5 amounts to 2–3%.

Uncertainties in the energy calibration and resolution of jets are applied with different correlations depending on their sources, which arise from the statistical limitations of the measurements used for calibration, the time-dependence of the energy measurements in data due to detector ageing, and bias corrections introduced to cover residual differences between simulation and data. They range from subpercent level to $\mathcal{O}(10\%)$, depending on the kinematic properties of the jets in the event. Similar uncertainties, with similar

ranges, are applied for the identification rates for b jets and for the misidentification rates for light-flavour quark or gluon jets.

Depending on the process under consideration, two independent uncertainties in $p_\mathrm{T}^\mathrm{miss}$ are applied. For processes that are subject to recoil corrections, i.e. $\mathrm{Z}/\gamma^* \to \ell\ell$, $\mathrm{W}+\mathrm{jets}$, h, or ϕ production, uncertainties in the calibration and resolution of the hadronic recoil are applied; they typically result in changes to the event yields ranging from 0–5%. For all other processes, an uncertainty in $\vec{p}_\mathrm{T}^\mathrm{miss}$ is derived from the amount of energy carried by unclustered particle candidates, which are not contained in jets, in the event [103]. This uncertainty typically results in changes to the event yields ranging from 0–10%.

The integrated luminosities of the 2016, 2017, and 2018 data-taking periods are individually known with uncertainties in the 1.2–2.5% range [150–152], while the total integrated luminosity for the years 2016–2018 has an uncertainty of 1.6%; the improvement in precision reflects the (uncorrelated) time evolution of some systematic effects. Uncertainties in the predictions of the normalizations of all simulated processes amount to 4% for $\mathrm{Z}/\gamma^* \to \ell\ell$ and $\mathrm{W}+\mathrm{jets}$ production [123], 6% for $\mathrm{t\bar{t}}$ production [124, 125], and 5% for diboson and single t quark production [125–127], where used in the analyses. These uncertainties are correlated across data-taking years. A shape-altering uncertainty is derived in the reweighting of the top quark p_T described in section 6.5 by applying the correction twice or not applying it at all. This uncertainty has only a very small effect on the final discriminant.

7.1.2 Uncertainties in the signal modelling

Theoretical uncertainties in the acceptance of $\mathrm{bb}\phi$ signal events are obtained from variations of the renormalization (μ_R) and factorization (μ_F) scales, the h_damp factor, and the PDFs. The scale uncertainty is obtained from the envelope of the six variations of μ_R and μ_F by factors of 0.5 and 2, omitting the variations where one scale is multiplied by 2 and the corresponding other scale by 0.5, as recommended in ref. [153]. The scale h_damp is varied by factors of $1/\sqrt{2}$ and $\sqrt{2}$. The uncertainty from the variation of μ_R and μ_F, and the uncertainty from the variation of h_damp are added linearly, following the recommendation in ref. [153], resulting in an overall uncertainty that ranges from 1–8% (1–5%) for the b tag ("no b tag") categories depending on the tested mass. The uncertainties due to PDF variations and the uncertainty in α_S are obtained following the PDF4LHC recommendations, taking the root mean square of the variation of the results when using different replicas of the default PDF4LHC sets as described, e.g., in ref. [139]. They range from 1–2%.

Uncertainties in the acceptance of the $\mathrm{gg}\phi$ process are also obtained from variations of μ_R, μ_F, and h_damp. The μ_R and μ_F scales are varied as described above for the $\mathrm{bb}\phi$ process, whereas the h_damp scale is varied by factors of 0.5 and 2 as suggested in ref. [135]. The influence of the former (latter) variation on the signal acceptance amounts to 20% (35%) for the smallest m_ϕ values. For larger m_ϕ values, the variation is at the subpercent level. In both cases the uncertainties also result in shape-altering effects in the overall model.

For the parameter scan in the MSSM interpretations, theoretical uncertainties in the $\mathrm{gg}\phi$ and $\mathrm{bb}\phi$ cross sections are included, as described in ref. [86]. This includes uncertainties in the μ_R and μ_F scales, PDFs, and α_S. The uncertainties are evaluated separately

for each m_A-$\tan\beta$ point under consideration. They are typically 5–20% (10–25%) for $gg\phi$ ($bb\phi$) production.

Several sources of theoretical uncertainty in the U_1 signal prediction are included. The uncertainty due to the μ_R and μ_F scale variations is about 15%. The uncertainties due to the PDFs and α_S variations are about 15 and 4%, respectively. The Q_{match} and parton shower uncertainties affect the signal acceptances in the "b tag" categories, with magnitudes of about 11 and 1% respectively, and in the "no b tag" categories, with magnitudes of 5 and 6% respectively. The uncertainty in the $\beta_L^{s\tau}$ parameter is estimated by varying the coupling strength by the uncertainties obtained in the fit presented in ref. [72] and summarized in table 1. The resulting uncertainty varies the signal yields by 4–12%. The uncertainty in the signal acceptance due to the choice of flavour scheme is estimated by comparing the predictions in the 4FS and 5FS calculations, which mainly affect the $N_{b\text{-jets}}$ distribution. The resulting uncertainty has a magnitude of 25% (18%) for the "b tag" ("no b tag") categories.

For all results shown in the following, the expectation for SM Higgs boson production is included in the model used for the statistical inference of the signal. Uncertainties due to different choices of μ_R and μ_F for the calculation of the production cross section of the SM Higgs boson amount to 3.9% for ggh, 0.4% for VBF, 2.8% for Zh, and 0.5% for Wh production [128–130, 154, 155]; uncertainties due to different choices for the PDFs and α_S amount to 3.2%, 2.1%, 1.6%, and 1.9% for these four production modes, respectively.

7.2 Uncertainties related to jets misidentified as an electron, muon, or τ_h candidate

For the F_F method, the following uncertainties apply. The F_F^i and their corrections are subject to statistical fluctuations in each corresponding DR^i and simulation. The corresponding uncertainties are split into a normalization and a shape-altering part and propagated into the final discriminant. They are typically 1–10% and are treated as uncorrelated across the kinematic and topological bins where they are derived. An additional uncertainty is defined by varying the choice of the functional form for the parametric fits.

Uncertainties are also applied to cover residual corrections and extrapolation factors, varying from a few percent to $\mathcal{O}(10\%)$, depending on the kinematic properties of the τ_h candidate and the topology of the event. These are both normalization and shape-altering uncertainties.

An additional source of uncertainty concerns the subtraction of processes other than the enriched process in each corresponding DR^i. These are subtracted from the data using simulated or τ-embedded events. The combined shape of the events to be removed is varied by 10%, and the measurements are repeated. The impacts of these variations are then propagated to the final discriminant as shape-altering uncertainties.

An uncertainty in the estimation of the three main background fractions in the AR is estimated from a variation of each individual contribution by 10%, increasing or decreasing the remaining fractions such that the sum of all contributions remains unchanged. The amount of variation is motivated by the uncertainty in the production cross sections and acceptances of the involved processes and the constraint on the process composition that

Uncertainty		Variation	Correlated across years
τ-emb.	Acceptance	4%	
	μμ closure	See text	✓
	t$\bar{\text{t}}$ fraction	0.1–8%	—
	p_T^{miss}	See text	—
μ	Identification	2%	✓
	Trigger	2%	—
e	Identification	2%	✓
	Trigger	2%	—
	Energy scale	See text	✓
τ_h	Identification	3–8%	—
	Trigger	5–10%	—
	Energy scale	0.2–1.1%	—
$\mu \to \tau_h$	Misidentification	7–67%	—
	Energy scale	1%	—
$e \to \tau_h$	Misidentification	18–41%	—
	Energy scale	1–6.5%	—
Jet → e misidentification		10%	✓
Jet → μ misidentification		10%	✓
μ → e misidentification		15–45%	—
Z/γ^* mass and p_T reweighting		<1%	
Jet energy scale & resolution		0.1–10%	✓
b-jet (mis)identification		1–10%	—
p_T^{miss} calibration		See text	✓
ECAL timing shift		2–3%	✓
t quark p_T reweighting		See text	✓
Integrated luminosity		1.2–2.5%	✓
Background cross sections		2–5%	✓
Signal theoretical uncertainties		See text	✓
F_F	Event count	$\mathcal{O}(1\text{–}10\%)$	—
	Corrections	$\mathcal{O}(10\%)$	—
	Non-F_F processes	10%	—
	F_F proc. composition	10%	—
QCD (eμ)	Event count	2–4%	—
	AR to SR extrapolations	$\mathcal{O}(10\%)$	—

Table 6. Summary of systematic uncertainties discussed in the text. The columns indicate the source of uncertainty, the variation, and how it is correlated between data-taking years. A checkmark is given also for partial correlations. More details are given in the text.

can be clearly obtained from the AR. The effect of this variation is found to be very small, since usually one of the contributions dominates the event composition in the AR.

Since the background from QCD multijet events in the eμ final state is also determined from a DR, uncertainties that account for the statistical uncertainty in the data and the subtracted backgrounds in this DR are applied in a similar way. These uncertainties amount to 2–4%. In addition, this background is subject to uncertainties related to the extrapolations from the DR to the corresponding SRs. These uncertainties are $\mathcal{O}(10\%)$ depending on $p_{\mathrm{T}}^{\mathrm{e}}$, p_{T}^{μ}, and $N_{\mathrm{b\text{-}jets}}$. Because of their mostly statistical nature, all uncertainties related to the F_{F} and SS methods are treated as uncorrelated across data-taking years.

In the eμ final state, the subdominant contribution to the jet $\to \ell$ and $\mu \to$ e backgrounds is estimated from simulation. Uncertainties in the simulated jet $\to$ e and jet $\to \mu$ misidentification rates are 10 and 12%, respectively. They are treated as correlated across data-taking years. The uncertainty in the $\mu \to$ e misidentification rate is 15–45%, and is treated as uncorrelated across data-taking years since it is mostly statistical in nature. A summary of all systematic uncertainties that have been discussed in this section is given in table 6, in which we also state the correlations between the data-taking years.

8 Results

The statistical model used to infer the signal from the data is defined by an extended binned likelihood of the form

$$\mathcal{L}\left(\{k_i\}, \{\mu_s\}, \{\theta_j\}\right) = \prod_i \mathcal{P}\Big(k_i | \sum_s \mu_s S_{si}(\{\theta_j\}) + \sum_b B_{bi}(\{\theta_j\})\Big) \prod_j \mathcal{C}(\widetilde{\theta}_j | \theta_j), \qquad (8.1)$$

where i labels the bins of the discriminating distributions of all categories, split by $\tau\tau$ final state and data-taking year. The function $\mathcal{P}(k_i | \sum \mu_s S_{si}(\{\theta_j\}) + \sum B_{bi}(\{\theta_j\}))$ corresponds to the Poisson probability to observe k_i events in bin i for a prediction of $\sum \mu_s S_{si}$ signal and $\sum B_{bi}$ background events. The predictions for S_{si} and B_{bi} are obtained from the signal and background models discussed in section 6. The parameters μ_s act as linear scaling parameters of the corresponding signal yields S_s. Systematic uncertainties are incorporated in the form of penalty terms for additional nuisance parameters $\{\theta_j\}$ in the likelihood, appearing as a product with predefined probability density functions $\mathcal{C}(\widetilde{\theta}_j | \theta_j)$, where $\widetilde{\theta}_j$ corresponds to the nominal value for θ_j. The predefined uncertainties in the $\widetilde{\theta}_j$, as discussed in section 7, may be constrained by the fit to the data.

The test statistic used for the inference of the signal is the profile likelihood ratio, as discussed in refs. [156, 157]:

$$q_{\mu_s} = -2\ln\left(\frac{\mathcal{L}(\{k_i\} | \sum_s \mu_s S_{si}(\{\hat{\theta}_{j,\mu_s}\}) + \sum_b B_{bi}(\{\hat{\theta}_{j,\mu_s}\}))}{\mathcal{L}(\{k_i\} | \sum_s \hat{\mu}_s S_{si}(\{\hat{\theta}_{j,\hat{\mu}_s}\}) + \sum_b B_{bi}(\{\hat{\theta}_{j,\hat{\mu}_s}\}))}\right), \quad 0 \le \hat{\mu}_s \le \mu_s, \qquad (8.2)$$

where one or more parameters μ_s are the parameters of interest (POIs) and $\hat{\mu}_s$, $\hat{\theta}_{j,\mu_s}$, and $\hat{\theta}_{j,\hat{\mu}_s}$ are the values of the given parameters that maximize the corresponding likelihood. The index of q_{μ_s} indicates that the test statistic is evaluated for a fixed value of μ_s. In the large number limit, the sampling distribution of q_{μ_s} can be approximated by analytic functions, from which the expected median and central intervals can be obtained as described in ref. [158]. The signal is inferred from the data in three different ways:

i) the model-independent ϕ search features a signal model for a single narrow resonance ϕ;

ii) for the search for vector leptoquarks, the data are interpreted in terms of the non-resonant U_1 t-channel exchange;

iii) the interpretation of the data in terms of MSSM benchmark scenarios relies on three resonances in the $\tau\tau$ mass spectrum with mass values and rates determined by the parameters of the corresponding scenario.

In all cases the $t\bar{t}$ control region, as defined in section 5 and shown in figures 5–6 is used to constrain the normalization of $t\bar{t}$ events and all $t\bar{t}$ related uncertainties. Detailed descriptions of the specific statistical procedures and the results obtained in each case are given in the following sections.

8.1 Model-independent ϕ search

For the model-independent ϕ search, we investigate $gg\phi$ and $bb\phi$ production corresponding to two independent POIs $\mu_{gg\phi}$ and $\mu_{bb\phi}$ in the likelihood of eq. (8.1). In the model, H(125) is treated as background assuming the production cross sections and branching fraction for the decay into τ leptons as expected from the SM. For $m_\phi \geq 250\,\text{GeV}$, the signal extraction is based on binned template distributions of m_T^{tot} in the 17 categories per data-taking year shown in figure 5, resulting in a total of 51 input distributions for signal extraction. For $60 \leq m_\phi < 250\,\text{GeV}$, binned template distributions of $m_{\tau\tau}$ are used in the 26 categories shown in figure 6, resulting in 78 input distributions for signal extraction. A few examples of these input distributions in a subset of the most sensitive categories per final state are shown in figures 8 and 9. In each figure the expected background distributions are represented by the stack of filled histograms in the upper panel of each subfigure, where each filled histogram corresponds to a process as discussed in section 6. The grey shaded band associated with the sum of filled histograms corresponds to the combination of all uncertainties discussed in section 7, including all correlations as obtained from the fit of the background model to the data. The lower panel of each subfigure shows the ratio of the data points to the expectation from the background model in each bin. The statistical uncertainty in the data is represented by the error bars and the uncertainty in the sum of all background processes, after the fit to the data, by the shaded band. The expected m_T^{tot} ($m_{\tau\tau}$) distributions for a $gg\phi$ or $bb\phi$ signal with $m_\phi = 1200\,(100)\,\text{GeV}$ are also shown.

Figure 10 shows the expected and observed 95% confidence level (CL) upper limits on the product of the cross sections and branching fraction for the decay into τ leptons for $gg\phi$ and $bb\phi$ production in a mass range of $60 \leq m_\phi \leq 3500\,\text{GeV}$. These limits have been obtained following the modified frequentist approach described in refs. [159, 160]. When setting the limit in one production mode the POI of the other production mode is profiled. The limits are shown with a separation into the low-mass ($m_\phi < 250\,\text{GeV}$) and high-mass ($m_\phi \geq 250\,\text{GeV}$) regions of the search.

The expected limits in the absence of a signal span four orders of magnitude between $\approx 10\,\text{pb}$ (at $m_\phi = 60\,\text{GeV}$) and $\approx 0.3\,\text{fb}$ (at $m_\phi = 3.5\,\text{TeV}$) for both production modes, with a
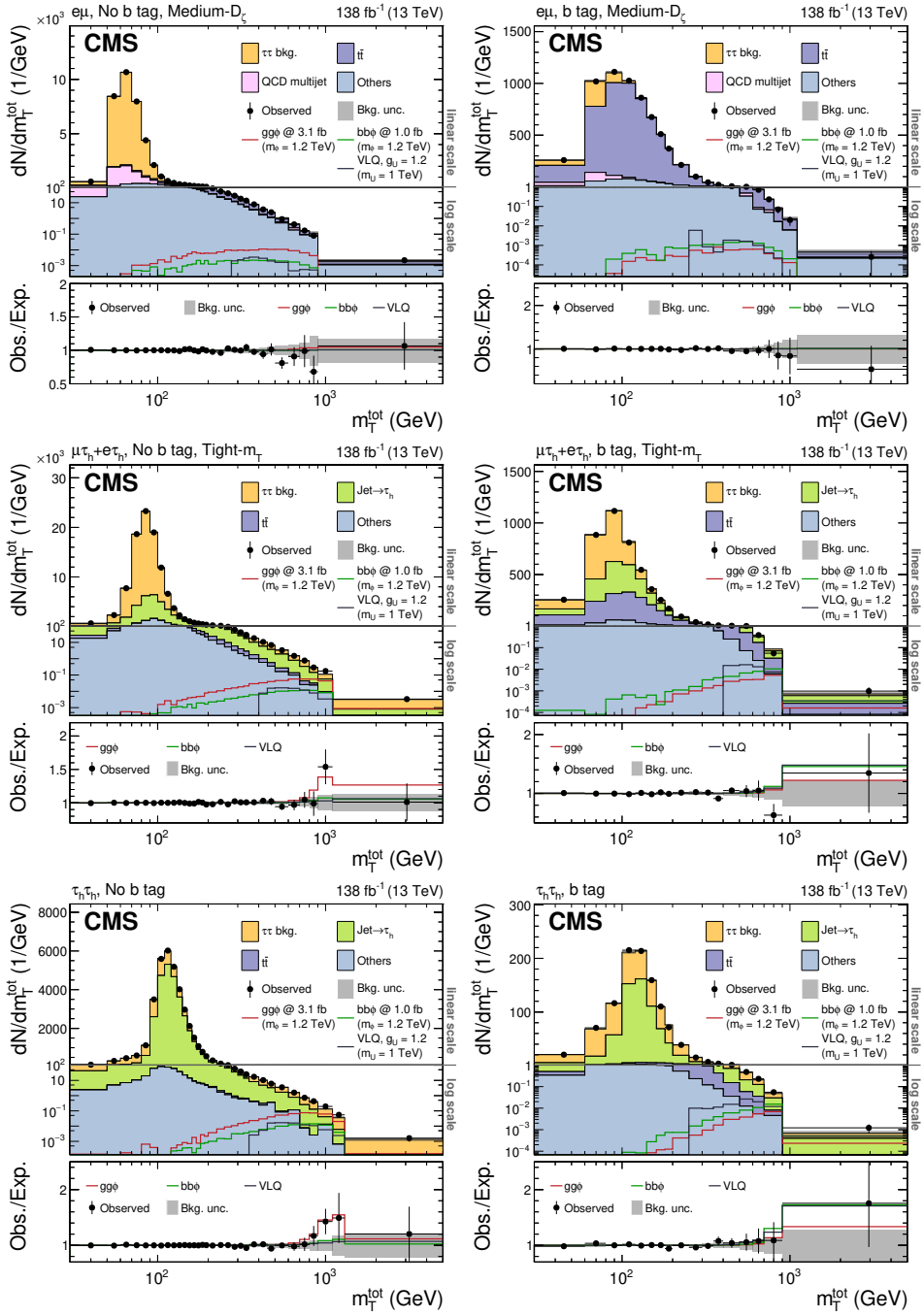
Figure 8. Distributions of m_T^{tot} in the global (left) "no b tag" and (right) "b tag" categories in the (upper) $e\mu$, (middle) $e\tau_h$ and $\mu\tau_h$, and (lower) $\tau_h\tau_h$ final states. For the $e\mu$ final state, the medium-D_ζ category is displayed; for the $e\tau_h$ and $\mu\tau_h$ final states the tight-m_T categories are shown. The solid histograms show the stacked background predictions after a background-only fit to the data. The best fit $gg\phi$ signal for $m_\phi = 1.2\,\text{TeV}$ is shown by the red line. The $bb\phi$ and U_1 signals are also shown for illustrative purposes. For all histograms, the bin contents show the event yields divided by the bin widths. The lower panel shows the ratio of the data to the background expectation after the background-only fit to the data.
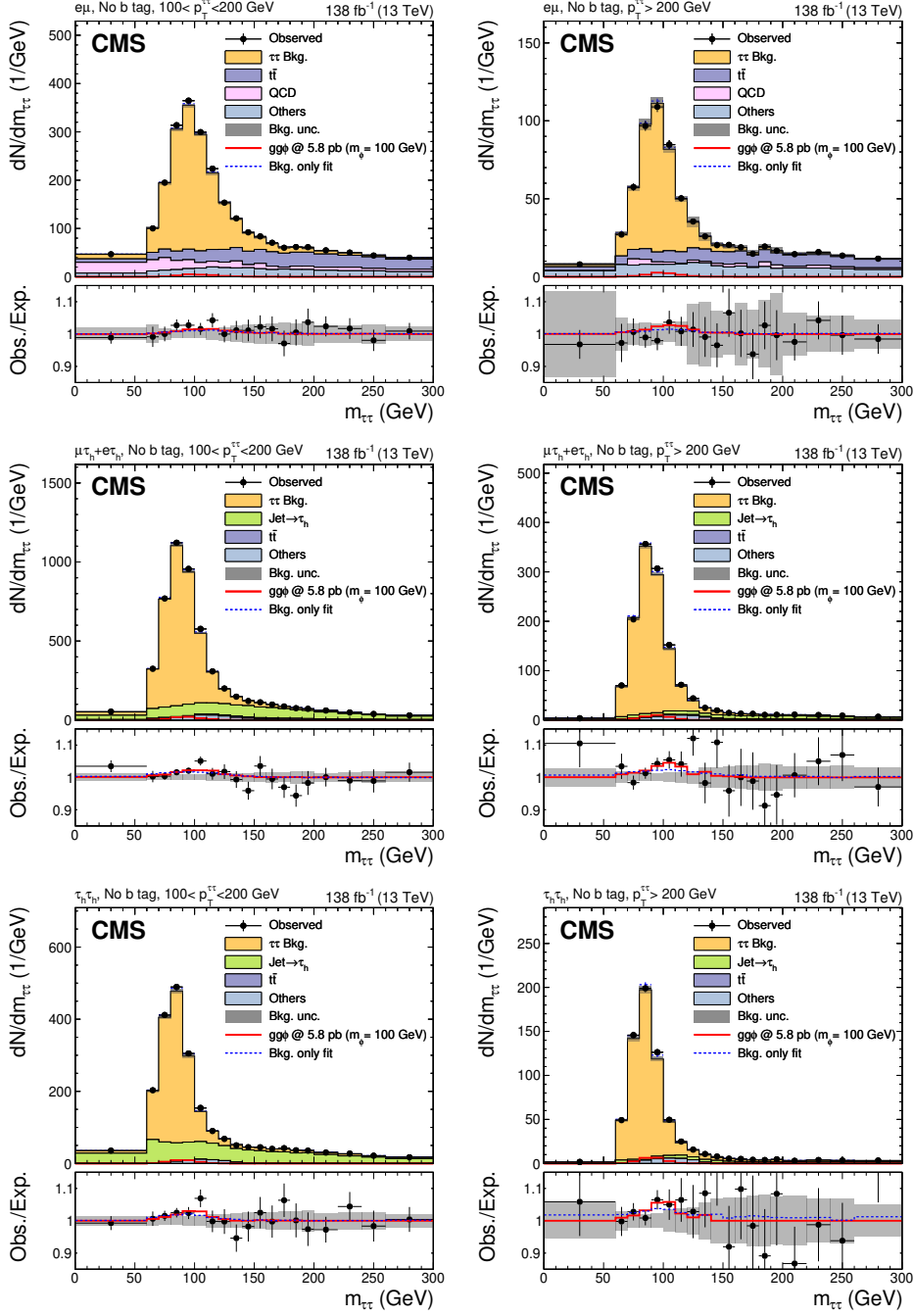
Figure 9. Distributions of $m_{\tau\tau}$ in the (left) $100 < p_T^{\tau\tau} < 200\,\mathrm{GeV}$ and (right) $p_T^{\tau\tau} > 200\,\mathrm{GeV}$ "no b tag" categories for the (upper) $e\mu$, (middle) $e\tau_h$ and $\mu\tau_h$, and (lower) $\tau_h\tau_h$ final states. The solid histograms show the stacked background predictions after a signal-plus-background fit to the data for $m_\phi = 100\,\mathrm{GeV}$. The best fit $gg\phi$ signal is shown by the red line. The total background prediction as estimated from a background-only fit to the data is shown by the dashed blue line for comparison. For all histograms, the bin contents show the event yields divided by the bin widths. The lower panel shows the ratio of the data to the background expectation after the signal-plus-background fit to the data. The signal-plus-background and background-only fit predictions are shown by the solid red and dashed blue lines, respectively, which are also shown relative to the background expectation obtained from the signal-plus-background fit to the data.
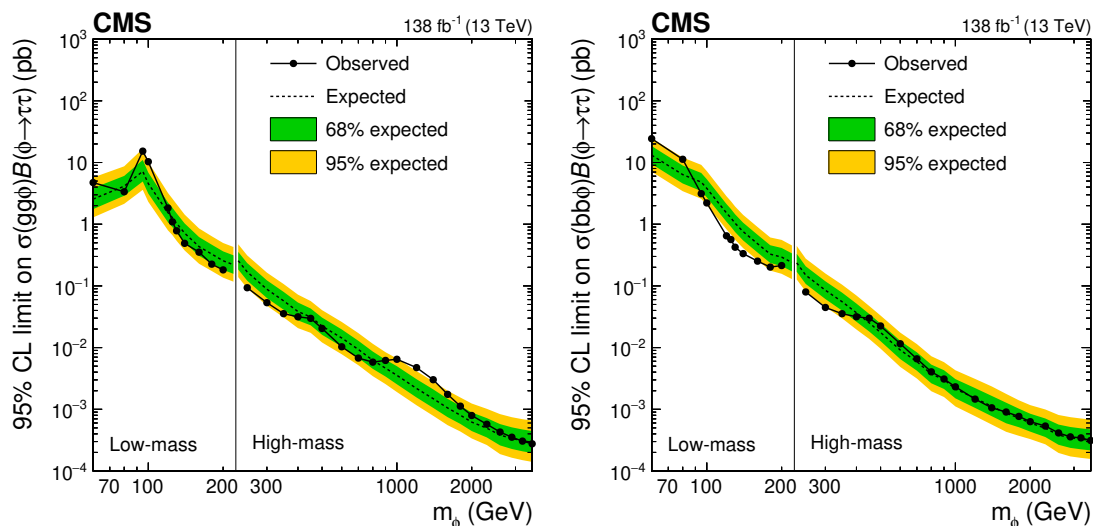
Figure 10. Expected and observed 95% CL upper limits on the product of the cross sections and branching fraction for the decay into τ leptons for (left) ggφ and (right) bbφ production in a mass range of $60 \leq m_\phi \leq 3500\,\mathrm{GeV}$, in addition to H(125). The expected median of the exclusion limit in the absence of signal is shown by the dashed line. The dark green and bright yellow bands indicate the central 68% and 95% intervals for the expected exclusion limit. The black dots correspond to the observed limits. The peak in the expected ggφ limit emerges from the loss of sensitivity around 90 GeV due to the background from $\mathrm{Z}/\gamma^* \to \tau\tau$ events.

falling slope for increasing values of m_ϕ. In general, the observation falls within the central 95% interval of the expectation. For the low-mass search, the largest deviation from the expectation is observed for ggφ production at $m_\phi = 100\,\mathrm{GeV}$ with a local (global) p-value equivalent to 3.1 (2.7) standard deviations (s.d.). To turn the local into a global p-value, a number N_{trial} of pseudo-data from the input distributions of the background model to the maximum likelihood fit is created. For each mass hypothesis in consideration, a fit of the signal model to these pseudo-data is performed and the fraction of cases, where the outcome of these fits with the maximal significance exceeds the observed significance, with respect to N_{trial} is determined. Finally, the local p-value is reduced by this fraction. The best fit value of the product of the cross section with the branching fraction for the decay into τ leptons is $\sigma_{\mathrm{gg}\phi}\mathcal{B}(\phi \to \tau\tau) = (5.8 \pm^{2.5}_{2.0})\,\mathrm{pb}$. The excess at $m_\phi = 100\,\mathrm{GeV}$ exhibits a p-value of 50% (58%) for the compatibility across ττ final states (data-taking years). Within the resolution of $m_{\tau\tau}$ this coincides with a similar excess observed in a previous search for low-mass resonances by the CMS Collaboration in the γγ final state, where the smallest local p-value corresponds to a significance of 2.8 s.d. for a mass of 95.3 GeV [161]. The local (global) significance for the ττ search evaluated at $m_\phi = 95\,\mathrm{GeV}$ is 2.6 (2.3) s.d. and the best fit value of the product of the cross section with the branching fraction for the decay into τ leptons is $\sigma_{\mathrm{gg}\phi}\mathcal{B}(\phi \to \tau\tau) = (7.8 \pm^{3.9}_{3.1})\,\mathrm{pb}$. For the high-mass search, the largest deviation from the expectation is observed for ggφ production at $m_\phi = 1.2\,\mathrm{TeV}$ with a local (global) p-value equivalent to 2.8 (2.2) s.d., where the best fit value of the product of the cross section with the branching fraction for the decay into τ leptons is
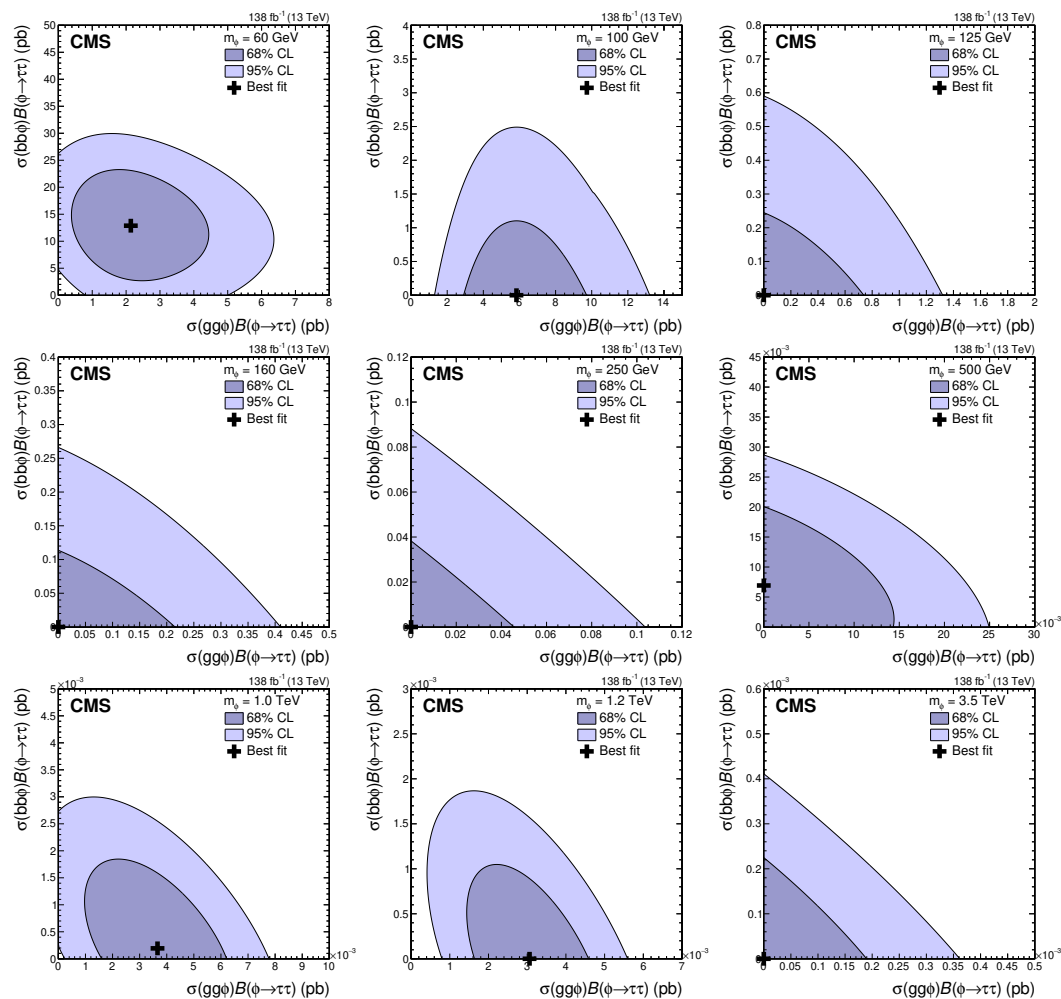
Figure 11. Maximum likelihood estimates, and 68% and 95% CL contours obtained from scans of the signal likelihood for the model-independent ϕ search. The scans are shown for selected values of m_ϕ between 60 GeV and 3.5 TeV. In each figure the SM expectation is $(0,0)$.

$\sigma_{\mathrm{gg}\phi}\mathcal{B}(\phi \to \tau\tau) = (3.1 \pm {}^{1.0}_{1.1})\,\mathrm{fb}$. The excess at $m_\phi = 1.2\,\mathrm{TeV}$ exhibits a p-value of 11% (63%) for the compatibility across $\tau\tau$ final states (data-taking years). For bbϕ production, no deviation from the expectation beyond the level of 2 s.d. is observed. Figure 11 shows the same results in the form of maximum likelihood estimates with 68% and 95% CL contours obtained from scans of the signal likelihood along the ggϕ and bbϕ cross sections, for selected values of m_ϕ between 60 GeV and 3.5 TeV.

8.2 Search for vector leptoquarks

The inputs for the search for vector leptoquarks are the binned template distributions of $m_{\mathrm{T}}^{\mathrm{tot}}$ in the categories shown in figure 5 resulting in 51 input distributions for signal extraction, for the years 2016–2018. Based on these inputs a signal is searched for in the range of $1 < m_{\mathrm{U}} < 5\,\mathrm{TeV}$.
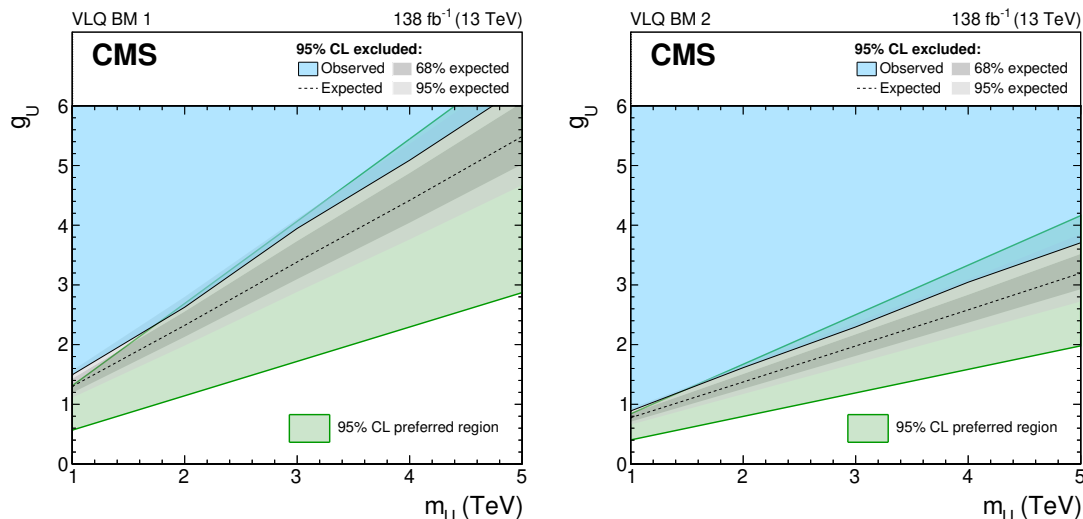
Figure 12. Expected and observed 95% CL upper limits on g_U in the VLQ BM (left) 1 and (right) 2 scenarios, in a mass range of $1 < m_U < 5\,\mathrm{TeV}$. The expected median of the exclusion limit in the absence of signal is shown by the dashed line. The dark and bright grey bands indicate the central 68% and 95% intervals of the expected exclusion limit. The observed excluded parameter space is indicated by the coloured blue area. For both scenarios, the 95% confidence interval for the preferred region from the global fit presented in ref. [72] is also shown by the green shaded area.

Due to the destructive interference with the $\mathrm{Z}/\gamma^* \to \tau\tau$ process discussed in section 6.4, depending on $m_\mathrm{T}^\mathrm{tot}$, a signal from U_1 t-channel exchange may result in an enhancement or a reduction of the yields as expected from the SM. A typical example of this effect for a signal with $m_U = 1\,\mathrm{TeV}$, $g_U = 1.5$, for the VLQ BM 1 scenario is shown in figure 7 (right). There, a reduction in yield (with respect to the SM) is expected for $m_\mathrm{T}^\mathrm{tot} \lesssim 250\,\mathrm{GeV}$ and an enhancement for $250 \lesssim m_\mathrm{T}^\mathrm{tot} \lesssim 1000\,\mathrm{GeV}$. In principle both effects contribute to the sensitivity of the analysis to the signal. However, the region of $m_\mathrm{T}^\mathrm{tot} \lesssim 250\,\mathrm{GeV}$, which features the deficit, suffers from large backgrounds, reducing the contribution of this effect to the overall sensitivity. Studies confirm that the sensitivity of the analysis to the signal is driven by the high $m_\mathrm{T}^\mathrm{tot}$ region, which consistently features an enhancement of the yields expected from the SM. Since the interference reduces this enhancement it also reduces the sensitivity of the analysis, compared to a signal without interference.

No statistically significant signal is observed and 95% CL upper limits on g_U are derived for the VLQ BM 1 and 2 scenarios, as shown in figure 12, again following the modified frequentist approach as for the previously discussed search. The expected sensitivity of the analysis drops for increasing values of m_U following a linear progression with values from $g_U = 1.3\,(0.8)$ to $5.6\,(3.2)$ for the VLQ BM 1 (2) scenario. The observed limits fall within the central 95% intervals for the expected limits in the absence of signal. The expected limits are also within the 95% confidence interval of the best fit results reported by ref. [72], indicating that the search is sensitive to a portion of the parameter space that can explain the b physics anomalies.

	Signal processes	
Categories	ggh, bbh, VBF, Vh	ggH/ggA, bbH/bbA
No b tag $m_{\tau\tau} < 250\,\text{GeV}$	✓	✓
No b tag $m_{\tau\tau} > 250\,\text{GeV}$	—	✓
b tag	✓	✓
Control regions	✓	—

Table 7. Contribution of MSSM signals to the $m_{\text{T}}^{\text{tot}}$ and NN output function template distributions used for signal extraction for the interpretation of the data in MSSM benchmark scenarios.

8.3   MSSM interpretation of the data

For the interpretation of the data in MSSM benchmark scenarios, the signal is based on the binned distributions of $m_{\text{T}}^{\text{tot}}$ in the categories shown in figure 5, complemented by distributions of the NN output function used for the stage-0 simplified template cross section measurement of ref. [109], as discussed in section 5.2, resulting in 129 input distributions for signal extraction.

In the MSSM, the signal constitutes a multiresonance structure with contributions from h, H, and A bosons. For the scenarios chosen for this paper h is associated with H(125). Any MSSM prediction has to match the observed properties of H(125), in particular its mass, cross sections for various production modes, and branching fraction for the decay into τ leptons. For the benchmark scenarios summarized in ref. [86], all model parameters have been chosen such that m_{h} is compatible with the observed H(125) mass of 125.38 GeV [8], within an uncertainty of $\pm 3\,\text{GeV}$ in most of the provided parameter space. The uncertainty of $\pm 3\,\text{GeV}$ in the prediction of m_{h} is supposed to reflect the unknown effect of higher-order corrections, as discussed in ref. [162]. The value of m_{h} is allowed to vary within these boundaries, according to a flat distribution. For the interpretation this is taken into account by simulating the h signal at the observed H(125) mass. For h production, the modes via ggh, b associated production (bbh), VBF, and Vh production are included, and all cross sections and the branching fraction for the decay into τ leptons are scaled according to the MSSM predictions. To remove any dependencies of these predictions on the exact value of m_{h}, they are scaled to the expectation for $m_{\text{h}} = 125.38\,\text{GeV}$, following the prescription of ref. [86]. For A and H production, gluon fusion (ggA, ggH) and b associated production (bbA, bbH) are included.

All kinematic distributions are modelled within the accuracies discussed in section 6.4. In particular, the H (A) boson p_{T} spectra in ggH (ggA) production are modelled as a function of $\tan\beta$ for each tested value of m_{A}, resulting in a softer progression for increasing values of $\tan\beta$. In the "no b tag" categories for $m_{\tau\tau} > 250\,\text{GeV}$ the h signal is expected to be negligible so it is dropped from the signal templates. A summary of the association of signals to the templates used for signal extraction is given in table 7. To interpolate the simulated mass points to the exact predicted values of m_{H}, a linear template morphing algorithm, as described in ref. [163], is used.

The m_{A}-$\tan\beta$ plane is scanned and for each tested point in (m_{A}, $\tan\beta$), the CL_{s} [160] value is calculated. Those points where CL_{s} falls below 5% define the 95% CL exclusion

contour for the benchmark scenario under consideration. The underlying test compares the MSSM hypothesis, with signal contributions for h (S_{h}), H (S_{H}), and A (S_{A}), with the SM hypothesis (S_{SM}), with only one signal contribution related to H(125). The test versus the SM hypothesis is justified by the properties of H(125) being in agreement with the SM expectation within the experimental accuracy of current measurements. For the hypothesis test the likelihood of eq. (8.1) is expressed in the form

$$\mathcal{L}\left(\{k_i\},\mu\right) = \prod_i \mathcal{P}\Big(k_i|\mu\big((S_{\mathrm{h}} - S_{\mathrm{SM}}) + S_{\mathrm{H}} + S_{\mathrm{A}}\big) + S_{\mathrm{SM}} + \sum_b B_b\Big), \qquad (8.3)$$

where for brevity the dependence on the nuisance parameters $\{\theta_j\}$ has been omitted. Equation (8.3) represents a nested likelihood model from which the MSSM hypothesis (with $\mu = 1$) evolves through continuous transformation from the SM hypothesis (with $\mu = 0$). We note that the only physically meaningful hypotheses in eq. (8.3) correspond to $\mu = 0$ and 1. On the other hand, in the large number limit this construction allows the application of the asymptotic formulas given in ref. [158], as analytic estimates of the sampling distributions for the MSSM and SM hypotheses, when using the profile likelihood ratio given in eq. (8.2) as the test statistic. We have verified the validity of the large number limit for masses of $m_{\mathrm{A}} > 1\,\mathrm{TeV}$ with the help of ensemble tests. Since we are using the same template distributions for S_{SM} and S_{h} the transition from $\mu = 0$ to 1 corresponds to a normalization change of the signal contribution related to H(125), only.

Figure 13 shows the exclusion contours in the m_{A}-$\tan\beta$ plane for two representative benchmark scenarios of the MSSM, M_{h}^{125} [83] and $M_{\mathrm{h,EFT}}^{125}$ [85]. The red hatched areas indicate the regions where the compatibility of m_{h} with the observed H(125) mass could not be achieved within the previously discussed $\pm 3\,\mathrm{GeV}$ boundary. For low values of $\tan\beta$, higher scales for the additional SUSY particle masses (referred to collectively as "m_{SUSY}") are required to accommodate a mass of $m_{\mathrm{h}} \approx 125\,\mathrm{GeV}$. In the M_{h}^{125} scenario, where m_{SUSY} is fixed, the prediction of m_{h} falls below $122\,\mathrm{GeV}$. In the $M_{\mathrm{h,EFT}}^{125}$ scenario, m_{SUSY} is adjusted to values that meet the required prediction for m_{h} in each point in (m_{A}, $\tan\beta$) individually. The growing logarithmic corrections associated with the large values of m_{SUSY} are resummed using an effective field theory approach. The $M_{\mathrm{h,EFT}}^{125}$ scenario can thus be viewed as a continuation of the M_{h}^{125} scenario for $\tan\beta \lesssim 10$. In this case the red hatched area at very low values of m_{A} in figure 13 (right) indicates the parameter space where the values required for m_{SUSY} exceed the GUT scale. For both scenarios the Higgs boson masses, mixing angle α, and effective Yukawa couplings have been calculated with the code FEYNHIGGS [164–171]. Branching fractions for the decay into τ leptons and other final states have been obtained from a combination of the codes FEYNHIGGS (and HDECAY [172, 173]) for the $M_{\mathrm{h,EFT}}^{125}$ (M_{h}^{125}) scenario, as described in ref. [86] following the prescriptions given in refs. [153, 174, 175].

Inclusive cross sections for the production via ggϕ have been calculated using the program SUSHI 1.7.0 [176, 177], including NLO corrections in α_{S} for the t- and b-quark contributions to the cross section [178, 179], NNLO corrections in α_{S} in the heavy t quark limit, for the t quark contribution [180–184], and next-to-NNLO contributions in α_{S} for h production [185–187]. Electroweak corrections mediated by light-flavour quarks are in-
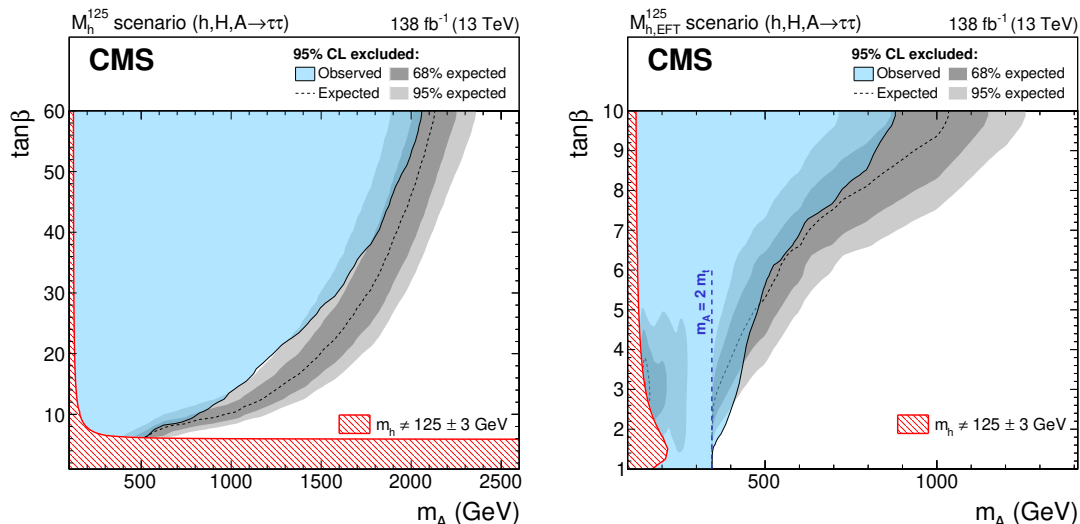
Figure 13. Expected and observed 95% CL exclusion contours in the MSSM (left) $M_{\rm h}^{125}$ and (right) $M_{\rm h,EFT}^{125}$ scenarios. The expected median in the absence of a signal is shown as a dashed black line. The dark and bright grey bands indicate the central 68% and 95% intervals of the expected exclusion. The observed exclusion contour is indicated by the coloured blue area. For both scenarios, those parts of the parameter space where $m_{\rm h}$ deviates by more then $\pm 3\,\text{GeV}$ from the mass of H(125) are indicated by a red hatched area. For the $M_{\rm h,EFT}^{125}$ scenario, the dashed blue line indicates the threshold at $m_{\rm A} = 2m_{\rm t}$ whereby the $\text{A} \to \text{t}\bar{\text{t}}$ decay starts to influence the $\text{A} \to \tau\tau$ branching fraction. The $\text{H} \to \tau\tau$ branching fraction is influenced more gradually close to this threshold since A and H are not completely degenerate in mass.

cluded at two-loop accuracy reweighting the SM results of refs. [188, 189]. Contributions from squarks and gluinos are included at NLO precision in $\alpha_{\rm S}$ following refs. [190–192]. The $\tan\beta$-enhanced SUSY contributions to the Higgs-b couplings have been resummed using the one-loop $\Delta_{\rm b}$ terms from ref. [193] as provided by FEYNHIGGS. Uncertainties in these $\Delta_{\rm b}$ terms which range $\approx 10\%$ are not included in the overall uncertainties in the predictions as they are subdominant with respect to the other theoretical uncertainties.

For bbH production, cross sections have been calculated for the SM Higgs boson as a function of its mass, based on soft-collinear effective theory [194, 195] which combines the merits of both the 4FS [196, 197] and 5FS [198, 199] calculations. These cross sections coincide with the results of the so-called "fixed order plus next-to-leading log" approach of refs. [200, 201]. The pure t- and loop-induced tb-interference contributions are separately reweighted with effective Higgs couplings, using an effective mixing angle α, and including the resummation of $\tan\beta$-enhanced SUSY contributions as in the $\text{gg}\phi$ case. The same SM cross sections are also used to obtain the reweighted cross section for bbA production. A more detailed discussion is given in ref. [86]. All Higgs boson masses, effective mixing angles α, Yukawa couplings, branching fractions, cross sections, and their uncertainties, which are included for the exclusion contours, are obtained from ref. [87].

In the figure, the exclusion sensitivity, estimated from the expected median in the absence of a signal, is indicated by the dashed black line. We note that the central 68%

and 95% intervals, also given for the exclusion sensitivity, should not be misinterpreted as an uncertainty in the analysis, but they rather reflect the variation of the expected signal yield in the probed parameter space of the chosen benchmark scenarios. For the $M_{\mathrm{h,EFT}}^{125}$ scenario the sensitivity sharply drops at $m_{\mathrm{A}} = 2\,m_{\mathrm{t}}$, caused by a drop of the branching fractions for the decay of A and H into τ leptons where the A and H decays into two on-shell t quarks become kinematically accessible. The distinct boundary is related to the fact that in FeynHiggs, which is used for the calculation of all branching fractions for this benchmark scenario, only the decay into on-shell $\mathrm{t\bar{t}}$ pairs is implemented. The parameter space of each benchmark scenario that is excluded at 95% CL by the data is indicated by the coloured blue area.

Both scenarios are excluded at 95% CL for $m_{\mathrm{A}} \lesssim 350\,\mathrm{GeV}$. The local excess observed at 1.2 TeV causes the deviation of the observed exclusion from the expectation. For $m_{\mathrm{A}} \lesssim 250\,\mathrm{GeV}$, most of the ggH/ggA events do not enter the "no b tag" categories due to the $m_{\tau\tau} > 250\,\mathrm{GeV}$ requirement, although these events still contribute to the signal yields in the NN categories. In this parameter space the sensitivity to the MSSM is driven by the measurements of the H(125) production rates, while the sensitivity to the H and A enters mainly via the bbϕ signal in the "b tag" categories, especially for increasing values of $\tan\beta$.

9 Summary

Three searches have been presented for signatures of physics beyond the standard model (SM) in $\tau\tau$ final states in proton-proton collisions at the LHC, using a data sample collected with the CMS detector at $\sqrt{s} = 13\,\mathrm{TeV}$, corresponding to an integrated luminosity of $138\,\mathrm{fb}^{-1}$. Upper limits at 95% confidence level (CL) have been set on the products of the branching fraction for the decay into τ leptons and the cross sections for the production of a resonance ϕ in addition to the observed Higgs boson via gluon fusion (ggϕ) or in association with b quarks, ranging from $\mathcal{O}(10\,\mathrm{pb})$ for a mass of 60 GeV to 0.3 fb for a mass of 3.5 TeV each. The data reveal two excesses for ggϕ production with local p-values equivalent to about three standard deviations at $m_\phi = 0.1$ and 1.2 TeV. Within the resolution of the reconstructed invariant mass of the $\tau\tau$ system, the excess at 100 GeV coincides with a similar excess observed in a previous search for low-mass resonances by the CMS Collaboration in the $\gamma\gamma$ final state at a mass of $\approx 95\,\mathrm{GeV}$. In a search for t-channel exchange of a vector leptoquark U_1, 95% CL upper limits are set on the U_1 coupling to quarks and τ leptons ranging from 1 for a mass of 1 TeV to 6 for a mass of 5 TeV, depending on the scenario. The search is sensitive to and excludes a portion of the parameter space that can explain the b physics anomalies. In the interpretation of the M_{h}^{125} and $M_{\mathrm{h,EFT}}^{125}$ minimal supersymmetric SM benchmark scenarios, additional Higgs bosons with masses below 350 GeV are excluded at 95% CL.

Acknowledgments

References

[1] ATLAS collaboration, *Observation of a new particle in the search for the Standard Model Higgs boson with the ATLAS detector at the LHC*, *Phys. Lett. B* **716** (2012) 1 [[arXiv:1207.7214](#)] [[INSPIRE](#)].

[2] CMS collaboration, *Observation of a new boson at a mass of* 125 *GeV with the CMS experiment at the LHC*, *Phys. Lett. B* **716** (2012) 30 [[arXiv:1207.7235](#)] [[INSPIRE](#)].

[3] CMS collaboration, *Observation of a new boson with mass near* 125 *GeV in pp collisions at* $\sqrt{s} = 7$ *and* 8 *TeV*, *JHEP* **06** (2013) 081 [[arXiv:1303.4571](#)] [[INSPIRE](#)].

[4] ATLAS and CMS collaborations, *Measurements of the Higgs boson production and decay rates and constraints on its couplings from a combined ATLAS and CMS analysis of the LHC pp collision data at* $\sqrt{s} = 7$ *and* 8 *TeV*, *JHEP* **08** (2016) 045 [[arXiv:1606.02266](#)] [[INSPIRE](#)].

[5] CMS collaboration, *Combined measurements of Higgs boson couplings in proton–proton collisions at* $\sqrt{s} = 13$ *TeV*, *Eur. Phys. J. C* **79** (2019) 421 [[arXiv:1809.10733](#)] [[INSPIRE](#)].

[6] ATLAS collaboration, *Combined measurements of Higgs boson production and decay using up to* 80 fb^{-1} *of proton-proton collision data at* $\sqrt{s} = 13$ *TeV collected with the ATLAS experiment*, *Phys. Rev. D* **101** (2020) 012002 [[arXiv:1909.02845](#)] [[INSPIRE](#)].

[7] CMS collaboration, *Measurements of the Higgs boson width and anomalous HVV couplings from on-shell and off-shell production in the four-lepton final state*, *Phys. Rev. D* **99** (2019) 112003 [[arXiv:1901.00174](#)] [[INSPIRE](#)].

[8] CMS collaboration, *A measurement of the Higgs boson mass in the diphoton decay channel*, *Phys. Lett. B* **805** (2020) 135425 [[arXiv:2002.06398](#)] [[INSPIRE](#)].

[9] Y.A. Golfand and E.P. Likhtman, *Extension of the algebra of Poincaré group generators and violation of p invariance*, *JETP Lett.* **13** (1971) 323 [[INSPIRE](#)].

[10] J. Wess and B. Zumino, *Supergauge transformations in four-dimensions*, *Nucl. Phys. B* **70** (1974) 39 [[INSPIRE](#)].

[11] P. Fayet, *Supergauge invariant extension of the Higgs mechanism and a model for the electron and its neutrino*, *Nucl. Phys. B* **90** (1975) 104 [[INSPIRE](#)].

[12] P. Fayet, *Spontaneously broken supersymmetric theories of weak, electromagnetic and strong interactions*, *Phys. Lett. B* **69** (1977) 489 [[INSPIRE](#)].

[13] ALEPH et al. collaborations, *Search for neutral MSSM Higgs bosons at LEP*, *Eur. Phys. J. C* **47** (2006) 547 [[hep-ex/0602042](#)] [[INSPIRE](#)].

[14] CDF collaboration, *Search for Higgs bosons predicted in two-Higgs-doublet models via decays to tau lepton pairs in* 1.96 *TeV* $p\bar{p}$ *collisions*, *Phys. Rev. Lett.* **103** (2009) 201801 [[arXiv:0906.1014](#)] [[INSPIRE](#)].

[15] D0 collaboration, *Search for neutral Higgs bosons in the multi-b-jet topology in* $5.2\,fb^{-1}$ *of* $p\bar{p}$ *collisions at* $\sqrt{s} = 1.96\,TeV$, *Phys. Lett. B* **698** (2011) 97 [arXiv:1011.1931] [INSPIRE].

[16] D0 collaboration, *Search for Higgs bosons decaying to* $\tau\tau$ *pairs in* $p\bar{p}$ *collisions at* $\sqrt{s} = 1.96\,TeV$, *Phys. Lett. B* **707** (2012) 323 [arXiv:1106.4555] [INSPIRE].

[17] CDF collaboration, *Search for Higgs bosons produced in association with b-quarks*, *Phys. Rev. D* **85** (2012) 032005 [arXiv:1106.4782] [INSPIRE].

[18] CMS collaboration, *Search for a Higgs boson decaying into a b-quark pair and produced in association with b quarks in proton–proton collisions at 7 TeV*, *Phys. Lett. B* **722** (2013) 207 [arXiv:1302.2892] [INSPIRE].

[19] CMS collaboration, *Search for neutral MSSM Higgs bosons decaying into a pair of bottom quarks*, *JHEP* **11** (2015) 071 [arXiv:1506.08329] [INSPIRE].

[20] CMS collaboration, *Search for beyond the standard model Higgs bosons decaying into a* $b\bar{b}$ *pair in pp collisions at* $\sqrt{s} = 13\,TeV$, *JHEP* **08** (2018) 113 [arXiv:1805.12191] [INSPIRE].

[21] ATLAS collaboration, *Search for heavy neutral Higgs bosons produced in association with b-quarks and decaying into b-quarks at* $\sqrt{s} = 13\,TeV$ *with the ATLAS detector*, *Phys. Rev. D* **102** (2020) 032004 [arXiv:1907.02749] [INSPIRE].

[22] ATLAS collaboration, *Search for the neutral Higgs bosons of the minimal supersymmetric standard model in pp collisions at* $\sqrt{s} = 7\,TeV$ *with the ATLAS detector*, *JHEP* **02** (2013) 095 [arXiv:1211.6956] [INSPIRE].

[23] CMS collaboration, *Search for neutral MSSM Higgs bosons decaying to* $\mu^+\mu^-$ *in pp collisions at* $\sqrt{s} = 7$ *and 8 TeV*, *Phys. Lett. B* **752** (2016) 221 [arXiv:1508.01437] [INSPIRE].

[24] CMS collaboration, *Search for MSSM Higgs bosons decaying to* $\mu^+\mu^-$ *in proton-proton collisions at s=13TeV*, *Phys. Lett. B* **798** (2019) 134992 [arXiv:1907.03152] [INSPIRE].

[25] ATLAS collaboration, *Search for scalar resonances decaying into* $\mu^+\mu^-$ *in events with and without b-tagged jets produced in proton-proton collisions at* $\sqrt{s} = 13\,TeV$ *with the ATLAS detector*, *JHEP* **07** (2019) 117 [arXiv:1901.08144] [INSPIRE].

[26] ATLAS collaboration, *Search for neutral Higgs bosons of the minimal supersymmetric standard model in pp collisions at* $\sqrt{s} = 8\,TeV$ *with the ATLAS detector*, *JHEP* **11** (2014) 056 [arXiv:1409.6064] [INSPIRE].

[27] ATLAS collaboration, *Search for minimal supersymmetric standard model Higgs bosons* h/A *and for a* Z' *boson in the* $\tau\tau$ *final state produced in pp collisions at* $\sqrt{s} = 13\,TeV$ *with the ATLAS Detector*, *Eur. Phys. J. C* **76** (2016) 585 [arXiv:1608.00890] [INSPIRE].

[28] ATLAS collaboration, *Search for additional heavy neutral Higgs and gauge bosons in the ditau final state produced in* $36\,fb^{-1}$ *of pp collisions at* $\sqrt{s} = 13\,TeV$ *with the ATLAS detector*, *JHEP* **01** (2018) 055 [arXiv:1709.07242] [INSPIRE].

[29] CMS collaboration, *Search for neutral MSSM Higgs bosons decaying to tau pairs in pp collisions at* $\sqrt{s} = 7\,TeV$, *Phys. Rev. Lett.* **106** (2011) 231801 [arXiv:1104.1619] [INSPIRE].

[30] CMS collaboration, *Search for neutral Higgs bosons decaying to tau pairs in pp collisions at* $\sqrt{s} = 7\,TeV$, *Phys. Lett. B* **713** (2012) 68 [arXiv:1202.4083] [INSPIRE].

[31] CMS collaboration, *Search for neutral MSSM Higgs bosons decaying to a pair of tau leptons in pp collisions*, *JHEP* **10** (2014) 160 [arXiv:1408.3316] [INSPIRE].

[32] CMS collaboration, *Search for additional neutral MSSM Higgs bosons in the* $\tau\tau$ *final state in proton-proton collisions at* $\sqrt{s} = 13\,TeV$, *JHEP* **09** (2018) 007 [arXiv:1803.06553] [INSPIRE].

[33] ATLAS collaboration, *Search for heavy Higgs bosons decaying into two tau leptons with the ATLAS detector using pp collisions at $\sqrt{s} = 13$ TeV*, *Phys. Rev. Lett.* **125** (2020) 051801 [arXiv:2002.12223] [INSPIRE].

[34] J. Steggemann, *Extended scalar sectors*, *Ann. Rev. Nucl. Part. Sci.* **70** (2020) 197 [INSPIRE].

[35] B. Diaz, M. Schmaltz and Y.-M. Zhong, *The leptoquark hunter's guide: Pair production*, *JHEP* **10** (2017) 097 [arXiv:1706.05033] [INSPIRE].

[36] M. Schmaltz and Y.-M. Zhong, *The leptoquark hunter's guide: large coupling*, *JHEP* **01** (2019) 132 [arXiv:1810.10017] [INSPIRE].

[37] CMS collaboration, *Search for third-generation scalar leptoquarks and heavy right-handed neutrinos in final states with two tau leptons and two jets in proton-proton collisions at $\sqrt{s} = 13$ TeV*, *JHEP* **07** (2017) 121 [arXiv:1703.03995] [INSPIRE].

[38] CMS collaboration, *Search for a singly produced third-generation scalar leptoquark decaying to a τ lepton and a bottom quark in proton-proton collisions at $\sqrt{s} = 13$ TeV*, *JHEP* **07** (2018) 115 [arXiv:1806.03472] [INSPIRE].

[39] CMS collaboration, *Search for heavy neutrinos and third-generation leptoquarks in hadronic states of two τ leptons and two jets in proton-proton collisions at $\sqrt{s} = 13$ TeV*, *JHEP* **03** (2019) 170 [arXiv:1811.00806] [INSPIRE].

[40] ATLAS collaboration, *Searches for third-generation scalar leptoquarks in $\sqrt{s} = 13$ TeV pp collisions with the ATLAS detector*, *JHEP* **06** (2019) 144 [arXiv:1902.08103] [INSPIRE].

[41] ATLAS collaboration, *Search for a scalar partner of the top quark in the all-hadronic $t\bar{t}$ plus missing transverse momentum final state at $\sqrt{s} = 13$ TeV with the ATLAS detector*, *Eur. Phys. J. C* **80** (2020) 737 [arXiv:2004.14060] [INSPIRE].

[42] CMS collaboration, *Search for singly and pair-produced leptoquarks coupling to third-generation fermions in proton-proton collisions at $\sqrt{s} = 13$ TeV*, *Phys. Lett. B* **819** (2021) 136446 [arXiv:2012.04178] [INSPIRE].

[43] ATLAS collaboration, *Search for new phenomena in pp collisions in final states with tau leptons, b-jets, and missing transverse momentum with the ATLAS detector*, *Phys. Rev. D* **104** (2021) 112005 [arXiv:2108.07665] [INSPIRE].

[44] ATLAS collaboration, *Search for new phenomena in final states with b-jets and missing transverse momentum in $\sqrt{s} = 13$ TeV pp collisions with the ATLAS detector*, *JHEP* **05** (2021) 093 [arXiv:2101.12527] [INSPIRE].

[45] ATLAS collaboration, *Search for pair production of third-generation scalar leptoquarks decaying into a top quark and a τ-lepton in pp collisions at $\sqrt{s} = 13$ TeV with the ATLAS detector*, *JHEP* **06** (2021) 179 [arXiv:2101.11582] [INSPIRE].

[46] CMS collaboration, *Searches for additional Higgs bosons and for vector leptoquarks in $\tau\tau$ final states in proton-proton collisions at $\sqrt{s} = 13$ TeV*, https://www.hepdata.net/record/ins2132368 [DOI:10.17182/HEPDATA.128147].

[47] W. Buchmuller, R. Ruckl and D. Wyler, *Leptoquarks in lepton-quark collisions*, *Phys. Lett. B* **191** (1987) 442 [INSPIRE].

[48] J.C. Pati and A. Salam, *Unified lepton-hadron symmetry and a gauge theory of the basic interactions*, *Phys. Rev. D* **8** (1973) 1240 [INSPIRE].

[49] J.C. Pati and A. Salam, *Lepton number as the fourth color*, *Phys. Rev. D* **10** (1974) 275 [INSPIRE].

[50] H. Georgi and S.L. Glashow, *Unity of all elementary particle forces*, *Phys. Rev. Lett.* **32** (1974) 438 [INSPIRE].

[51] H. Fritzsch and P. Minkowski, *Unified interactions of leptons and hadrons*, *Annals Phys.* **93** (1975) 193 [INSPIRE].

[52] S. Dimopoulos and L. Susskind, *Mass without scalars*, *Nucl. Phys. B* **155** (1979) 237 [INSPIRE].

[53] S. Dimopoulos, *Technicolored signatures*, *Nucl. Phys. B* **168** (1980) 69 [INSPIRE].

[54] E. Farhi and L. Susskind, *Technicolor*, *Phys. Rept.* **74** (1981) 277 [INSPIRE].

[55] K.D. Lane and M.V. Ramana, *Walking technicolor signatures at hadron colliders*, *Phys. Rev. D* **44** (1991) 2678 [INSPIRE].

[56] B. Schrempp and F. Schrempp, *Light leptoquarks*, *Phys. Lett. B* **153** (1985) 101 [INSPIRE].

[57] B. Gripaios, *Composite leptoquarks at the LHC*, *JHEP* **02** (2010) 045 [arXiv:0910.1789] [INSPIRE].

[58] G.R. Farrar and P. Fayet, *Phenomenology of the production, decay, and detection of new hadronic states associated with supersymmetry*, *Phys. Lett. B* **76** (1978) 575 [INSPIRE].

[59] P. Ramond, *Dual theory for free fermions*, *Phys. Rev. D* **3** (1971) 2415 [INSPIRE].

[60] A. Neveu and J.H. Schwarz, *Factorizable dual model of pions*, *Nucl. Phys. B* **31** (1971) 86 [INSPIRE].

[61] D.V. Volkov and V.P. Akulov, *Possible universal neutrino interaction*, *JETP Lett.* **16** (1972) 438 [INSPIRE].

[62] J. Wess and B. Zumino, *A Lagrangian model invariant under supergauge transformations*, *Phys. Lett. B* **49** (1974) 52 [INSPIRE].

[63] H.P. Nilles, *Supersymmetry, supergravity and particle physics*, *Phys. Rept.* **110** (1984) 1 [INSPIRE].

[64] R. Barbier et al., *R-parity violating supersymmetry*, *Phys. Rept.* **420** (2005) 1 [hep-ph/0406039] [INSPIRE].

[65] M. Tanaka and R. Watanabe, *New physics in the weak interaction of $\bar{B} \to D^{(*)}\tau\bar{\nu}$*, *Phys. Rev. D* **87** (2013) 034028 [arXiv:1212.1878] [INSPIRE].

[66] R. Barbieri, G. Isidori, A. Pattori and F. Senia, *Anomalies in B-decays and $U(2)$ flavour symmetry*, *Eur. Phys. J. C* **76** (2016) 67 [arXiv:1512.01560] [INSPIRE].

[67] D.A. Faroughy, A. Greljo and J.F. Kamenik, *Confronting lepton flavor universality violation in B decays with high-p_T tau lepton searches at LHC*, *Phys. Lett. B* **764** (2017) 126 [arXiv:1609.07138] [INSPIRE].

[68] M. Bordone, C. Cornella, J. Fuentes-Martin and G. Isidori, *A three-site gauge model for flavor hierarchies and flavor anomalies*, *Phys. Lett. B* **779** (2018) 317 [arXiv:1712.01368] [INSPIRE].

[69] L. Di Luzio, A. Greljo and M. Nardecchia, *Gauge leptoquark as the origin of B-physics anomalies*, *Phys. Rev. D* **96** (2017) 115011 [arXiv:1708.08450] [INSPIRE].

[70] A. Greljo and B.A. Stefanek, *Third family quark–lepton unification at the TeV scale*, *Phys. Lett. B* **782** (2018) 131 [arXiv:1802.04274] [INSPIRE].

[71] A. Angelescu et al., *Single leptoquark solutions to the B-physics anomalies*, *Phys. Rev. D* **104** (2021) 055017 [arXiv:2103.12504] [INSPIRE].

[72] C. Cornella et al., *Reading the footprints of the B-meson flavor anomalies*, *JHEP* **08** (2021) 050 [arXiv:2103.16558] [INSPIRE].

[73] LHCB collaboration, *Test of lepton universality in beauty-quark decays*, *Nature Phys.* **18** (2022) 277 [arXiv:2103.11769] [INSPIRE].

[74] BaBar collaboration, *Evidence for an excess of $\bar{B} \to D^{(*)}\tau^-\bar{\nu}_\tau$ decays*, *Phys. Rev. Lett.* **109** (2012) 101802 [arXiv:1205.5442] [InSPIRE].

[75] BaBar collaboration, *Measurement of an excess of $\bar{B} \to D^{(*)}\tau^-\bar{\nu}_\tau$ decays and implications for charged Higgs bosons*, *Phys. Rev. D* **88** (2013) 072012 [arXiv:1303.0571] [InSPIRE].

[76] Belle collaboration, *Measurement of the branching ratio of $\bar{B} \to D^{(*)}\tau^-\bar{\nu}_\tau$ relative to $\bar{B} \to D^{(*)}\ell^-\bar{\nu}_\ell$ decays with hadronic tagging at Belle*, *Phys. Rev. D* **92** (2015) 072014 [arXiv:1507.03233] [InSPIRE].

[77] LHCb collaboration, *Measurement of the ratio of branching fractions $\mathcal{B}(\bar{B}^0 \to D^{*+}\tau^-\bar{\nu}_\tau)/\mathcal{B}(\bar{B}^0 \to D^{*+}\mu^-\bar{\nu}_\mu)$*, *Phys. Rev. Lett.* **115** (2015) 111803 [*Erratum ibid.* **115** (2015) 159901] [arXiv:1506.08614] [InSPIRE].

[78] Belle collaboration, *Measurement of the τ lepton polarization and $R(D^*)$ in the decay $\bar{B} \to D^*\tau^-\bar{\nu}_\tau$*, *Phys. Rev. Lett.* **118** (2017) 211801 [arXiv:1612.00529] [InSPIRE].

[79] LHCb collaboration, *Test of Lepton Flavor Universality by the measurement of the $B^0 \to D^{*-}\tau^+\nu_\tau$ branching fraction using three-prong τ decays*, *Phys. Rev. D* **97** (2018) 072013 [arXiv:1711.02505] [InSPIRE].

[80] LHCb collaboration, *Measurement of the ratio of the $B^0 \to D^{*-}\tau^+\nu_\tau$ and $B^0 \to D^{*-}\mu^+\nu_\mu$ branching fractions using three-prong τ-lepton decays*, *Phys. Rev. Lett.* **120** (2018) 171802 [arXiv:1708.08856] [InSPIRE].

[81] T.D. Lee, *A theory of spontaneous T Violation*, *Phys. Rev. D* **8** (1973) 1226 [InSPIRE].

[82] G.C. Branco et al., *Theory and phenomenology of two-Higgs-doublet models*, *Phys. Rept.* **516** (2012) 1 [arXiv:1106.0034] [InSPIRE].

[83] E. Bagnaschi et al., *MSSM Higgs boson searches at the LHC: benchmark scenarios for Run 2 and beyond*, *Eur. Phys. J. C* **79** (2019) 617 [arXiv:1808.07542] [InSPIRE].

[84] H. Bahl et al., *HL-LHC and ILC sensitivities in the hunt for heavy Higgs bosons*, *Eur. Phys. J. C* **80** (2020) 916 [arXiv:2005.14536] [InSPIRE].

[85] H. Bahl, S. Liebler and T. Stefaniak, *MSSM Higgs benchmark scenarios for Run 2 and beyond: the low $\tan\beta$ region*, *Eur. Phys. J. C* **79** (2019) 279 [arXiv:1901.05933] [InSPIRE].

[86] E.A. Bagnaschi et al., *Benchmark scenarios for MSSM Higgs boson searches at the LHC*, LHCHWG-2021-001, CERN, Geneva (2021).

[87] LHC Higgs Cross Section Working Group — MSSM subgroup, *LHCHWG MSSM ROOT files*, https://zenodo.org/record/6793918 [DOI:10.5281/ZENODO.6793918].

[88] CMS collaboration, *Performance of the CMS Level-1 trigger in proton-proton collisions at $\sqrt{s} = 13$ TeV*, 2020 *JINST* **15** P10017 [arXiv:2006.10165] [InSPIRE].

[89] CMS collaboration, *The CMS trigger system*, 2017 *JINST* **12** P01020 [arXiv:1609.02366] [InSPIRE].

[90] CMS collaboration, *The CMS experiment at the CERN LHC*, 2008 *JINST* **3** S08004 [InSPIRE].

[91] CMS collaboration, *Particle-flow reconstruction and global event description with the CMS detector*, 2017 *JINST* **12** P10003 [arXiv:1706.04965] [InSPIRE].

[92] D. Contardo et al., *Technical proposal for the Phase-II upgrade of the CMS detector*, CERN-LHCC-2015-010 (2015) [DOI:10.17181/CERN.VU8I.D59J].

[93] CMS collaboration, *Performance of electron reconstruction and selection with the CMS detector in proton-proton collisions at $\sqrt{s} = 8$ TeV*, 2015 *JINST* **10** P06005 [arXiv:1502.02701] [InSPIRE].

[94] CMS collaboration, *Electron and photon reconstruction and identification with the CMS experiment at the CERN LHC*, 2021 *JINST* **16** P05014 [`arXiv:2012.06888`] [IɴSPIRE].

[95] CMS collaboration, *Performance of the CMS muon detector and muon reconstruction with proton-proton collisions at $\sqrt{s} = 13$ TeV*, 2018 *JINST* **13** P06015 [`arXiv:1804.04528`] [IɴSPIRE].

[96] M. Cacciari, G.P. Salam and G. Soyez, *The anti-k_t jet clustering algorithm*, *JHEP* **04** (2008) 063 [`arXiv:0802.1189`] [IɴSPIRE].

[97] M. Cacciari, G.P. Salam and G. Soyez, *FastJet user manual*, *Eur. Phys. J. C* **72** (2012) 1896 [`arXiv:1111.6097`] [IɴSPIRE].

[98] CMS collaboration, *Identification of heavy-flavour jets with the CMS detector in pp collisions at 13 TeV*, 2018 *JINST* **13** P05011 [`arXiv:1712.07158`] [IɴSPIRE].

[99] E. Bols et al., *Jet flavour classification using DeepJet*, 2020 *JINST* **15** P12012 [`arXiv:2008.10519`] [IɴSPIRE].

[100] CMS collaboration, *Performance of the DeepJet b tagging algorithm using 41.9/fb of data from proton-proton collisions at 13 TeV with Phase 1 CMS detector*, CMS-DP-2018-058 (2018).

[101] CMS collaboration, *Performance of reconstruction and identification of τ leptons decaying to hadrons and ν_τ in pp collisions at $\sqrt{s} = 13$ TeV*, 2018 *JINST* **13** P10005 [`arXiv:1809.02816`] [IɴSPIRE].

[102] CMS collaboration, *Identification of hadronic tau lepton decays using a deep neural network*, 2022 *JINST* **17** P07023 [`arXiv:2201.08458`] [IɴSPIRE].

[103] CMS collaboration, *Performance of missing transverse momentum reconstruction in proton-proton collisions at $\sqrt{s} = 13$ TeV using the CMS detector*, 2019 *JINST* **14** P07004 [`arXiv:1903.06078`] [IɴSPIRE].

[104] D. Bertolini, P. Harris, M. Low and N. Tran, *Pileup per particle identification*, *JHEP* **10** (2014) 059 [`arXiv:1407.6013`] [IɴSPIRE].

[105] CDF collaboration, *Search for neutral MSSM Higgs bosons decaying to tau pairs in $p\bar{p}$ collisions at $\sqrt{s} = 1.96$ TeV*, *Phys. Rev. Lett.* **96** (2006) 011802 [`hep-ex/0508051`] [IɴSPIRE].

[106] L. Bianchini, J. Conway, E.K. Friis and C. Veelken, *Reconstruction of the Higgs mass in $H \to \tau\tau$ events by dynamical likelihood techniques*, *J. Phys. Conf. Ser.* **513** (2014) 022035 [IɴSPIRE].

[107] B.K. Bullock, K. Hagiwara and A.D. Martin, *Tau polarization and its correlations as a probe of new physics*, *Nucl. Phys. B* **395** (1993) 499 [IɴSPIRE].

[108] PARTICLE DATA GROUP collaboration, *Review of particle physics*, *PTEP* **2020** (2020) 083C01 [IɴSPIRE].

[109] CMS collaboration, *Measurements of Higgs boson production in the decay channel with a pair of τ leptons in proton-proton collisions at $\sqrt{s} = 13$ TeV*, `arXiv:2204.12957` [IɴSPIRE].

[110] CMS collaboration, *An embedding technique to determine $\tau\tau$ backgrounds in proton-proton collision data*, 2019 *JINST* **14** P06032 [`arXiv:1903.01216`] [IɴSPIRE].

[111] CMS collaboration, *Measurement of the $Z\gamma^* \to \tau\tau$ cross section in pp collisions at $\sqrt{s} = 13$ TeV and validation of τ lepton analysis techniques*, *Eur. Phys. J. C* **78** (2018) 708 [`arXiv:1801.03535`] [IɴSPIRE].

[112] J. Alwall et al., *MadGraph 5: going beyond*, *JHEP* **06** (2011) 128 [`arXiv:1106.0522`] [IɴSPIRE].

[113] J. Alwall et al., *The automated computation of tree-level and next-to-leading order differential cross sections, and their matching to parton shower simulations*, *JHEP* **07** (2014) 079 [arXiv:1405.0301] [INSPIRE].

[114] R. Frederix and S. Frixione, *Merging meets matching in MC@NLO*, *JHEP* **12** (2012) 061 [arXiv:1209.6215] [INSPIRE].

[115] J. Alwall et al., *Comparative study of various algorithms for the merging of parton showers and matrix elements in hadronic collisions*, *Eur. Phys. J. C* **53** (2008) 473 [arXiv:0706.2569] [INSPIRE].

[116] S. Alioli, S.-O. Moch and P. Uwer, *Hadronic top-quark pair-production with one jet and parton showering*, *JHEP* **01** (2012) 137 [arXiv:1110.5251] [INSPIRE].

[117] R. Frederix, E. Re and P. Torrielli, *Single-top t-channel hadroproduction in the four-flavour scheme with POWHEG and aMC@NLO*, *JHEP* **09** (2012) 130 [arXiv:1207.5391] [INSPIRE].

[118] P. Nason, *A new method for combining NLO QCD with shower Monte Carlo algorithms*, *JHEP* **11** (2004) 040 [hep-ph/0409146] [INSPIRE].

[119] S. Frixione, P. Nason and C. Oleari, *Matching NLO QCD computations with Parton Shower simulations: the POWHEG method*, *JHEP* **11** (2007) 070 [arXiv:0709.2092] [INSPIRE].

[120] S. Alioli, P. Nason, C. Oleari and E. Re, *A general framework for implementing NLO calculations in shower Monte Carlo programs: the POWHEG BOX*, *JHEP* **06** (2010) 043 [arXiv:1002.2581] [INSPIRE].

[121] T. Ježo and P. Nason, *On the treatment of resonances in next-to-leading order calculations matched to a parton shower*, *JHEP* **12** (2015) 065 [arXiv:1509.09071] [INSPIRE].

[122] E. Re, *Single-top Wt-channel production matched with parton showers using the POWHEG method*, *Eur. Phys. J. C* **71** (2011) 1547 [arXiv:1009.2450] [INSPIRE].

[123] K. Melnikov and F. Petriello, *Electroweak gauge boson production at hadron colliders through $O(\alpha_s^2)$*, *Phys. Rev. D* **74** (2006) 114017 [hep-ph/0609070] [INSPIRE].

[124] M. Czakon and A. Mitov, *Top++: a program for the calculation of the top-pair cross-section at hadron colliders*, *Comput. Phys. Commun.* **185** (2014) 2930 [arXiv:1112.5675] [INSPIRE].

[125] N. Kidonakis, *Top Quark Production*, in the proceedings of the *Helmholtz International Summer School on Physics of Heavy Quarks and Hadrons*, (2014), p. 139–168 [DOI:10.3204/DESY-PROC-2013-03/Kidonakis] [arXiv:1311.0283] [INSPIRE].

[126] J.M. Campbell, R.K. Ellis and C. Williams, *Vector boson pair production at the LHC*, *JHEP* **07** (2011) 018 [arXiv:1105.0020] [INSPIRE].

[127] T. Gehrmann et al., *W^+W^- production at hadron colliders in next to next to leading order QCD*, *Phys. Rev. Lett.* **113** (2014) 212001 [arXiv:1408.5243] [INSPIRE].

[128] E. Bagnaschi, G. Degrassi, P. Slavich and A. Vicini, *Higgs production via gluon fusion in the POWHEG approach in the SM and in the MSSM*, *JHEP* **02** (2012) 088 [arXiv:1111.2854] [INSPIRE].

[129] P. Nason and C. Oleari, *NLO Higgs boson production via vector-boson fusion matched with shower in POWHEG*, *JHEP* **02** (2010) 037 [arXiv:0911.5299] [INSPIRE].

[130] G. Luisoni, P. Nason, C. Oleari and F. Tramontano, *$HW^\pm/HZ$ + 0 and 1 jet at NLO with the POWHEG BOX interfaced to GoSam and their merging within MiNLO*, *JHEP* **10** (2013) 083 [arXiv:1306.2542] [INSPIRE].

[131] F. Granata, J.M. Lindert, C. Oleari and S. Pozzorini, *NLO QCD+EW predictions for HV and HV +jet production including parton-shower effects*, *JHEP* **09** (2017) 012 [arXiv:1706.03522] [INSPIRE].

[132] K. Hamilton, P. Nason, E. Re and G. Zanderighi, *NNLOPS simulation of Higgs boson production*, *JHEP* **10** (2013) 222 [arXiv:1309.0017] [INSPIRE].

[133] K. Hamilton, P. Nason and G. Zanderighi, *Finite quark-mass effects in the NNLOPS POWHEG+MiNLO Higgs generator*, *JHEP* **05** (2015) 140 [arXiv:1501.04637] [INSPIRE].

[134] R.V. Harlander, H. Mantler and M. Wiesemann, *Transverse momentum resummation for Higgs production via gluon fusion in the MSSM*, *JHEP* **11** (2014) 116 [arXiv:1409.0531] [INSPIRE].

[135] E. Bagnaschi et al., *Resummation ambiguities in the Higgs transverse-momentum spectrum in the Standard Model and beyond*, *JHEP* **01** (2016) 090 [arXiv:1510.08850] [INSPIRE].

[136] E. Bagnaschi and A. Vicini, *The Higgs transverse momentum distribution in gluon fusion as a multiscale problem*, *JHEP* **01** (2016) 056 [arXiv:1505.00735] [INSPIRE].

[137] B. Jager, L. Reina and D. Wackeroth, *Higgs boson production in association with b jets in the POWHEG BOX*, *Phys. Rev. D* **93** (2016) 014030 [arXiv:1509.05843] [INSPIRE].

[138] M.J. Baker, J. Fuentes-Martín, G. Isidori and M. König, *High-p_T signatures in vector–leptoquark models*, *Eur. Phys. J. C* **79** (2019) 334 [arXiv:1901.10480] [INSPIRE].

[139] J. Butterworth et al., *PDF4LHC recommendations for LHC Run II*, *J. Phys. G* **43** (2016) 023001 [arXiv:1510.03865] [INSPIRE].

[140] NNPDF collaboration, *Parton distributions from high-precision collider data*, *Eur. Phys. J. C* **77** (2017) 663 [arXiv:1706.00428] [INSPIRE].

[141] NNPDF collaboration, *Parton distributions for the LHC Run II*, *JHEP* **04** (2015) 040 [arXiv:1410.8849] [INSPIRE].

[142] CMS collaboration, *Event generator tunes obtained from underlying event and multiparton scattering measurements*, *Eur. Phys. J. C* **76** (2016) 155 [arXiv:1512.00815] [INSPIRE].

[143] CMS collaboration, *Extraction and validation of a new set of CMS PYTHIA8 tunes from underlying-event measurements*, *Eur. Phys. J. C* **80** (2020) 4 [arXiv:1903.12179] [INSPIRE].

[144] T. Sjöstrand et al., *An introduction to PYTHIA 8.2*, *Comput. Phys. Commun.* **191** (2015) 159 [arXiv:1410.3012] [INSPIRE].

[145] GEANT4 collaboration, *GEANT4 — a simulation toolkit*, *Nucl. Instrum. Meth. A* **506** (2003) 250 [INSPIRE].

[146] CMS collaboration, *Measurements of inclusive W and Z cross sections in pp collisions at $\sqrt{s} = 7$ TeV*, *JHEP* **01** (2011) 080 [arXiv:1012.2466] [INSPIRE].

[147] CMS collaboration, *Measurement of the differential cross section for top quark pair production in pp collisions at $\sqrt{s} = 8$ TeV*, *Eur. Phys. J. C* **75** (2015) 542 [arXiv:1505.04480] [INSPIRE].

[148] R.J. Barlow and C. Beeston, *Fitting using finite Monte Carlo samples*, *Comput. Phys. Commun.* **77** (1993) 219 [INSPIRE].

[149] J.S. Conway, *Incorporating Nuisance Parameters in Likelihoods for Multisource Spectra*, in the proceedings of the *PHYSTAT 2011*, (2011), p. 115–120 [DOI:10.5170/CERN-2011-006.115] [arXiv:1103.0354] [INSPIRE].

[150] CMS collaboration, *Precision luminosity measurement in proton-proton collisions at* $\sqrt{s} = 13$ *TeV in 2015 and 2016 at CMS*, *Eur. Phys. J. C* **81** (2021) 800 [arXiv:2104.01927] [INSPIRE].

[151] CMS collaboration, *CMS luminosity measurement for the 2017 data-taking period at* $\sqrt{s} = 13$ *TeV*, CMS-PAS-LUM-17-004, CERN, Geneva (2018).

[152] CMS collaboration, *CMS luminosity measurement for the 2018 data-taking period at* $\sqrt{s} = 13$ *TeV*, CMS-PAS-LUM-18-002, CERN, Geneva (2019).

[153] LHC HIGGS CROSS SECTION WORKING GROUP collaboration, *Handbook of LHC Higgs Cross Sections: 4. Deciphering the Nature of the Higgs Sector*, arXiv:1610.07922 [DOI:10.23731/CYRM-2017-002] [INSPIRE].

[154] S. Alioli, P. Nason, C. Oleari and E. Re, *NLO Higgs boson production via gluon fusion matched with shower in POWHEG*, *JHEP* **04** (2009) 002 [arXiv:0812.0578] [INSPIRE].

[155] H.B. Hartanto, B. Jager, L. Reina and D. Wackeroth, *Higgs boson production in association with top quarks in the POWHEG BOX*, *Phys. Rev. D* **91** (2015) 094003 [arXiv:1501.04498] [INSPIRE].

[156] ATLAS collaboration, *Improved common* $t\bar{t}$ *Monte-Carlo settings for ATLAS and CMS*, ATL-PHYS-PUB-2023-016, CERN, Geneva (2023).

[157] CMS collaboration, *Combined results of searches for the standard model Higgs boson in pp collisions at* $\sqrt{s} = 7$ *TeV*, *Phys. Lett. B* **710** (2012) 26 [arXiv:1202.1488] [INSPIRE].

[158] G. Cowan, K. Cranmer, E. Gross and O. Vitells, *Asymptotic formulae for likelihood-based tests of new physics*, *Eur. Phys. J. C* **71** (2011) 1554 [*Erratum ibid.* **73** (2013) 2501] [arXiv:1007.1727] [INSPIRE].

[159] T. Junk, *Confidence level computation for combining searches with small statistics*, *Nucl. Instrum. Meth. A* **434** (1999) 435 [hep-ex/9902006] [INSPIRE].

[160] A.L. Read, *Presentation of search results: the* CL_s *technique*, *J. Phys. G* **28** (2002) 2693 [INSPIRE].

[161] CMS collaboration, *Search for a standard model-like Higgs boson in the mass range between 70 and 110 GeV in the diphoton final state in proton-proton collisions at* $\sqrt{s} = 8$ *and 13 TeV*, *Phys. Lett. B* **793** (2019) 320 [arXiv:1811.08459] [INSPIRE].

[162] P. Slavich et al., *Higgs-mass predictions in the MSSM and beyond*, *Eur. Phys. J. C* **81** (2021) 450 [arXiv:2012.15629] [INSPIRE].

[163] A.L. Read, *Linear interpolation of histograms*, *Nucl. Instrum. Meth. A* **425** (1999) 357 [INSPIRE].

[164] S. Heinemeyer, W. Hollik and G. Weiglein, *FeynHiggs: a program for the calculation of the masses of the neutral CP even Higgs bosons in the MSSM*, *Comput. Phys. Commun.* **124** (2000) 76 [hep-ph/9812320] [INSPIRE].

[165] S. Heinemeyer, W. Hollik and G. Weiglein, *The Masses of the neutral CP-even Higgs bosons in the MSSM: accurate analysis at the two loop level*, *Eur. Phys. J. C* **9** (1999) 343 [hep-ph/9812472] [INSPIRE].

[166] G. Degrassi et al., *Towards high precision predictions for the MSSM Higgs sector*, *Eur. Phys. J. C* **28** (2003) 133 [hep-ph/0212020] [INSPIRE].

[167] M. Frank et al., *The Higgs boson masses and mixings of the complex MSSM in the Feynman-diagrammatic approach*, *JHEP* **02** (2007) 047 [hep-ph/0611326] [INSPIRE].

[168] T. Hahn et al., *High-precision predictions for the light CP-even Higgs boson mass of the Minimal Supersymmetric Standard Model*, *Phys. Rev. Lett.* **112** (2014) 141801 [arXiv:1312.4937] [INSPIRE].

[169] H. Bahl and W. Hollik, *Precise prediction for the light MSSM Higgs boson mass combining effective field theory and fixed-order calculations*, *Eur. Phys. J. C* **76** (2016) 499 [arXiv:1608.01880] [INSPIRE].

[170] H. Bahl, S. Heinemeyer, W. Hollik and G. Weiglein, *Reconciling EFT and hybrid calculations of the light MSSM Higgs-boson mass*, *Eur. Phys. J. C* **78** (2018) 57 [arXiv:1706.00346] [INSPIRE].

[171] H. Bahl et al., *Precision calculations in the MSSM Higgs-boson sector with FeynHiggs 2.14*, *Comput. Phys. Commun.* **249** (2020) 107099 [arXiv:1811.09073] [INSPIRE].

[172] A. Djouadi, J. Kalinowski and M. Spira, *HDECAY: A Program for Higgs boson decays in the standard model and its supersymmetric extension*, *Comput. Phys. Commun.* **108** (1998) 56 [hep-ph/9704448] [INSPIRE].

[173] HDECAY collaboration, *HDECAY: Twenty$_{++}$ years after*, *Comput. Phys. Commun.* **238** (2019) 214 [arXiv:1801.09506] [INSPIRE].

[174] LHC Higgs Cross Section Working Group collaboration, *Handbook of LHC Higgs cross sections: 3. Higgs properties*, arXiv:1307.1347 [DOI:10.5170/CERN-2013-004] [INSPIRE].

[175] A. Denner et al., *Standard model Higgs-boson branching ratios with uncertainties*, *Eur. Phys. J. C* **71** (2011) 1753 [arXiv:1107.5909] [INSPIRE].

[176] R.V. Harlander, S. Liebler and H. Mantler, *SusHi: a program for the calculation of Higgs production in gluon fusion and bottom-quark annihilation in the Standard Model and the MSSM*, *Comput. Phys. Commun.* **184** (2013) 1605 [arXiv:1212.3249] [INSPIRE].

[177] R.V. Harlander, S. Liebler and H. Mantler, *SusHi Bento: beyond NNLO and the heavy-top limit*, *Comput. Phys. Commun.* **212** (2017) 239 [arXiv:1605.03190] [INSPIRE].

[178] M. Spira, A. Djouadi, D. Graudenz and P.M. Zerwas, *Higgs boson production at the LHC*, *Nucl. Phys. B* **453** (1995) 17 [hep-ph/9504378] [INSPIRE].

[179] R. Harlander and P. Kant, *Higgs production and decay: analytic results at next-to-leading order QCD*, *JHEP* **12** (2005) 015 [hep-ph/0509189] [INSPIRE].

[180] R.V. Harlander and W.B. Kilgore, *Next-to-next-to-leading order Higgs production at hadron colliders*, *Phys. Rev. Lett.* **88** (2002) 201801 [hep-ph/0201206] [INSPIRE].

[181] C. Anastasiou and K. Melnikov, *Higgs boson production at hadron colliders in NNLO QCD*, *Nucl. Phys. B* **646** (2002) 220 [hep-ph/0207004] [INSPIRE].

[182] V. Ravindran, J. Smith and W.L. van Neerven, *NNLO corrections to the total cross-section for Higgs boson production in hadron hadron collisions*, *Nucl. Phys. B* **665** (2003) 325 [hep-ph/0302135] [INSPIRE].

[183] R.V. Harlander and W.B. Kilgore, *Production of a pseudoscalar Higgs boson at hadron colliders at next-to-next-to leading order*, *JHEP* **10** (2002) 017 [hep-ph/0208096] [INSPIRE].

[184] C. Anastasiou and K. Melnikov, *Pseudoscalar Higgs boson production at hadron colliders in NNLO QCD*, *Phys. Rev. D* **67** (2003) 037501 [hep-ph/0208115] [INSPIRE].

[185] C. Anastasiou et al., *Higgs boson gluon-fusion production beyond threshold in N^3LO QCD*, *JHEP* **03** (2015) 091 [arXiv:1411.3584] [INSPIRE].

[186] C. Anastasiou et al., *Soft expansion of double-real-virtual corrections to Higgs production at N^3LO*, *JHEP* **08** (2015) 051 [arXiv:1505.04110] [INSPIRE].
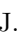
[187] C. Anastasiou et al., *High precision determination of the gluon fusion Higgs boson cross-section at the LHC*, *JHEP* **05** (2016) 058 [arXiv:1602.00695] [INSPIRE].

[188] U. Aglietti, R. Bonciani, G. Degrassi and A. Vicini, *Two loop light fermion contribution to Higgs production and decays*, *Phys. Lett. B* **595** (2004) 432 [hep-ph/0404071] [INSPIRE].

[189] R. Bonciani, G. Degrassi and A. Vicini, *On the generalized harmonic polylogarithms of one complex variable*, *Comput. Phys. Commun.* **182** (2011) 1253 [arXiv:1007.1891] [INSPIRE].

[190] G. Degrassi and P. Slavich, *NLO QCD bottom corrections to Higgs boson production in the MSSM*, *JHEP* **11** (2010) 044 [arXiv:1007.3465] [INSPIRE].

[191] G. Degrassi, S. Di Vita and P. Slavich, *NLO QCD corrections to pseudoscalar Higgs production in the MSSM*, *JHEP* **08** (2011) 128 [arXiv:1107.0914] [INSPIRE].

[192] G. Degrassi, S. Di Vita and P. Slavich, *On the NLO QCD corrections to the production of the heaviest neutral Higgs scalar in the MSSM*, *Eur. Phys. J. C* **72** (2012) 2032 [arXiv:1204.1016] [INSPIRE].

[193] L. Hofer, U. Nierste and D. Scherer, *Resummation of tan-beta-enhanced supersymmetric loop corrections beyond the decoupling limit*, *JHEP* **10** (2009) 081 [arXiv:0907.5408] [INSPIRE].

[194] M. Bonvini, A.S. Papanastasiou and F.J. Tackmann, *Resummation and matching of b-quark mass effects in $b\bar{b}H$ production*, *JHEP* **11** (2015) 196 [arXiv:1508.03288] [INSPIRE].

[195] M. Bonvini, A.S. Papanastasiou and F.J. Tackmann, *Matched predictions for the $b\bar{b}H$ cross section at the 13 TeV LHC*, *JHEP* **10** (2016) 053 [arXiv:1605.01733] [INSPIRE].

[196] S. Dittmaier, M. Krämer and M. Spira, *Higgs radiation off bottom quarks at the Tevatron and the CERN LHC*, *Phys. Rev. D* **70** (2004) 074010 [hep-ph/0309204] [INSPIRE].

[197] S. Dawson, C.B. Jackson, L. Reina and D. Wackeroth, *Exclusive Higgs boson production with bottom quarks at hadron colliders*, *Phys. Rev. D* **69** (2004) 074027 [hep-ph/0311067] [INSPIRE].

[198] R.V. Harlander and W.B. Kilgore, *Higgs boson production in bottom quark fusion at next-to-next-to leading order*, *Phys. Rev. D* **68** (2003) 013001 [hep-ph/0304035] [INSPIRE].

[199] C. Duhr, F. Dulat and B. Mistlberger, *Higgs boson production in bottom-quark fusion to third order in the strong coupling*, *Phys. Rev. Lett.* **125** (2020) 051804 [arXiv:1904.09990] [INSPIRE].

[200] S. Forte, D. Napoletano and M. Ubiali, *Higgs production in bottom-quark fusion in a matched scheme*, *Phys. Lett. B* **751** (2015) 331 [arXiv:1508.01529] [INSPIRE].

[201] S. Forte, D. Napoletano and M. Ubiali, *Higgs production in bottom-quark fusion: matching beyond leading order*, *Phys. Lett. B* **763** (2016) 190 [arXiv:1607.00389] [INSPIRE].

The CMS collaboration

Yerevan Physics Institute, Yerevan, Armenia

A. Tumasyan [1]

Institut für Hochenergiephysik, Vienna, Austria

W. Adam, J.W. Andrejkovic, T. Bergauer, S. Chatterjee, K. Damanakis,
M. Dragicevic, A. Escalante Del Valle, P.S. Hussain, M. Jeitler [2], N. Krammer,
L. Lechner, D. Liko, I. Mikulec, P. Paulitsch, F.M. Pitters, J. Schieck [2], R. Schöfbeck,
D. Schwarz, S. Templ, W. Waltenberger, C.-E. Wulz [2]
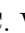
Universiteit Antwerpen, Antwerpen, Belgium

M.R. Darwish [3], T. Janssen, T. Kello [4], H. Rejeb Sfar, P. Van Mechelen

Vrije Universiteit Brussel, Brussel, Belgium

E.S. Bols, J. D'Hondt, A. De Moor, M. Delcourt, H. El Faham, S. Lowette,
S. Moortgat, A. Morton, D. Müller, A.R. Sahasransu, S. Tavernier, W. Van Doninck,
D. Vannerom
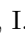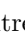
Université Libre de Bruxelles, Bruxelles, Belgium

B. Clerbaux, G. De Lentdecker, L. Favart, D. Hohov, J. Jaramillo, K. Lee,
M. Mahdavikhorrami, I. Makarenko, A. Malara, S. Paredes, L. Pétré, N. Postiau,
E. Starling, L. Thomas, M. Vanden Bemden, C. Vander Velde, P. Vanlaer

Ghent University, Ghent, Belgium

D. Dobur, J. Knolle, L. Lambrecht, G. Mestdach, M. Niedziela, C. Rendón, C. Roskas,
A. Samalan, K. Skovpen, M. Tytgat, N. Van Den Bossche, B. Vermassen, L. Wezenbeek
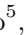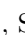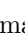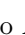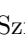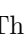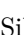
Université Catholique de Louvain, Louvain-la-Neuve, Belgium

A. Benecke, G. Bruno, F. Bury, C. Caputo, P. David, C. Delaere, I.S. Donertas,
A. Giammanco, K. Jaffel, Sa. Jain, V. Lemaitre, K. Mondal, J. Prisciandaro,
A. Taliercio, T.T. Tran, P. Vischia, S. Wertz

Centro Brasileiro de Pesquisas Fisicas, Rio de Janeiro, Brazil

G.A. Alves, E. Coelho, C. Hensel, A. Moraes, P. Rebello Teles

Universidade do Estado do Rio de Janeiro, Rio de Janeiro, Brazil

W.L. Aldá Júnior, M. Alves Gallo Pereira, M. Barroso Ferreira Filho,
H. Brandao Malbouisson, W. Carvalho, J. Chinellato [5], E.M. Da Costa,
G.G. Da Silveira [6], D. De Jesus Damiao, V. Dos Santos Sousa, S. Fonseca De Souza,
J. Martins [7], C. Mora Herrera, K. Mota Amarilo, L. Mundim, H. Nogima,
A. Santoro, S.M. Silva Do Amaral, A. Sznajder, M. Thiel,
F. Torres Da Silva De Araujo [8], A. Vilela Pereira

Universidade Estadual Paulista, Universidade Federal do ABC, São Paulo, Brazil

C.A. Bernardes [6], L. Calligaris, T.R. Fernandez Perez Tomei, E.M. Gregores, P.G. Mercadante, S.F. Novaes, Sandra S. Padula

Institute for Nuclear Research and Nuclear Energy, Bulgarian Academy of Sciences, Sofia, Bulgaria

A. Aleksandrov, G. Antchev, R. Hadjiiska, P. Iaydjiev, M. Misheva, M. Rodozov, M. Shopova, G. Sultanov
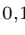
University of Sofia, Sofia, Bulgaria

A. Dimitrov, T. Ivanov, L. Litov, B. Pavlov, P. Petkov, A. Petrov, E. Shumka
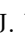
Beihang University, Beijing, China

T. Cheng, T. Javaid [9], M. Mittal, L. Yuan

Department of Physics, Tsinghua University, Beijing, China

M. Ahmad, G. Bauer [10], Z. Hu, S. Lezki, K. Yi [10,11]

Institute of High Energy Physics, Beijing, China

G.M. Chen [9], H.S. Chen [9], M. Chen [9], F. Iemmi, C.H. Jiang, A. Kapoor, H. Liao, Z.-A. Liu [12], V. Milosevic, F. Monti, R. Sharma, J. Tao, J. Thomas-Wilsker, J. Wang, H. Zhang, J. Zhao

State Key Laboratory of Nuclear Physics and Technology, Peking University, Beijing, China

A. Agapitos, Y. An, Y. Ban, C. Chen, A. Levin, C. Li, Q. Li, X. Lyu, Y. Mao, S.J. Qian, X. Sun, D. Wang, J. Xiao, H. Yang

Sun Yat-Sen University, Guangzhou, China

J. Li, M. Lu, Z. You

Institute of Modern Physics and Key Laboratory of Nuclear Physics and Ion-beam Application (MOE) - Fudan University, Shanghai, China

X. Gao [4], D. Leggat, H. Okawa, Y. Zhang

Zhejiang University, Hangzhou, Zhejiang, China

Z. Lin, C. Lu, M. Xiao

Universidad de Los Andes, Bogota, Colombia
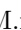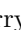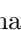
C. Avila, D.A. Barbosa Trujillo, A. Cabrera, C. Florez, J. Fraga

Universidad de Antioquia, Medellin, Colombia
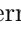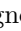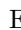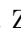
J. Mejia Guisao, F. Ramirez, M. Rodriguez, J.D. Ruiz Alvarez

University of Split, Faculty of Electrical Engineering, Mechanical Engineering and Naval Architecture, Split, Croatia
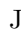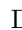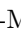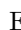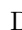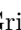
D. Giljanovic, N. Godinovic, D. Lelas, I. Puljak

University of Split, Faculty of Science, Split, Croatia

Z. Antunovic, M. Kovac ©, T. Sculac ©

Institute Rudjer Boskovic, Zagreb, Croatia

V. Brigljevic ©, B.K. Chitroda ©, D. Ferencek ©, D. Majumder ©, M. Roguljic ©,
A. Starodumov ©[13], T. Susa ©

University of Cyprus, Nicosia, Cyprus

A. Attikis ©, K. Christoforou ©, G. Kole ©, M. Kolosova ©, S. Konstantinou ©, J. Mousa ©,
C. Nicolaou, F. Ptochos ©, P.A. Razis ©, H. Rykaczewski, H. Saka ©

Charles University, Prague, Czech Republic

M. Finger ©[13], M. Finger Jr. ©[13], A. Kveton ©

Escuela Politecnica Nacional, Quito, Ecuador

E. Ayala ©

Universidad San Francisco de Quito, Quito, Ecuador

E. Carrera Jarrin ©

**Academy of Scientific Research and Technology of the Arab Republic of
Egypt, Egyptian Network of High Energy Physics, Cairo, Egypt**

H. Abdalla ©[14], Y. Assran[15,16]

**Center for High Energy Physics (CHEP-FU), Fayoum University, El-Fayoum,
Egypt**

M. Abdullah Al-Mashad ©, M.A. Mahmoud ©

National Institute of Chemical Physics and Biophysics, Tallinn, Estonia

S. Bhowmik ©, R.K. Dewanjee ©, K. Ehataht ©, M. Kadastik, T. Lange ©, S. Nandan ©,
C. Nielsen ©, J. Pata ©, M. Raidal ©, L. Tani ©, C. Veelken ©

Department of Physics, University of Helsinki, Helsinki, Finland

P. Eerola ©, H. Kirschenmann ©, K. Osterberg ©, M. Voutilainen ©

Helsinki Institute of Physics, Helsinki, Finland

S. Bharthuar ©, E. Brücken ©, F. Garcia ©, J. Havukainen ©, M.S. Kim ©, R. Kinnunen,
T. Lampén ©, K. Lassila-Perini ©, S. Lehti ©, T. Lindén ©, M. Lotti, L. Martikainen ©,
M. Myllymäki ©, J. Ott ©, M.m. Rantanen ©, H. Siikonen ©, E. Tuominen ©, J. Tuominiemi ©

Lappeenranta-Lahti University of Technology, Lappeenranta, Finland

P. Luukka ©, H. Petrow ©, T. Tuuva

IRFU, CEA, Université Paris-Saclay, Gif-sur-Yvette, France

C. Amendola ©, M. Besancon ©, F. Couderc ©, M. Dejardin ©, D. Denegri, J.L. Faure, F. Ferri ©,
S. Ganjour ©, P. Gras ©, G. Hamel de Monchenault ©, P. Jarry ©, V. Lohezic, J. Malcles ©,
J. Rander, A. Rosowsky ©, M.Ö. Sahin ©, A. Savoy-Navarro ©[17], P. Simkina ©, M. Titov ©
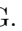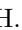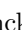
Laboratoire Leprince-Ringuet, CNRS/IN2P3, Ecole Polytechnique, Institut Polytechnique de Paris, Palaiseau, France

C. Baldenegro Barrera ⓘ, F. Beaudette ⓘ, A. Buchot Perraguin ⓘ, P. Busson ⓘ, A. Cappati ⓘ, C. Charlot ⓘ, F. Damas ⓘ, O. Davignon ⓘ, B. Diab ⓘ, G. Falmagne ⓘ, B.A. Fontana Santos Alves ⓘ, S. Ghosh ⓘ, R. Granier de Cassagnac ⓘ, A. Hakimi ⓘ, B. Harikrishnan ⓘ, G. Liu ⓘ, J. Motta ⓘ, M. Nguyen ⓘ, C. Ochando ⓘ, L. Portales ⓘ, J. Rembser ⓘ, R. Salerno ⓘ, U. Sarkar ⓘ, J.B. Sauvan ⓘ, Y. Sirois ⓘ, A. Tarabini ⓘ, E. Vernazza ⓘ, A. Zabi ⓘ, A. Zghiche ⓘ

Université de Strasbourg, CNRS, IPHC UMR 7178, Strasbourg, France

J.-L. Agram ⓘ[18], J. Andrea ⓘ, D. Apparu ⓘ, D. Bloch ⓘ, G. Bourgatte ⓘ, J.-M. Brom ⓘ, E.C. Chabert ⓘ, C. Collard ⓘ, D. Darej, U. Goerlach ⓘ, C. Grimault, A.-C. Le Bihan ⓘ, P. Van Hove ⓘ

Institut de Physique des 2 Infinis de Lyon (IP2I), Villeurbanne, France

S. Beauceron ⓘ, C. Bernet ⓘ, B. Blancon ⓘ, G. Boudoul ⓘ, A. Carle, N. Chanon ⓘ, J. Choi ⓘ, D. Contardo ⓘ, P. Depasse ⓘ, C. Dozen ⓘ[19], H. El Mamouni, J. Fay ⓘ, S. Gascon ⓘ, M. Gouzevitch ⓘ, G. Grenier ⓘ, B. Ille ⓘ, I.B. Laktineh, M. Lethuillier ⓘ, L. Mirabito, S. Perries, V. Sordini ⓘ, L. Torterotot ⓘ, M. Vander Donckt ⓘ, P. Verdier ⓘ, S. Viret
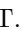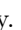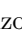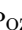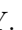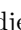
Georgian Technical University, Tbilisi, Georgia

D. Chokheli ⓘ, I. Lomidze ⓘ, Z. Tsamalaidze ⓘ[13]
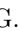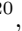
RWTH Aachen University, I. Physikalisches Institut, Aachen, Germany

V. Botta ⓘ, L. Feld ⓘ, K. Klein ⓘ, M. Lipinski ⓘ, D. Meuser ⓘ, A. Pauls ⓘ, N. Röwert ⓘ, M. Teroerde ⓘ
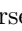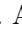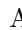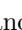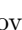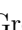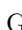
RWTH Aachen University, III. Physikalisches Institut A, Aachen, Germany

S. Diekmann ⓘ, A. Dodonova ⓘ, N. Eich ⓘ, D. Eliseev ⓘ, M. Erdmann ⓘ, P. Fackeldey ⓘ, D. Fasanella ⓘ, B. Fischer ⓘ, T. Hebbeker ⓘ, K. Hoepfner ⓘ, F. Ivone ⓘ, M.y. Lee ⓘ, L. Mastrolorenzo, M. Merschmeyer ⓘ, A. Meyer ⓘ, S. Mondal ⓘ, S. Mukherjee ⓘ, D. Noll ⓘ, A. Novak ⓘ, F. Nowotny, A. Pozdnyakov ⓘ, Y. Rath, W. Redjeb ⓘ, H. Reithler ⓘ, A. Schmidt ⓘ, S.C. Schuler, A. Sharma ⓘ, L. Vigilante, S. Wiedenbeck ⓘ, S. Zaleski

RWTH Aachen University, III. Physikalisches Institut B, Aachen, Germany
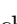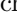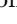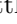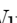
C. Dziwok ⓘ, G. Flügge ⓘ, W. Haj Ahmad ⓘ[20], O. Hlushchenko, T. Kress ⓘ, A. Nowack ⓘ, O. Pooth ⓘ, A. Stahl ⓘ[21], T. Ziemons ⓘ, A. Zotz ⓘ

Deutsches Elektronen-Synchrotron, Hamburg, Germany
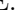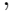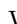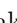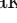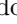
H. Aarup Petersen ⓘ, M. Aldaya Martin ⓘ, P. Asmuss, S. Baxter ⓘ, M. Bayatmakou ⓘ, O. Behnke ⓘ, A. Bermúdez Martínez ⓘ, S. Bhattacharya ⓘ, A.A. Bin Anuar ⓘ, F. Blekman ⓘ[22], K. Borras ⓘ[23], D. Brunner ⓘ, A. Campbell ⓘ, A. Cardini ⓘ, C. Cheng, F. Colombina, S. Consuegra Rodríguez ⓘ, G. Correia Silva ⓘ, M. De Silva ⓘ, L. Didukh ⓘ, G. Eckerlin, D. Eckstein ⓘ, L.I. Estevez Banos ⓘ, O. Filatov ⓘ, E. Gallo ⓘ[22], A. Geiser ⓘ, A. Giraldi ⓘ, G. Greau, A. Grohsjean ⓘ, V. Guglielmi ⓘ, M. Guthoff ⓘ, A. Jafari ⓘ[24], N.Z. Jomhari ⓘ,

B. Kaech, A. Kasem[23], M. Kasemann, H. Kaveh, C. Kleinwort, R. Kogler,
M. Komm, D. Krücker, W. Lange, D. Leyva Pernia, K. Lipka, W. Lohmann[25],
R. Mankel, I.-A. Melzer-Pellmann, M. Mendizabal Morentin, J. Metwally, A.B. Meyer,
G. Milella, M. Mormile, A. Mussgiller, A. Nürnberg, Y. Otarid, D. Pérez Adán,
A. Raspereza, B. Ribeiro Lopes, J. Rübenach, A. Saggio, A. Saibel, M. Savitskyi,
M. Scham[26,23], V. Scheurer, S. Schnake[23], P. Schütze, C. Schwanenberger[22],
M. Shchedrolosiev, R.E. Sosa Ricardo, D. Stafford, N. Tonon[†], M. Van De Klundert,
F. Vazzoler, A. Ventura Barroso, R. Walsh, D. Walter, Q. Wang, Y. Wen,
K. Wichmann, L. Wiens[23], C. Wissing, S. Wuchterl, Y. Yang,
A. Zimermmane Castro Santos

University of Hamburg, Hamburg, Germany

R. Aggleton, A. Albrecht, S. Albrecht, M. Antonello, S. Bein, L. Benato,
M. Bonanomi, P. Connor, K. De Leo, M. Eich, K. El Morabit, F. Feindt, A. Fröhlich,
C. Garbers, E. Garutti, M. Hajheidari, J. Haller, A. Hinzmann, H.R. Jabusch,
G. Kasieczka, R. Klanner, W. Korcari, T. Kramer, V. Kutzner, J. Lange,
A. Lobanov, C. Matthies, A. Mehta, L. Moureaux, M. Mrowietz, A. Nigamova,
Y. Nissan, A. Paasch, K.J. Pena Rodriguez, M. Rieger, O. Rieger, P. Schleper,
M. Schröder, J. Schwandt, H. Stadie, G. Steinbrück, A. Tews, M. Wolf
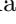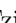
Karlsruher Institut fuer Technologie, Karlsruhe, Germany

J. Bechtel, S. Brommer, M. Burkart, E. Butz, R. Caspart, T. Chwalek,
A. Dierlamm, A. Droll, N. Faltermann, M. Giffels, J.O. Gosewisch, A. Gottmann,
F. Hartmann[21], M. Horzela, U. Husemann, P. Keicher, M. Klute, R. Koppenhöfer,
S. Maier, S. Mitra, Th. Müller, M. Neukum, G. Quast, K. Rabbertz, J. Rauser,
D. Savoiu, M. Schnepf, D. Seith, I. Shvetsov, H.J. Simonis, N. Trevisani, R. Ulrich,
J. van der Linden, R.F. Von Cube, M. Wassmer, M. Weber, S. Wieland, R. Wolf,
S. Wozniewski, S. Wunsch

Institute of Nuclear and Particle Physics (INPP), NCSR Demokritos, Aghia Paraskevi, Greece

G. Anagnostou, P. Assiouras, G. Daskalakis, A. Kyriakis, A. Stakia

National and Kapodistrian University of Athens, Athens, Greece

M. Diamantopoulou, D. Karasavvas, P. Kontaxakis, A. Manousakis-Katsikakis,
A. Panagiotou, I. Papavergou, N. Saoulidou, K. Theofilatos, E. Tziaferi, K. Vellidis,
E. Vourliotis, I. Zisopoulos

National Technical University of Athens, Athens, Greece

G. Bakas, T. Chatzistavrou, K. Kousouris, I. Papakrivopoulos, G. Tsipolitis,
A. Zacharopoulou

University of Ioánnina, Ioánnina, Greece

K. Adamidis, I. Bestintzanos, I. Evangelou, C. Foudas, P. Gianneios, C. Kamtsikis,
P. Katsoulis, P. Kokkas, P.G. Kosmoglou Kioseoglou, N. Manthos, I. Papadopoulos,
J. Strologas

MTA-ELTE Lendület CMS Particle and Nuclear Physics Group, Eötvös Loránd University, Budapest, Hungary

M. Csanád [iD], K. Farkas [iD], M.M.A. Gadallah [iD][27], S. Lökös [iD][28], P. Major [iD], K. Mandal [iD], G. Pásztor [iD], A.J. Rádl [iD][29], O. Surányi [iD], G.I. Veres [iD]

Wigner Research Centre for Physics, Budapest, Hungary

M. Bartók [iD][30], G. Bencze, C. Hajdu [iD], D. Horvath [iD][31,32], F. Sikler [iD], V. Veszpremi [iD]

Institute of Nuclear Research ATOMKI, Debrecen, Hungary

N. Beni [iD], S. Czellar, J. Karancsi [iD][30], J. Molnar, Z. Szillasi, D. Teyssier [iD]

Institute of Physics, University of Debrecen, Debrecen, Hungary

P. Raics, B. Ujvari [iD][33]
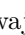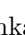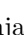
Karoly Robert Campus, MATE Institute of Technology, Gyongyos, Hungary

T. Csorgo [iD][29], F. Nemes [iD][29], T. Novak [iD]
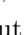
Panjab University, Chandigarh, India

J. Babbar [iD], S. Bansal [iD], S.B. Beri, V. Bhatnagar [iD], G. Chaudhary [iD], S. Chauhan [iD], N. Dhingra [iD][34], R. Gupta, A. Kaur [iD], A. Kaur [iD], H. Kaur [iD], M. Kaur [iD], S. Kumar [iD], P. Kumari [iD], M. Meena [iD], K. Sandeep [iD], T. Sheokand, J.B. Singh [iD][35], A. Singla, A. K. Virdi [iD]
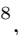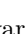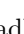
University of Delhi, Delhi, India

A. Ahmed [iD], A. Bhardwaj [iD], B.C. Choudhary [iD], M. Gola, S. Keshri [iD], A. Kumar [iD], M. Naimuddin [iD], P. Priyanka [iD], K. Ranjan [iD], S. Saumya [iD], A. Shah [iD]

Saha Institute of Nuclear Physics, HBNI, Kolkata, India

S. Baradia [iD], S. Barman [iD][36], S. Bhattacharya [iD], D. Bhowmik, S. Dutta [iD], S. Dutta, B. Gomber [iD][37], M. Maity[36], P. Palit [iD], P.K. Rout [iD], G. Saha [iD], B. Sahu [iD], S. Sarkar

Indian Institute of Technology Madras, Madras, India

P.K. Behera [iD], S.C. Behera [iD], P. Kalbhor [iD], J.R. Komaragiri [iD][38], D. Kumar [iD][38], A. Muhammad [iD], L. Panwar [iD][38], R. Pradhan [iD], P.R. Pujahari [iD], A. Sharma [iD], A.K. Sikdar [iD], P.C. Tiwari [iD][38], S. Verma [iD]

Bhabha Atomic Research Centre, Mumbai, India

K. Naskar [iD][39]

Tata Institute of Fundamental Research-A, Mumbai, India

T. Aziz, I. Das [iD], S. Dugad, M. Kumar [iD], G.B. Mohanty [iD], P. Suryadevara

Tata Institute of Fundamental Research-B, Mumbai, India

S. Banerjee [iD], R. Chudasama [iD], M. Guchait [iD], S. Karmakar [iD], S. Kumar [iD], G. Majumder [iD], K. Mazumdar [iD], S. Mukherjee [iD], A. Thachayath [iD]

National Institute of Science Education and Research, An OCC of Homi Bhabha National Institute, Bhubaneswar, Odisha, India

S. Bahinipati [40], A.K. Das, C. Kar, P. Mal, T. Mishra, V.K. Muraleedharan Nair Bindhu [41], A. Nayak [41], P. Saha, N. Sur, S.K. Swain, D. Vats [41]

Indian Institute of Science Education and Research (IISER), Pune, India

A. Alpana, S. Dube, B. Kansal, A. Laha, S. Pandey, A. Rastogi, S. Sharma

Isfahan University of Technology, Isfahan, Iran

H. Bakhshiansohi [42], E. Khazaie, M. Zeinali [43]
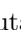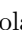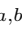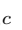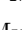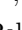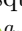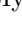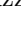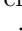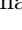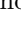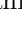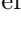
Institute for Research in Fundamental Sciences (IPM), Tehran, Iran

S. Chenarani [44], S.M. Etesami, M. Khakzad, M. Mohammadi Najafabadi
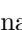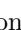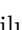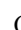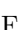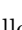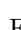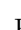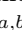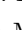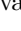
University College Dublin, Dublin, Ireland

M. Grunewald

INFN Sezione di Bari[a]**, Università di Bari**[b]**, Politecnico di Bari**[c]**, Bari, Italy**

M. Abbrescia [a,b], R. Aly [a,c,45], C. Aruta [a,b], A. Colaleo [a], D. Creanza [a,c], N. De Filippis [a,c], M. De Palma [a,b], A. Di Florio [a,b], W. Elmetenawee [a,b], F. Errico [a,b], L. Fiore [a], G. Iaselli [a,c], M. Ince [a,b], G. Maggi [a,c], M. Maggi [a], I. Margjeka [a,b], V. Mastrapasqua [a,b], S. My [a,b], S. Nuzzo [a,b], A. Pellecchia [a,b], A. Pompili [a,b], G. Pugliese [a,c], R. Radogna [a], D. Ramos [a], A. Ranieri [a], G. Selvaggi [a,b], L. Silvestris [a], F.M. Simone [a,b], Ü. Sözbilir [a], A. Stamerra [a], R. Venditti [a], P. Verwilligen [a]
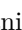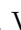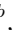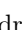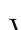
INFN Sezione di Bologna[a]**, Università di Bologna**[b]**, Bologna, Italy**

G. Abbiendi [a], C. Battilana [a,b], D. Bonacorsi [a,b], L. Borgonovi [a], L. Brigliadori[a], R. Campanini [a,b], P. Capiluppi [a,b], A. Castro [a,b], F.R. Cavallo [a], M. Cuffiani [a,b], G.M. Dallavalle [a], T. Diotalevi [a,b], F. Fabbri [a], A. Fanfani [a,b], P. Giacomelli [a], L. Giommi [a,b], C. Grandi [a], L. Guiducci [a,b], S. Lo Meo [a,46], L. Lunerti [a,b], S. Marcellini [a], G. Masetti [a], F.L. Navarria [a,b], A. Perrotta [a], F. Primavera [a,b], A.M. Rossi [a,b], T. Rovelli [a,b], G.P. Siroli [a,b]

INFN Sezione di Catania[a]**, Università di Catania**[b]**, Catania, Italy**

S. Costa [a,b,47], A. Di Mattia [a], R. Potenza[a,b], A. Tricomi [a,b,47], C. Tuve [a,b]

INFN Sezione di Firenze[a]**, Università di Firenze**[b]**, Firenze, Italy**

G. Barbagli [a], B. Camaiani [a,b], A. Cassese [a], R. Ceccarelli [a,b], V. Ciulli [a,b], C. Civinini [a], R. D'Alessandro [a,b], E. Focardi [a,b], G. Latino [a,b], P. Lenzi [a,b], M. Lizzo [a,b], M. Meschini [a], S. Paoletti [a], R. Seidita [a,b], G. Sguazzoni [a], L. Viliani [a]
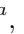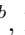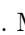
INFN Laboratori Nazionali di Frascati, Frascati, Italy

L. Benussi, S. Bianco, S. Meola [21], D. Piccolo
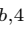
INFN Sezione di Genova[a]**, Università di Genova**[b]**, Genova, Italy**

M. Bozzo [a,b], F. Ferro [a], R. Mulargia [a], E. Robutti [a], S. Tosi [a,b]
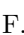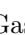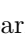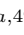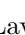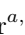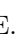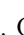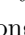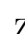
INFN Sezione di Milano-Bicocca^a, Università di Milano-Bicocca^b, Milano, Italy

A. Benaglia ^{a}, G. Boldrini ^{a}, F. Brivio ^{a,b}, F. Cetorelli ^{a,b}, F. De Guio ^{a,b}, M.E. Dinardo ^{a,b}, P. Dini ^{a}, S. Gennai ^{a}, A. Ghezzi ^{a,b}, P. Govoni ^{a,b}, L. Guzzi ^{a,b}, M.T. Lucchini ^{a,b}, M. Malberti ^{a}, S. Malvezzi ^{a}, A. Massironi ^{a}, D. Menasce ^{a}, L. Moroni ^{a}, M. Paganoni ^{a,b}, D. Pedrini ^{a}, B.S. Pinolini^a, S. Ragazzi ^{a,b}, N. Redaelli ^{a}, T. Tabarelli de Fatis ^{a,b}, D. Zuolo ^{a,b}
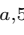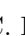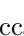
INFN Sezione di Napoli^a, Università di Napoli 'Federico II'^{b}, Napoli, Italy; Università della Basilicata^c, Potenza, Italy; Università G. Marconi^d, Roma, Italy

S. Buontempo ^{a}, F. Carnevali^{a,b}, N. Cavallo ^{a,c}, A. De Iorio ^{a,b}, F. Fabozzi ^{a,c}, A.O.M. Iorio ^{a,b}, L. Lista ^{a,b,48}, P. Paolucci ^{a,21}, B. Rossi ^{a}, C. Sciacca ^{a,b}
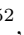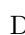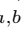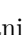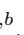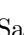
INFN Sezione di Padova^a, Università di Padova^b, Padova, Italy; Università di Trento^c, Trento, Italy

P. Azzi ^{a}, D. Bisello ^{a,b}, P. Bortignon ^{a}, A. Bragagnolo ^{a,b}, R. Carlin ^{a,b}, P. Checchia ^{a}, T. Dorigo ^{a}, F. Gasparini ^{a,b}, U. Gasparini ^{a,b}, G. Govi^a, A. Gozzelino ^{a}, G. Grosso^a, M. Gulmini ^{a,49}, L. Layer^{a,50}, E. Lusiani ^{a}, M. Margoni ^{a,b}, J. Pazzini ^{a,b}, P. Ronchese ^{a,b}, R. Rossin ^{a,b}, G. Strong ^{a}, M. Tosi ^{a,b}, H. Yarar^{a,b}, M. Zanetti ^{a,b}, P. Zotto ^{a,b}, A. Zucchetta ^{a,b}, G. Zumerle ^{a,b}
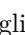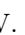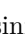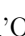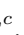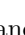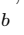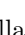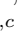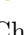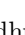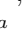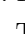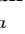
INFN Sezione di Pavia^a, Università di Pavia^b, Pavia, Italy

S. Abu Zeid ^{a,51}, C. Aimè ^{a,b}, A. Braghieri ^{a}, S. Calzaferri ^{a,b}, D. Fiorina ^{a,b}, P. Montagna ^{a,b}, V. Re ^{a}, C. Riccardi ^{a,b}, P. Salvini ^{a}, I. Vai ^{a}, P. Vitulo ^{a,b}
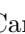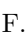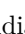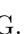
INFN Sezione di Perugia^a, Università di Perugia^b, Perugia, Italy

P. Asenov ^{a,52}, G.M. Bilei ^{a}, D. Ciangottini ^{a,b}, L. Fanò ^{a,b}, M. Magherini ^{a,b}, G. Mantovani^{a,b}, V. Mariani ^{a,b}, M. Menichelli ^{a}, F. Moscatelli ^{a,52}, A. Piccinelli ^{a,b}, M. Presilla ^{a,b}, A. Rossi ^{a,b}, A. Santocchia ^{a,b}, D. Spiga ^{a}, T. Tedeschi ^{a,b}

INFN Sezione di Pisa^a, Università di Pisa^b, Scuola Normale Superiore di Pisa^c, Pisa, Italy; Università di Siena^d, Siena, Italy
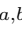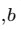
P. Azzurri ^{a}, G. Bagliesi ^{a}, V. Bertacchi ^{a,c}, R. Bhattacharya ^{a}, L. Bianchini ^{a,b}, T. Boccali ^{a}, E. Bossini ^{a,b}, D. Bruschini ^{a,c}, R. Castaldi ^{a}, M.A. Ciocci ^{a,b}, V. D'Amante ^{a,d}, R. Dell'Orso ^{a}, M.R. Di Domenico ^{a,d}, S. Donato ^{a}, A. Giassi ^{a}, F. Ligabue ^{a,c}, E. Manca ^{a,c}, G. Mandorli ^{a,c}, D. Matos Figueiredo ^{a}, A. Messineo ^{a,b}, M. Musich ^{a,b}, F. Palla ^{a}, S. Parolia ^{a,b}, G. Ramirez-Sanchez ^{a,c}, A. Rizzi ^{a,b}, G. Rolandi ^{a,c}, S. Roy Chowdhury ^{a,c}, T. Sarkar ^{a,36}, A. Scribano ^{a}, N. Shafiei ^{a,b}, P. Spagnolo ^{a}, R. Tenchini ^{a}, G. Tonelli ^{a,b}, N. Turini ^{a,d}, A. Venturi ^{a}, P.G. Verdini ^{a}

INFN Sezione di Roma^a, Sapienza Università di Roma^b, Roma, Italy
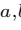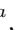
P. Barria ^{a}, M. Campana ^{a,b}, F. Cavallari ^{a}, D. Del Re ^{a,b}, E. Di Marco ^{a}, M. Diemoz ^{a}, E. Longo ^{a,b}, P. Meridiani ^{a}, G. Organtini ^{a,b}, F. Pandolfi ^{a}, R. Paramatti ^{a,b},

C. Quaranta<img>^{a,b}, S. Rahatlou<img>^{a,b}, C. Rovelli<img>^{a}, F. Santanastasio<img>^{a,b}, L. Soffi<img>^{a},
R. Tramontano<img>^{a,b}

INFN Sezione di Torino^{a}, Università di Torino^{b}, Torino, Italy; Università del Piemonte Orientale^{c}, Novara, Italy

N. Amapane<img>^{a,b}, R. Arcidiacono<img>^{a,c}, S. Argiro<img>^{a,b}, M. Arneodo<img>^{a,c}, N. Bartosik<img>^{a},
R. Bellan<img>^{a,b}, A. Bellora<img>^{a,b}, J. Berenguer Antequera<img>^{a,b}, C. Biino<img>^{a}, N. Cartiglia<img>^{a},
M. Costa<img>^{a,b}, R. Covarelli<img>^{a,b}, N. Demaria<img>^{a}, M. Grippo<img>^{a,b}, B. Kiani<img>^{a,b}, F. Legger<img>^{a},
C. Mariotti<img>^{a}, S. Maselli<img>^{a}, A. Mecca<img>^{a,b}, E. Migliore<img>^{a,b}, E. Monteil<img>^{a,b}, M. Monteno<img>^{a},
M.M. Obertino<img>^{a,b}, G. Ortona<img>^{a}, L. Pacher<img>^{a,b}, N. Pastrone<img>^{a}, M. Pelliccioni<img>^{a},
M. Ruspa<img>^{a,c}, K. Shchelina<img>^{a}, F. Siviero<img>^{a,b}, V. Sola<img>^{a}, A. Solano<img>^{a,b}, D. Soldi<img>^{a,b},
A. Staiano<img>^{a}, M. Tornago<img>^{a,b}, D. Trocino<img>^{a}, G. Umoret<img>^{a,b}, A. Vagnerini<img>^{a,b}

INFN Sezione di Trieste^{a}, Università di Trieste^{b}, Trieste, Italy

S. Belforte<img>^{a}, V. Candelise<img>^{a,b}, M. Casarsa<img>^{a}, F. Cossutti<img>^{a}, A. Da Rold<img>^{a,b},
G. Della Ricca<img>^{a,b}, G. Sorrentino<img>^{a,b}

Kyungpook National University, Daegu, Korea

S. Dogra<img>, C. Huh<img>, B. Kim<img>, D.H. Kim<img>, G.N. Kim<img>, J. Kim, J. Lee<img>, S.W. Lee<img>,
C.S. Moon<img>, Y.D. Oh<img>, S.I. Pak<img>, M.S. Ryu<img>, S. Sekmen<img>, Y.C. Yang<img>
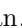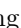
Chonnam National University, Institute for Universe and Elementary Particles, Kwangju, Korea

H. Kim<img>, D.H. Moon<img>

Hanyang University, Seoul, Korea

E. Asilar<img>, T.J. Kim<img>, J. Park<img>

Korea University, Seoul, Korea

S. Cho, S. Choi<img>, S. Han, B. Hong<img>, K. Lee, K.S. Lee<img>, J. Lim, J. Park, S.K. Park, J. Yoo<img>

Kyung Hee University, Department of Physics, Seoul, Korea

J. Goh<img>
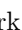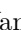
Sejong University, Seoul, Korea

H. S. Kim<img>, Y. Kim, S. Lee

Seoul National University, Seoul, Korea

J. Almond, J.H. Bhyun, J. Choi<img>, S. Jeon<img>, W. Jun<img>, J. Kim<img>, J. Kim<img>, J.S. Kim, S. Ko<img>,
H. Kwon<img>, H. Lee<img>, J. Lee<img>, S. Lee, B.H. Oh<img>, M. Oh<img>, S.B. Oh<img>, H. Seo<img>, U.K. Yang,
I. Yoon<img>

University of Seoul, Seoul, Korea

W. Jang<img>, D.Y. Kang, Y. Kang<img>, D. Kim<img>, S. Kim<img>, B. Ko, J.S.H. Lee<img>, Y. Lee<img>,
J.A. Merlin, I.C. Park<img>, Y. Roh, D. Song, Watson, I.J.<img>, S. Yang<img>

Yonsei University, Department of Physics, Seoul, Korea

S. Ha , H.D. Yoo

Sungkyunkwan University, Suwon, Korea

M. Choi , M.R. Kim , H. Lee, Y. Lee , Y. Lee , I. Yu

College of Engineering and Technology, American University of the Middle East (AUM), Dasman, Kuwait

T. Beyrouthy, Y. Maghrbi

Riga Technical University, Riga, Latvia

K. Dreimanis , A. Gaile , A. Potrebko , T. Torims , V. Veckalns

Vilnius University, Vilnius, Lithuania

M. Ambrozas , A. Carvalho Antunes De Oliveira , A. Juodagalvis , A. Rinkevicius , G. Tamulaitis

National Centre for Particle Physics, Universiti Malaya, Kuala Lumpur, Malaysia

N. Bin Norjoharuddeen , S.Y. Hoh [53], I. Yusuff [53], Z. Zolkapli

Universidad de Sonora (UNISON), Hermosillo, Mexico

J.F. Benitez , A. Castaneda Hernandez , H.A. Encinas Acosta, L.G. Gallegos Maríñez, M. León Coello , J.A. Murillo Quijada , A. Sehrawat , L. Valencia Palomo

Centro de Investigacion y de Estudios Avanzados del IPN, Mexico City, Mexico

G. Ayala , H. Castilla-Valdez , I. Heredia-De La Cruz [54], R. Lopez-Fernandez , C.A. Mondragon Herrera, D.A. Perez Navarro , A. Sánchez Hernández

Universidad Iberoamericana, Mexico City, Mexico

C. Oropeza Barrera , F. Vazquez Valencia

Benemerita Universidad Autonoma de Puebla, Puebla, Mexico

I. Pedraza , H.A. Salazar Ibarguen , C. Uribe Estrada

University of Montenegro, Podgorica, Montenegro

I. Bubanja, J. Mijuskovic [55], N. Raicevic

National Centre for Physics, Quaid-I-Azam University, Islamabad, Pakistan

A. Ahmad , M.I. Asghar, A. Awais , M.I.M. Awan, M. Gul , H.R. Hoorani , W.A. Khan , M. Shoaib , M. Waqas

AGH University of Science and Technology Faculty of Computer Science, Electronics and Telecommunications, Krakow, Poland

V. Avati, L. Grzanka , M. Malawski

National Centre for Nuclear Research, Swierk, Poland

H. Bialkowska , M. Bluj , B. Boimska , M. Górski , M. Kazana , M. Szleper ,
P. Zalewski

Institute of Experimental Physics, Faculty of Physics, University of Warsaw, Warsaw, Poland

K. Bunkowski , K. Doroba , A. Kalinowski , M. Konecki , J. Krolikowski
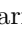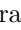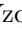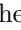
Laboratório de Instrumentação e Física Experimental de Partículas, Lisboa, Portugal

M. Araujo , P. Bargassa , D. Bastos , A. Boletti , P. Faccioli , M. Gallinaro , J. Hollar ,
N. Leonardo , T. Niknejad , M. Pisano , J. Seixas , O. Toldaiev , J. Varela

VINCA Institute of Nuclear Sciences, University of Belgrade, Belgrade, Serbia

P. Adzic [56], M. Dordevic , P. Milenovic , J. Milosevic
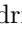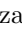
Centro de Investigaciones Energéticas Medioambientales y Tecnológicas (CIEMAT), Madrid, Spain

M. Aguilar-Benitez, J. Alcaraz Maestre , A. Álvarez Fernández , M. Barrio Luna,
Cristina F. Bedoya , C.A. Carrillo Montoya , M. Cepeda , M. Cerrada , N. Colino ,
B. De La Cruz , A. Delgado Peris , D. Fernández Del Val , J.P. Fernández Ramos ,
J. Flix , M.C. Fouz , O. Gonzalez Lopez , S. Goy Lopez , J.M. Hernandez , M.I. Josa ,
J. León Holgado , D. Moran , C. Perez Dengra , A. Pérez-Calero Yzquierdo ,
J. Puerta Pelayo , I. Redondo , D.D. Redondo Ferrero , L. Romero, S. Sánchez Navas ,
J. Sastre , L. Urda Gómez , J. Vazquez Escobar , C. Willmott
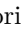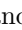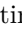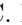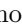
Universidad Autónoma de Madrid, Madrid, Spain

J.F. de Trocóniz

Universidad de Oviedo, Instituto Universitario de Ciencias y Tecnologías Espaciales de Asturias (ICTEA), Oviedo, Spain

B. Alvarez Gonzalez , J. Cuevas , J. Fernandez Menendez , S. Folgueras ,
I. Gonzalez Caballero , J.R. González Fernández , E. Palencia Cortezon ,
C. Ramón Álvarez , V. Rodríguez Bouza , A. Soto Rodríguez , A. Trapote ,
C. Vico Villalba
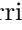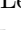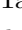
Instituto de Física de Cantabria (IFCA), CSIC-Universidad de Cantabria, Santander, Spain

J.A. Brochero Cifuentes , I.J. Cabrillo , A. Calderon , J. Duarte Campderros ,
M. Fernandez , C. Fernandez Madrazo , A. García Alonso, G. Gomez , C. Lasaosa García ,
C. Martinez Rivero , P. Martinez Ruiz del Arbol , F. Matorras , P. Matorras Cuevas ,
J. Piedra Gomez , C. Prieels, A. Ruiz-Jimeno , L. Scodellaro , I. Vila , J.M. Vizan Garcia
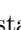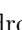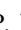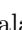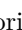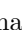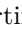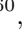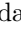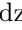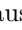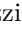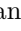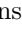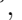
University of Colombo, Colombo, Sri Lanka

M.K. Jayananda , B. Kailasapathy [57], D.U.J. Sonnadara , D.D.C. Wickramarathna
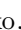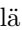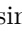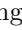
University of Ruhuna, Department of Physics, Matara, Sri Lanka

W.G.D. Dharmaratna [ID], K. Liyanage [ID], N. Perera [ID], N. Wickramage [ID]

CERN, European Organization for Nuclear Research, Geneva, Switzerland

D. Abbaneo [ID], J. Alimena [ID], E. Auffray [ID], G. Auzinger [ID], J. Baechler, P. Baillon[†], D. Barney [ID], J. Bendavid [ID], M. Bianco [ID], B. Bilin [ID], A. Bocci [ID], E. Brondolin [ID], C. Caillol [ID], T. Camporesi [ID], G. Cerminara [ID], N. Chernyavskaya [ID], S.S. Chhibra [ID], S. Choudhury, M. Cipriani [ID], L. Cristella [ID], D. d'Enterria [ID], A. Dabrowski [ID], A. David [ID], A. De Roeck [ID], M.M. Defranchis [ID], M. Deile [ID], M. Dobson [ID], M. Dünser [ID], N. Dupont, A. Elliott-Peisert, F. Fallavollita[58], A. Florent [ID], L. Forthomme [ID], G. Franzoni [ID], W. Funk [ID], S. Ghosh [ID], S. Giani, D. Gigi, K. Gill [ID], F. Glege [ID], L. Gouskos [ID], E. Govorkova [ID], M. Haranko [ID], J. Hegeman [ID], V. Innocente [ID], T. James [ID], P. Janot [ID], J. Kaspar [ID], J. Kieseler [ID], N. Kratochwil [ID], S. Laurila [ID], P. Lecoq [ID], E. Leutgeb [ID], A. Lintuluoto [ID], C. Lourenço [ID], B. Maier [ID], L. Malgeri [ID], M. Mannelli [ID], A.C. Marini [ID], F. Meijers [ID], S. Mersi [ID], E. Meschi [ID], F. Moortgat [ID], M. Mulders [ID], S. Orfanelli, L. Orsini, F. Pantaleo [ID], E. Perez, M. Peruzzi [ID], A. Petrilli [ID], G. Petrucciani [ID], A. Pfeiffer [ID], M. Pierini [ID], D. Piparo [ID], M. Pitt, H. Qu [ID], T. Quast, D. Rabady [ID], A. Racz, G. Reales Gutiérrez, M. Rovere [ID], H. Sakulin [ID], J. Salfeld-Nebgen [ID], S. Scarfi [ID], M. Selvaggi [ID], A. Sharma [ID], P. Silva [ID], P. Sphicas [ID][59], A.G. Stahl Leiton [ID], S. Summers [ID], K. Tatar [ID], V.R. Tavolaro [ID], D. Treille [ID], P. Tropea [ID], A. Tsirou, J. Wanczyk [ID][60], K.A. Wozniak [ID], W.D. Zeuner

Paul Scherrer Institut, Villigen, Switzerland

L. Caminada [ID][61], A. Ebrahimi [ID], W. Erdmann [ID], R. Horisberger [ID], Q. Ingram [ID], H.C. Kaestli [ID], D. Kotlinski [ID], C. Lange [ID], M. Missiroli [ID][61], L. Noehte [ID][61], T. Rohe [ID]

ETH Zurich - Institute for Particle Physics and Astrophysics (IPA), Zurich, Switzerland

T.K. Aarrestad [ID], K. Androsov [ID][60], M. Backhaus [ID], P. Berger, A. Calandri [ID], K. Datta [ID], A. De Cosa [ID], G. Dissertori [ID], M. Dittmar, M. Donegà [ID], F. Eble [ID], M. Galli [ID], K. Gedia [ID], F. Glessgen [ID], T.A. Gómez Espinosa [ID], C. Grab [ID], D. Hits [ID], W. Lustermann [ID], A.-M. Lyon [ID], R.A. Manzoni [ID], L. Marchese [ID], C. Martin Perez [ID], A. Mascellani [ID][60], M.T. Meinhard [ID], F. Nessi-Tedaldi [ID], J. Niedziela [ID], F. Pauss [ID], V. Perovic [ID], S. Pigazzini [ID], M.G. Ratti [ID], M. Reichmann [ID], C. Reissel [ID], T. Reitenspiess [ID], B. Ristic [ID], F. Riti [ID], D. Ruini, D.A. Sanz Becerra [ID], J. Steggemann [ID][60], D. Valsecchi [ID][21], R. Wallny [ID]

Universität Zürich, Zurich, Switzerland

C. Amsler [ID][62], P. Bärtschi [ID], C. Botta [ID], D. Brzhechko, M.F. Canelli [ID], K. Cormier [ID], A. De Wit [ID], R. Del Burgo, J.K. Heikkilä [ID], M. Huwiler [ID], W. Jin [ID], A. Jofrehei [ID], B. Kilminster [ID], S. Leontsinis [ID], S.P. Liechti [ID], A. Macchiolo [ID], P. Meiring [ID], V.M. Mikuni [ID], U. Molinatti [ID], I. Neutelings [ID], A. Reimers [ID], P. Robmann, S. Sanchez Cruz [ID], K. Schweiger [ID], M. Senger [ID], Y. Takahashi [ID]

National Central University, Chung-Li, Taiwan

C. Adloff[63], C.M. Kuo, W. Lin, S.S. Yu [ID]

National Taiwan University (NTU), Taipei, Taiwan

L. Ceard, Y. Chao, K.F. Chen, P.s. Chen, H. Cheng, W.-S. Hou, Y.y. Li, R.-S. Lu, E. Paganis, A. Psallidas, A. Steen, H.y. Wu, E. Yazgan, P.r. Yu

Chulalongkorn University, Faculty of Science, Department of Physics, Bangkok, Thailand

C. Asawatangtrakuldee, N. Srimanobhas

Çukurova University, Physics Department, Science and Art Faculty, Adana, Turkey

D. Agyel, F. Boran, Z.S. Demiroglu, F. Dolek, I. Dumanoglu[64], E. Eskut, Y. Guler[65], E. Gurpinar Guler[65], C. Isik, O. Kara, A. Kayis Topaksu, U. Kiminsu, G. Onengut, K. Ozdemir[66], A. Polatoz, A.E. Simsek, B. Tali[67], U.G. Tok, S. Turkcapar, E. Uslan, I.S. Zorbakir

Middle East Technical University, Physics Department, Ankara, Turkey

G. Karapinar[68], K. Ocalan[69], M. Yalvac[70]

Bogazici University, Istanbul, Turkey

B. Akgun, I.O. Atakisi, E. Gülmez, M. Kaya[71], O. Kaya[72], Ö. Özçelik, S. Tekten[73]

Istanbul Technical University, Istanbul, Turkey

A. Cakir, K. Cankocak[64], Y. Komurcu, S. Sen[74]

Istanbul University, Istanbul, Turkey

O. Aydilek, S. Cerci[67], B. Hacisahinoglu, I. Hos[75], B. Isildak[76], B. Kaynak, S. Ozkorucuklu, C. Simsek, D. Sunar Cerci[67]

Institute for Scintillation Materials of National Academy of Science of Ukraine, Kharkiv, Ukraine

B. Grynyov
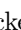
National Science Centre, Kharkiv Institute of Physics and Technology, Kharkiv, Ukraine

L. Levchuk

University of Bristol, Bristol, United Kingdom
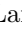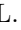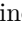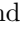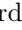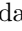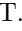
D. Anthony, E. Bhal, J.J. Brooke, A. Bundock, E. Clement, D. Cussans, H. Flacher, M. Glowacki, J. Goldstein, G.P. Heath, H.F. Heath, L. Kreczko, B. Krikler, S. Paramesvaran, S. Seif El Nasr-Storey, V.J. Smith, N. Stylianou[77], K. Walkingshaw Pass, R. White

Rutherford Appleton Laboratory, Didcot, United Kingdom

A.H. Ball, K.W. Bell, A. Belyaev[78], C. Brew, R.M. Brown, D.J.A. Cockerill, C. Cooke, K.V. Ellis, K. Harder, S. Harper, M.-L. Holmberg[79], J. Linacre,

K. Manolopoulos, D.M. Newbold , E. Olaiya, D. Petyt , T. Reis , G. Salvi , T. Schuh,
C.H. Shepherd-Themistocleous , I.R. Tomalin, T. Williams
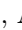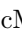
Imperial College, London, United Kingdom
R. Bainbridge , P. Bloch , S. Bonomally, J. Borg , S. Breeze, C.E. Brown , O. Buchmuller,
V. Cacchio, V. Cepaitis , G.S. Chahal [80], D. Colling , J.S. Dancu, P. Dauncey ,
G. Davies , J. Davies, M. Della Negra , S. Fayer, G. Fedi , G. Hall , M.H. Hassanshahi ,
A. Howard, G. Iles , J. Langford , L. Lyons , A.-M. Magnan , S. Malik, A. Martelli ,
M. Mieskolainen , D.G. Monk , J. Nash [81], M. Pesaresi, B.C. Radburn-Smith ,
D.M. Raymond, A. Richards, A. Rose , E. Scott , C. Seez , A. Shtipliyski, R. Shukla ,
A. Tapper , K. Uchida , G.P. Uttley , L.H. Vage, T. Virdee [21], M. Vojinovic ,
N. Wardle , S.N. Webb , D. Winterbottom
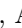
Brunel University, Uxbridge, United Kingdom
K. Coldham, J.E. Cole , A. Khan, P. Kyberd , I.D. Reid

Baylor University, Waco, Texas, USA
S. Abdullin , A. Brinkerhoff , B. Caraway , J. Dittmann , K. Hatakeyama ,
A.R. Kanuganti , B. McMaster , M. Saunders , S. Sawant , C. Sutantawibul , J. Wilson
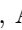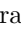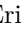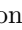
Catholic University of America, Washington, DC, USA
R. Bartek , A. Dominguez , R. Uniyal , A.M. Vargas Hernandez
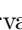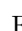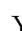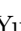
The University of Alabama, Tuscaloosa, Alabama, USA
A. Buccilli , S.I. Cooper , D. Di Croce , S.V. Gleyzer , C. Henderson , C.U. Perez ,
P. Rumerio [82], C. West
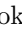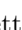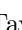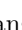
Boston University, Boston, Massachusetts, USA
A. Akpinar , A. Albert , D. Arcaro , C. Cosby , Z. Demiragli , C. Erice , E. Fontanesi ,
D. Gastler , S. May , J. Rohlf , K. Salyer , D. Sperka , D. Spitzbart , I. Suarez ,
A. Tsatsos , S. Yuan

Brown University, Providence, Rhode Island, USA
G. Benelli , B. Burkle , X. Coubez [23], D. Cutts , M. Hadley , U. Heintz , J.M. Hogan [83],
T. Kwon , G. Landsberg , K.T. Lau , D. Li , J. Luo , M. Narain , N. Pervan ,
S. Sagir [84], F. Simpson , E. Usai , W.Y. Wong , X. Yan , D. Yu , W. Zhang

University of California, Davis, Davis, California, USA
J. Bonilla , C. Brainerd , R. Breedon , M. Calderon De La Barca Sanchez , M. Chertok ,
J. Conway , P.T. Cox , R. Erbacher , G. Haza , F. Jensen , O. Kukral , G. Mocellin ,
M. Mulhearn , D. Pellett , B. Regnery , D. Taylor , Y. Yao , F. Zhang
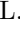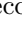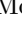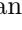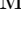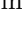
University of California, Los Angeles, California, USA
M. Bachtis , R. Cousins , A. Datta , D. Hamilton , J. Hauser , M. Ignatenko ,
M.A. Iqbal , T. Lam , W.A. Nash , S. Regnard , D. Saltzberg , B. Stone , V. Valuev
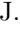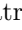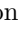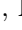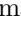
University of California, Riverside, Riverside, California, USA

Y. Chen, R. Clare [iD], J.W. Gary [iD], M. Gordon, G. Hanson [iD], G. Karapostoli [iD], O.R. Long [iD], N. Manganelli [iD], W. Si [iD], S. Wimpenny [iD]

University of California, San Diego, La Jolla, California, USA

J.G. Branson, P. Chang [iD], S. Cittolin, S. Cooperstein [iD], D. Diaz [iD], J. Duarte [iD], R. Gerosa [iD], L. Giannini [iD], J. Guiang [iD], R. Kansal [iD], V. Krutelyov [iD], R. Lee [iD], J. Letts [iD], M. Masciovecchio [iD], F. Mokhtar [iD], M. Pieri [iD], B.V. Sathia Narayanan [iD], V. Sharma [iD], M. Tadel [iD], F. Würthwein [iD], Y. Xiang [iD], A. Yagil [iD]
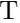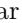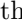
University of California, Santa Barbara - Department of Physics, Santa Barbara, California, USA

N. Amin, C. Campagnari [iD], M. Citron [iD], G. Collura [iD], A. Dorsett [iD], V. Dutta [iD], J. Incandela [iD], M. Kilpatrick [iD], J. Kim [iD], A.J. Li [iD], B. Marsh, P. Masterson [iD], H. Mei [iD], M. Oshiro [iD], M. Quinnan [iD], J. Richman [iD], U. Sarica [iD], R. Schmitz, F. Setti [iD], J. Sheplock [iD], P. Siddireddy, D. Stuart [iD], S. Wang [iD]
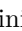
California Institute of Technology, Pasadena, California, USA

A. Bornheim [iD], O. Cerri, I. Dutta [iD], J.M. Lawhorn [iD], N. Lu [iD], J. Mao [iD], H.B. Newman [iD], T. Q. Nguyen [iD], M. Spiropulu [iD], J.R. Vlimant [iD], C. Wang [iD], S. Xie [iD], R.Y. Zhu [iD]
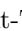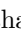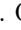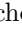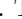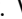
Carnegie Mellon University, Pittsburgh, Pennsylvania, USA

J. Alison [iD], S. An [iD], M.B. Andrews [iD], P. Bryant [iD], T. Ferguson [iD], A. Harilal [iD], C. Liu [iD], T. Mudholkar [iD], S. Murthy [iD], M. Paulini [iD], A. Roberts [iD], A. Sanchez [iD], W. Terrill [iD]
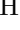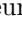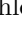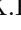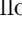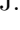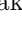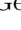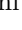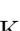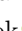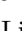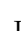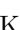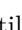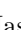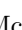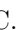
University of Colorado Boulder, Boulder, Colorado, USA

J.P. Cumalat [iD], W.T. Ford [iD], A. Hassani [iD], G. Karathanasis [iD], E. MacDonald, F. Marini [iD], R. Patel, A. Perloff [iD], C. Savard [iD], N. Schonbeck [iD], K. Stenson [iD], K.A. Ulmer [iD], S.R. Wagner [iD], N. Zipper [iD]

Cornell University, Ithaca, New York, USA
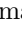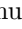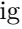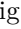
J. Alexander [iD], S. Bright-Thonney [iD], X. Chen [iD], D.J. Cranshaw [iD], J. Fan [iD], X. Fan [iD], D. Gadkari [iD], S. Hogan [iD], J. Monroy [iD], J.R. Patterson [iD], D. Quach [iD], J. Reichert [iD], M. Reid [iD], A. Ryd [iD], J. Thom [iD], P. Wittich [iD], R. Zou [iD]

Fermi National Accelerator Laboratory, Batavia, Illinois, USA

M. Albrow [iD], M. Alyari [iD], G. Apollinari [iD], A. Apresyan [iD], L.A.T. Bauerdick [iD], D. Berry [iD], J. Berryhill [iD], P.C. Bhat [iD], K. Burkett [iD], J.N. Butler [iD], A. Canepa [iD], G.B. Cerati [iD], H.W.K. Cheung [iD], F. Chlebana [iD], K.F. Di Petrillo [iD], J. Dickinson [iD], V.D. Elvira [iD], Y. Feng [iD], J. Freeman [iD], A. Gandrakota [iD], Z. Gecse [iD], L. Gray [iD], D. Green, S. Grünendahl [iD], O. Gutsche [iD], R.M. Harris [iD], R. Heller [iD], T.C. Herwig [iD], J. Hirschauer [iD], L. Horyn [iD], B. Jayatilaka [iD], S. Jindariani [iD], M. Johnson [iD], U. Joshi [iD], T. Klijnsma [iD], B. Klima [iD], K.H.M. Kwok [iD], S. Lammel [iD], D. Lincoln [iD], R. Lipton [iD], T. Liu [iD], C. Madrid [iD], K. Maeshima [iD], C. Mantilla [iD], D. Mason [iD], P. McBride [iD], P. Merkel [iD], S. Mrenna [iD], S. Nahn [iD], J. Ngadiuba [iD], D. Noonan [iD], V. Papadimitriou [iD], N. Pastika [iD], K. Pedro [iD], C. Pena [iD][85],

F. Ravera ⓘ, A. Reinsvold Hall ⓘ[86], L. Ristori ⓘ, E. Sexton-Kennedy ⓘ, N. Smith ⓘ, A. Soha ⓘ, L. Spiegel ⓘ, J. Strait ⓘ, L. Taylor ⓘ, S. Tkaczyk ⓘ, N.V. Tran ⓘ, L. Uplegger ⓘ, E.W. Vaandering ⓘ, H.A. Weber ⓘ, I. Zoi ⓘ

University of Florida, Gainesville, Florida, USA

P. Avery ⓘ, D. Bourilkov ⓘ, L. Cadamuro ⓘ, V. Cherepanov ⓘ, R.D. Field, D. Guerrero ⓘ, M. Kim, E. Koenig ⓘ, J. Konigsberg ⓘ, A. Korytov ⓘ, K.H. Lo, K. Matchev ⓘ, N. Menendez ⓘ, G. Mitselmakher ⓘ, A. Muthirakalayil Madhu ⓘ, N. Rawal ⓘ, D. Rosenzweig ⓘ, S. Rosenzweig ⓘ, K. Shi ⓘ, J. Wang ⓘ, Z. Wu ⓘ
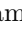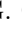
Florida State University, Tallahassee, Florida, USA

T. Adams ⓘ, A. Askew ⓘ, R. Habibullah ⓘ, V. Hagopian ⓘ, R. Khurana, T. Kolberg ⓘ, G. Martinez, H. Prosper ⓘ, C. Schiber, O. Viazlo ⓘ, R. Yohay ⓘ, J. Zhang
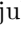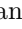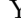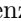
Florida Institute of Technology, Melbourne, Florida, USA

M.M. Baarmand ⓘ, S. Butalla ⓘ, T. Elkafrawy ⓘ[51], M. Hohlmann ⓘ, R. Kumar Verma ⓘ, M. Rahmani, F. Yumiceva ⓘ

University of Illinois at Chicago (UIC), Chicago, Illinois, USA

M.R. Adams ⓘ, H. Becerril Gonzalez ⓘ, R. Cavanaugh ⓘ, S. Dittmer ⓘ, O. Evdokimov ⓘ, C.E. Gerber ⓘ, D.J. Hofman ⓘ, D. S. Lemos ⓘ, A.H. Merrit ⓘ, C. Mills ⓘ, G. Oh ⓘ, T. Roy ⓘ, S. Rudrabhatla ⓘ, M.B. Tonjes ⓘ, N. Varelas ⓘ, X. Wang ⓘ, Z. Ye ⓘ, J. Yoo ⓘ
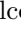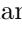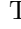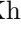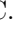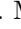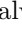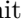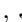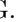
The University of Iowa, Iowa City, Iowa, USA

M. Alhusseini ⓘ, K. Dilsiz ⓘ[87], L. Emediato ⓘ, R.P. Gandrajula ⓘ, G. Karaman ⓘ, O.K. Köseyan ⓘ, J.-P. Merlo, A. Mestvirishvili ⓘ[88], J. Nachtman ⓘ, O. Neogi, H. Ogul ⓘ[89], Y. Onel ⓘ, A. Penzo ⓘ, C. Snyder, E. Tiras ⓘ[90]
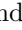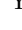
Johns Hopkins University, Baltimore, Maryland, USA

O. Amram ⓘ, B. Blumenfeld ⓘ, L. Corcodilos ⓘ, J. Davis ⓘ, A.V. Gritsan ⓘ, L. Kang ⓘ, S. Kyriacou ⓘ, P. Maksimovic ⓘ, J. Roskes ⓘ, S. Sekhar ⓘ, M. Swartz ⓘ, T.Á. Vámi ⓘ

The University of Kansas, Lawrence, Kansas, USA

A. Abreu ⓘ, L.F. Alcerro Alcerro ⓘ, J. Anguiano ⓘ, P. Baringer ⓘ, A. Bean ⓘ, Z. Flowers ⓘ, T. Isidori ⓘ, S. Khalil ⓘ, J. King ⓘ, G. Krintiras ⓘ, M. Lazarovits ⓘ, C. Le Mahieu, C. Lindsey, J. Marquez ⓘ, N. Minafra ⓘ, M. Murray ⓘ, M. Nickel ⓘ, C. Rogan ⓘ, C. Royon ⓘ, R. Salvatico ⓘ, S. Sanders ⓘ, E. Schmitz ⓘ, C. Smith ⓘ, Q. Wang ⓘ, J. Williams ⓘ, G. Wilson ⓘ
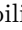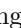
Kansas State University, Manhattan, Kansas, USA

B. Allmond ⓘ, S. Duric, R. Gujju Gurunadha ⓘ, A. Ivanov ⓘ, K. Kaadze ⓘ, D. Kim, Y. Maravin ⓘ, T. Mitchell, A. Modak, K. Nam, J. Natoli ⓘ, D. Roy ⓘ
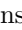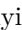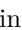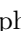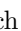
Lawrence Livermore National Laboratory, Livermore, California, USA

F. Rebassoo ⓘ, D. Wright ⓘ
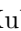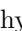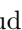
University of Maryland, College Park, Maryland, USA

E. Adams ⓘ, A. Baden ⓘ, O. Baron, A. Belloni ⓘ, A. Bethani ⓘ, S.C. Eno ⓘ, N.J. Hadley ⓘ, S. Jabeen ⓘ, R.G. Kellogg ⓘ, T. Koeth ⓘ, Y. Lai ⓘ, S. Lascio ⓘ, A.C. Mignerey ⓘ, S. Nabili ⓘ, C. Palmer ⓘ, C. Papageorgakis ⓘ, M. Seidel ⓘ, L. Wang ⓘ, K. Wong ⓘ

Massachusetts Institute of Technology, Cambridge, Massachusetts, USA

D. Abercrombie, R. Bi, W. Busza ⓘ, I.A. Cali ⓘ, Y. Chen ⓘ, M. D'Alfonso ⓘ, J. Eysermans ⓘ, C. Freer ⓘ, G. Gomez-Ceballos ⓘ, M. Goncharov, P. Harris, M. Hu ⓘ, D. Kovalskyi ⓘ, J. Krupa ⓘ, Y.-J. Lee ⓘ, K. Long ⓘ, C. Mironov ⓘ, C. Paus ⓘ, D. Rankin ⓘ, C. Roland ⓘ, G. Roland ⓘ, Z. Shi ⓘ, G.S.F. Stephans ⓘ, J. Wang, Z. Wang ⓘ, B. Wyslouch ⓘ
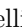
University of Minnesota, Minneapolis, Minnesota, USA

R.M. Chatterjee, B. Crossman ⓘ, A. Evans ⓘ, J. Hiltbrand ⓘ, Sh. Jain ⓘ, B.M. Joshi ⓘ, C. Kapsiak ⓘ, M. Krohn ⓘ, Y. Kubota ⓘ, J. Mans ⓘ, M. Revering ⓘ, R. Rusack ⓘ, R. Saradhy ⓘ, N. Schroeder ⓘ, N. Strobbe ⓘ, M.A. Wadud ⓘ
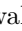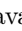
University of Mississippi, Oxford, Mississippi, USA

L.M. Cremaldi ⓘ
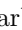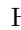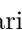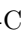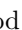
University of Nebraska-Lincoln, Lincoln, Nebraska, USA

K. Bloom ⓘ, M. Bryson, D.R. Claes ⓘ, C. Fangmeier ⓘ, L. Finco ⓘ, F. Golf ⓘ, C. Joo ⓘ, I. Kravchenko ⓘ, I. Reed ⓘ, J.E. Siado ⓘ, G.R. Snow[†], W. Tabb ⓘ, A. Wightman ⓘ, F. Yan ⓘ, A.G. Zecchinelli ⓘ

State University of New York at Buffalo, Buffalo, New York, USA

G. Agarwal ⓘ, H. Bandyopadhyay ⓘ, L. Hay ⓘ, I. Iashvili ⓘ, A. Kharchilava ⓘ, C. McLean ⓘ, M. Morris ⓘ, D. Nguyen ⓘ, J. Pekkanen ⓘ, S. Rappoccio ⓘ, A. Williams ⓘ
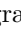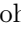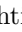
Northeastern University, Boston, Massachusetts, USA

G. Alverson ⓘ, E. Barberis ⓘ, Y. Haddad ⓘ, Y. Han ⓘ, A. Krishna ⓘ, J. Li ⓘ, J. Lidrych ⓘ, G. Madigan ⓘ, B. Marzocchi ⓘ, D.M. Morse ⓘ, V. Nguyen ⓘ, T. Orimoto ⓘ, A. Parker ⓘ, L. Skinnari ⓘ, A. Tishelman-Charny ⓘ, T. Wamorkar ⓘ, B. Wang ⓘ, A. Wisecarver ⓘ, D. Wood ⓘ

Northwestern University, Evanston, Illinois, USA

S. Bhattacharya ⓘ, J. Bueghly, Z. Chen ⓘ, A. Gilbert ⓘ, T. Gunter ⓘ, K.A. Hahn ⓘ, Y. Liu ⓘ, N. Odell ⓘ, M.H. Schmitt ⓘ, M. Velasco

University of Notre Dame, Notre Dame, Indiana, USA

R. Band ⓘ, R. Bucci, S. Castells ⓘ, M. Cremonesi, A. Das ⓘ, R. Goldouzian ⓘ, M. Hildreth ⓘ, K. Hurtado Anampa ⓘ, C. Jessop ⓘ, K. Lannon ⓘ, J. Lawrence ⓘ, N. Loukas ⓘ, L. Lutton ⓘ, J. Mariano, N. Marinelli, I. Mcalister, T. McCauley ⓘ, C. Mcgrady ⓘ, K. Mohrman ⓘ, C. Moore ⓘ, Y. Musienko ⓘ[13], H. Nelson ⓘ, R. Ruchti ⓘ, A. Townsend ⓘ, M. Wayne ⓘ, H. Yockey, M. Zarucki ⓘ, L. Zygala ⓘ

The Ohio State University, Columbus, Ohio, USA

B. Bylsma, M. Carrigan ©, L.S. Durkin ©, B. Francis ©, C. Hill ©, A. Lesauvage ©,
M. Nunez Ornelas ©, K. Wei, B.L. Winer ©, B. R. Yates ©

Princeton University, Princeton, New Jersey, USA

F.M. Addesa ©, B. Bonham ©, P. Das ©, G. Dezoort ©, P. Elmer ©, A. Frankenthal ©,
B. Greenberg ©, N. Haubrich ©, S. Higginbotham ©, A. Kalogeropoulos ©, G. Kopp ©, S. Kwan ©,
D. Lange ©, D. Marlow ©, K. Mei ©, I. Ojalvo ©, J. Olsen ©, D. Stickland ©, C. Tully ©

University of Puerto Rico, Mayaguez, Puerto Rico, USA

S. Malik ©, S. Norberg

Purdue University, West Lafayette, Indiana, USA

A.S. Bakshi ©, V.E. Barnes ©, R. Chawla ©, S. Das ©, L. Gutay, M. Jones ©, A.W. Jung ©,
D. Kondratyev ©, A.M. Koshy, M. Liu ©, G. Negro ©, N. Neumeister ©, G. Paspalaki ©,
S. Piperov ©, A. Purohit ©, J.F. Schulte ©, M. Stojanovic ©, J. Thieman ©, F. Wang ©,
R. Xiao ©, W. Xie ©

Purdue University Northwest, Hammond, Indiana, USA

J. Dolen ©, N. Parashar ©

Rice University, Houston, Texas, USA

D. Acosta ©, A. Baty ©, T. Carnahan ©, M. Decaro, S. Dildick ©, K.M. Ecklund ©,
P.J. Fernández Manteca ©, S. Freed, P. Gardner, F.J.M. Geurts ©, A. Kumar ©, W. Li ©,
B.P. Padley ©, R. Redjimi, J. Rotter ©, W. Shi ©, S. Yang ©, E. Yigitbasi ©, L. Zhang[91],
Y. Zhang ©, X. Zuo ©

University of Rochester, Rochester, New York, USA

A. Bodek ©, P. de Barbaro ©, R. Demina ©, J.L. Dulemba ©, C. Fallon, T. Ferbel ©, M. Galanti,
A. Garcia-Bellido ©, O. Hindrichs ©, A. Khukhunaishvili ©, E. Ranken ©, R. Taus ©,
G.P. Van Onsem ©

The Rockefeller University, New York, New York, USA

K. Goulianos ©

Rutgers, The State University of New Jersey, Piscataway, New Jersey, USA

B. Chiarito, J.P. Chou ©, Y. Gershtein ©, E. Halkiadakis ©, A. Hart ©, M. Heindl ©,
D. Jaroslawski ©, O. Karacheban ©[25], I. Laflotte ©, A. Lath ©, R. Montalvo, K. Nash,
M. Osherson ©, S. Salur ©, S. Schnetzer, S. Somalwar ©, R. Stone ©, S.A. Thayil ©, S. Thomas,
H. Wang ©

University of Tennessee, Knoxville, Tennessee, USA

H. Acharya, A.G. Delannoy ©, S. Fiorendi ©, T. Holmes ©, E. Nibigira ©, S. Spanier ©

Texas A&M University, College Station, Texas, USA

O. Bouhali [92], M. Dalchenko, A. Delgado, R. Eusebi, J. Gilmore, T. Huang, T. Kamon [93], H. Kim, S. Luo, S. Malhotra, R. Mueller, D. Overton, D. Rathjens, A. Safonov

Texas Tech University, Lubbock, Texas, USA

N. Akchurin, J. Damgov, V. Hegde, K. Lamichhane, S.W. Lee, T. Mengke, S. Muthumuni, T. Peltola, I. Volobouev, Z. Wang, A. Whitbeck

Vanderbilt University, Nashville, Tennessee, USA

E. Appelt, S. Greene, A. Gurrola, W. Johns, A. Melo, F. Romeo, P. Sheldon, S. Tuo, J. Velkovska, J. Viinikainen

University of Virginia, Charlottesville, Virginia, USA

B. Cardwell, B. Cox, G. Cummings, J. Hakala, R. Hirosky, M. Joyce, A. Ledovskoy, A. Li, C. Neu, C.E. Perez Lara, B. Tannenwald

Wayne State University, Detroit, Michigan, USA

P.E. Karchin, N. Poudyal

University of Wisconsin - Madison, Madison, Wisconsin, USA

S. Banerjee, K. Black, T. Bose, S. Dasu, I. De Bruyn, P. Everaerts, C. Galloni, H. He, M. Herndon, A. Herve, C.K. Koraka, A. Lanaro, A. Loeliger, R. Loveless, J. Madhusudanan Sreekala, A. Mallampalli, A. Mohammadi, S. Mondal, G. Parida, D. Pinna, A. Savin, V. Shang, V. Sharma, W.H. Smith, D. Teague, H.F. Tsoi, W. Vetens

Authors affiliated with an institute or an international laboratory covered by a cooperation agreement with CERN

S. Afanasiev, V. Andreev, Yu. Andreev, T. Aushev, M. Azarkin, A. Babaev, A. Belyaev, V. Blinov [94], E. Boos, V. Borshch, D. Budkouski, V. Bunichev, O. Bychkova, M. Chadeeva [94], V. Chekhovsky, A. Dermenev, T. Dimova [94], I. Dremin, M. Dubinin [85], L. Dudko, V. Epshteyn, G. Gavrilov, V. Gavrilov, S. Gninenko, V. Golovtcov, N. Golubev, I. Golutvin, I. Gorbunov, A. Gribushin, V. Ivanchenko, Y. Ivanov, V. Kachanov, L. Kardapoltsev [94], V. Karjavine, A. Karneyeu, V. Kim [94], M. Kirakosyan, D. Kirpichnikov, M. Kirsanov, V. Klyukhin, O. Kodolova [95], D. Konstantinov, V. Korenkov, A. Kozyrev [94], N. Krasnikov, E. Kuznetsova [96], A. Lanev, P. Levchenko, A. Litomin, N. Lychkovskaya, V. Makarenko, A. Malakhov, V. Matveev [94,97], V. Murzin, A. Nikitenko [98], S. Obraztsov, V. Okhotnikov, A. Oskin, I. Ovtin [94], V. Palichik, P. Parygin, V. Perelygin, M. Perfilov, S. Petrushanko, G. Pivovarov, V. Popov, E. Popova, O. Radchenko [94], V. Rusinov, M. Savina, V. Savrin, V. Shalaev, S. Shmatov, S. Shulha, Y. Skovpen [94], S. Slabospitskii, V. Smirnov, D. Sosnov, A. Stepennov, V. Sulimov, E. Tcherniaev, A. Terkulov, O. Teryaev, I. Tlisova, M. Toms, A. Toropin, L. Uvarov, A. Uzunian, E. Vlasov, A. Vorobyev, N. Voytishin, B.S. Yuldashev [99], A. Zarubin, I. Zhizhin, A. Zhokin

† *Deceased*

1 *Also at Yerevan State University, Yerevan, Armenia*

2 *Also at TU Wien, Vienna, Austria*

3 *Also at Institute of Basic and Applied Sciences, Faculty of Engineering, Arab Academy for Science, Technology and Maritime Transport, Alexandria, Egypt*

4 *Also at Université Libre de Bruxelles, Bruxelles, Belgium*

5 *Also at Universidade Estadual de Campinas, Campinas, Brazil*

6 *Also at Federal University of Rio Grande do Sul, Porto Alegre, Brazil*

7 *Also at UFMS, Nova Andradina, Brazil*

8 *Also at The University of the State of Amazonas, Manaus, Brazil*

9 *Also at University of Chinese Academy of Sciences, Beijing, China*

10 *Also at Nanjing Normal University Department of Physics, Nanjing, China*

11 *Now at The University of Iowa, Iowa City, Iowa, USA*

12 *Also at University of Chinese Academy of Sciences, Beijing, China*

13 *Also at an institute or an international laboratory covered by a cooperation agreement with CERN*

14 *Also at Cairo University, Cairo, Egypt*

15 *Also at Suez University, Suez, Egypt*

16 *Now at British University in Egypt, Cairo, Egypt*

17 *Also at Purdue University, West Lafayette, Indiana, USA*

18 *Also at Université de Haute Alsace, Mulhouse, France*

19 *Also at Department of Physics, Tsinghua University, Beijing, China*

20 *Also at Erzincan Binali Yildirim University, Erzincan, Turkey*

21 *Also at CERN, European Organization for Nuclear Research, Geneva, Switzerland*

22 *Also at University of Hamburg, Hamburg, Germany*

23 *Also at RWTH Aachen University, III. Physikalisches Institut A, Aachen, Germany*

24 *Also at Isfahan University of Technology, Isfahan, Iran*

25 *Also at Brandenburg University of Technology, Cottbus, Germany*

26 *Also at Forschungszentrum Jülich, Juelich, Germany*

27 *Also at Physics Department, Faculty of Science, Assiut University, Assiut, Egypt*

28 *Also at Karoly Robert Campus, MATE Institute of Technology, Gyongyos, Hungary*

29 *Also at Wigner Research Centre for Physics, Budapest, Hungary*

30 *Also at Institute of Physics, University of Debrecen, Debrecen, Hungary*

31 *Also at Institute of Nuclear Research ATOMKI, Debrecen, Hungary*

32 *Now at Universitatea Babes-Bolyai - Facultatea de Fizica, Cluj-Napoca, Romania*

33 *Also at Faculty of Informatics, University of Debrecen, Debrecen, Hungary*

34 *Also at Punjab Agricultural University, Ludhiana, India*

35 *Also at UPES - University of Petroleum and Energy Studies, Dehradun, India*

36 *Also at University of Visva-Bharati, Santiniketan, India*

37 *Also at University of Hyderabad, Hyderabad, India*

38 *Also at Indian Institute of Science (IISc), Bangalore, India*

39 *Also at Indian Institute of Technology (IIT), Mumbai, India*

40 *Also at IIT Bhubaneswar, Bhubaneswar, India*

41 *Also at Institute of Physics, Bhubaneswar, India*

42 *Also at Deutsches Elektronen-Synchrotron, Hamburg, Germany*

43 *Also at Sharif University of Technology, Tehran, Iran*

44 *Also at Department of Physics, University of Science and Technology of Mazandaran, Behshahr, Iran*

45 *Also at Helwan University, Cairo, Egypt*

46 *Also at Italian National Agency for New Technologies, Energy and Sustainable Economic Development, Bologna, Italy*

47 *Also at Centro Siciliano di Fisica Nucleare e di Struttura Della Materia, Catania, Italy*

48 *Also at Scuola Superiore Meridionale, Università di Napoli 'Federico II', Napoli, Italy*

49 *Also at Laboratori Nazionali di Legnaro dell'INFN, Legnaro, Italy*

50 *Also at Università di Napoli 'Federico II', Napoli, Italy*

[51] *Also at Ain Shams University, Cairo, Egypt*

[52] *Also at Consiglio Nazionale delle Ricerche - Istituto Officina dei Materiali, Perugia, Italy*

[53] *Also at Department of Applied Physics, Faculty of Science and Technology, Universiti Kebangsaan Malaysia, Bangi, Malaysia*

[54] *Also at Consejo Nacional de Ciencia y Tecnología, Mexico City, Mexico*

[55] *Also at IRFU, CEA, Université Paris-Saclay, Gif-sur-Yvette, France*

[56] *Also at Faculty of Physics, University of Belgrade, Belgrade, Serbia*

[57] *Also at Trincomalee Campus, Eastern University, Sri Lanka, Nilaveli, Sri Lanka*

[58] *Also at INFN Sezione di Pavia, Università di Pavia, Pavia, Italy*

[59] *Also at National and Kapodistrian University of Athens, Athens, Greece*

[60] *Also at Ecole Polytechnique Fédérale Lausanne, Lausanne, Switzerland*

[61] *Also at Universität Zürich, Zurich, Switzerland*

[62] *Also at Stefan Meyer Institute for Subatomic Physics, Vienna, Austria*

[63] *Also at Laboratoire d'Annecy-le-Vieux de Physique des Particules, IN2P3-CNRS, Annecy-le-Vieux, France*

[64] *Also at Near East University, Research Center of Experimental Health Science, Mersin, Turkey*

[65] *Also at Konya Technical University, Konya, Turkey*

[66] *Also at Izmir Bakircay University, Izmir, Turkey*

[67] *Also at Adiyaman University, Adiyaman, Turkey*

[68] *Also at Istanbul Gedik University, Istanbul, Turkey*

[69] *Also at Necmettin Erbakan University, Konya, Turkey*

[70] *Also at Bozok Universitetesi Rektörlügü, Yozgat, Turkey*

[71] *Also at Marmara University, Istanbul, Turkey*

[72] *Also at Milli Savunma University, Istanbul, Turkey*

[73] *Also at Kafkas University, Kars, Turkey*

[74] *Also at Hacettepe University, Ankara, Turkey*

[75] *Also at Istanbul University - Cerrahpasa, Faculty of Engineering, Istanbul, Turkey*

[76] *Also at Yildiz Technical University, Istanbul, Turkey*

[77] *Also at Vrije Universiteit Brussel, Brussel, Belgium*

[78] *Also at School of Physics and Astronomy, University of Southampton, Southampton, United Kingdom*

[79] *Also at University of Bristol, Bristol, United Kingdom*

[80] *Also at IPPP Durham University, Durham, United Kingdom*

[81] *Also at Monash University, Faculty of Science, Clayton, Australia*

[82] *Also at Università di Torino, Torino, Italy*

[83] *Also at Bethel University, St. Paul, Minnesota, USA*

[84] *Also at Karamanoğlu Mehmetbey University, Karaman, Turkey*

[85] *Also at California Institute of Technology, Pasadena, California, USA*

[86] *Also at United States Naval Academy, Annapolis, Maryland, USA*

[87] *Also at Bingol University, Bingol, Turkey*

[88] *Also at Georgian Technical University, Tbilisi, Georgia*

[89] *Also at Sinop University, Sinop, Turkey*

[90] *Also at Erciyes University, Kayseri, Turkey*

[91] *Also at Institute of Modern Physics and Key Laboratory of Nuclear Physics and Ion-beam Application (MOE) - Fudan University, Shanghai, China*

[92] *Also at Texas A&M University at Qatar, Doha, Qatar*

[93] *Also at Kyungpook National University, Daegu, Korea*

[94] *Also at another institute or international laboratory covered by a cooperation agreement with CERN*

[95] *Also at Yerevan Physics Institute, Yerevan, Armenia*

[96] *Now at University of Florida, Gainesville, Florida, USA*

[97] *Now at another institute or international laboratory covered by a cooperation agreement with CERN*

[98] *Also at Imperial College, London, United Kingdom*

[99] *Also at Institute of Nuclear Physics of the Uzbekistan Academy of Sciences, Tashkent, Uzbekistan*